CREATION OF TRANSPORT PATHWAYS ACROSS SKIN BY MICRONEEDLES FOR DRUG DELIVERY

LI HAIRUI

NATIONAL UNIVERSITY OF SINGAPORE

2016

CREATION OF TRANSPORT PATHWAYS ACROSS SKIN BY MICRONEEDLES FOR DRUG DELIVERY

LI HAIRUI

(M. S., China Pharmaceutical University)

A THESIS SUBMITTED

FOR THE DEGREE OF DOCTOR OF PHILOSOPHY

DEPARTMENT OF PHARMACY

NATIONAL UNIVERSITY OF SINGAPORE

2016

Declaration

I hereby declare that this thesis is my original work and it has been written by me in its entirety. I have duly acknowledged all the sources of information which have been used in the thesis.

This thesis has also not been submitted for any degree in any university previously.

_____

Li Hairui

24 Sep 2016

Acknowledgements

Firstly, I would like to thank Dr. Kang Lifeng for his encouragement, enthusiasm, support and guidance throughout my Ph.D. studies. His mentorship and training has inspired me tremendously throughout the journey.

I would like to thank my 3M supervisor, Dr. Lee Chi-Ying for advising me critically and helping me grow professionally, especially at the early stage of my Ph.D. journey. My heartfelt gratitude goes to Dr. Melvin Zin, who gives his time generously and provides me valuable and insightful advices on my research. I am especially grateful to Dr. Li Bo for being both a good supervisor and a friend, and providing me with help and suggestions whenever I need. I would also express my great gratitude to Dr. Bao Hongqian for inspiring me in antimicrobial material development, to Dr. Melvina Leolukman for her helpful suggestions and support. My thanks also go to my other 3M colleagues for supporting me at some point or the other in the journey: Dr. Sun Shuangyong, Chu Wenhong, Yeo Siew Ping, Dr. Soon Boon Yi, Yee Meng Hun, Dr. David Julius, Dr. Lim Boon Kiat, Dr. Jesudoss Arokiaraj and Jaslyn Tan.

I would like to thank my Thesis Advisory Committee members, A/P Giorgia Pastorin and Dr Ciprian Iliescu, who helped me make progress in my project by raising critical questions.

I am grateful to EDB, NUS and 3M Singapore for providing me the industrial postgraduate scholarship, financial and facility support which allowed me to carry out my scientific pursuit.

My gratitude goes to the past and present members of the Kang lab who have been not only great colleagues and but also great friends: Dr. Jaspreet Singh Kochhar, Dr. Pan Jing, Dr. Li Fang, Sara Dana, Himanshu Kathuria, Lim Seng Han, Justin Tan Jia Yao and Sun

Yuanyuan. I also wish to extend my appreciation to the Final Year Project students, Chong Hui Ping, Low Yong Sheng Jason, Bok Ke Xin, Teh Xiang Sheng, Toh Pei Zhen, and Lin Shu'E for the time spent together in research. I also thank the lab-support and administrative staff of NUS *Pharmily* for their timely assistance.

I am blessed to have a loving and supportive family who helped me through the tough journey. I am deeply thankful to my husband, Zhao Jinwei who accompanied and supported me all the time, to my parents and my parents-in-law for their sacrifices and taking care of us and the children. Last but not least, I would like to thank you, my children, Sihan and Siyuan, for bringing countless joy to our family. You have been an endless source of my strength and courage to continue my Ph.D. study.

Dedicated to my husband, my children,

my parents and my parents-in-law

for their love, sacrifice and tremendous support

Table of Contents

Summary

Microneedles can act as an effective enhancer for transdermal drug delivery by painlessly breaching the skin surface and providing an alternative transport pathway. Increasing studies have been carried out on microneedles for transdermal drug delivery, most of the publications focus on fabrication technology of microneedles and general application of microneedles. However, there are still a number of issues that limit the widespread use of microneedles in pharmaceutical and cosmetic fields, including the exact mechanism of microneedles in facilitating the skin permeability of drug, reasonable design of microneedle product for effective drug delivery, and safety concerns over the use of microneedles. The safety issues include the potential toxicity resulted from enhanced delivery of active ingredients and excipients, and the potential infection risk associated with a compromised *stratum corneum*. This thesis is focused on these issues that will influence the commercialization of microneedle products.

A tripeptide copper complex (GHK-Cu) was used in this thesis to study the factors influencing microneedle-mediated transdermal drug delivery efficacy with the aim to explore the underlying mechanisms of enhanced delivery by microneedles. It was demonstrated that microneedle application force can influence the performance of skin permeation of copper peptide by affecting the penetration properties in skin. This finding is very important for the design of microneedles and the correct use of microneedles for effective skin permeation enhancement. Besides, it was found that human epidermis and rat skin may not be suitable models for *in vitro* skin permeation study when microneedles are used, although they are good models for conventional transdermal delivery.

Microneedles showed a dramatic enhancement in the skin permeation of GHK-Cu, which may potentially be useful in providing delivery of copper through the skin to exert its

beneficial effects. However, whether other copper compounds can be used together with microneedles for copper delivery and whether enhanced delivery of copper through skin can cause any toxicity to skin are unknown. Therefore, the skin toxicity potential of copper peptide (GHK-Cu) was compared with two other copper compounds, copper chloride and copper acetate by an *in vitro* skin irritation test with multiple biomarkers used. It was demonstrated that GHK-Cu has a low potential of inducing skin irritation response when compared to copper chloride and copper acetate. The proposed *in vitro* skin irritancy test approach may also be useful to assess the irritancy potential of other similar inorganic compounds or minerals through the skin.

The use of microneedle in percutaneous drug delivery is also associated with the risk of infection because of the compromised SC. We managed to develop novel quaternary ammonium silane (QAS) antimicrobial copolymers which showed lower toxicity compared to the commercial QAS agent and the resulted coatings showed enhanced effectiveness and durability. Furthermore, microneedles with effective antimicrobial property was developed by coating with the synthesized copolymer, PDT-10% and good biocompatibility of the coated microneedles was demonstrated. The antimicrobial microneedles can potentially minimize the infection associated with microneedle usage.

Lastly, we fabricated an adhesive-free and solvent-free skin patch, namely dry patch, for the percutaneous delivery of lidocaine, to be applied together with microneedles. By comparing the percutaneous delivery of lidocaine and lidocaine HCl, it was found that the hydrophilic molecule, lidocaine HCl is the preferred molecule for a microneedle-assisted drug delivery system other than lidocaine. The new patch system can achieve a similar effectiveness as the commercial patch yet with a faster onset, although 40 times less drug was loaded in the new patch system.

List of Publications

1. **Li H**, Li B, Kathuria H, Pan J, Lee C-Y, Zin MT, Bao H, Leolukman M, and Kang L. Development of Lidocaine HCl dry patch with microneedle pretreatment for fast anesthetic effect. To be submitted.

2. **Li H**, Bao H, Lee C-Y, Li B, Zin MT and Kang L. Antibacterial activity of dental composites containing DMA-C_{16}Br against *Streptococcus mutans*. To be submitted.

3. **Li H**, Toh PZ, Zin MT, Lee C-Y, Li B, Leolukman M, Bao H, Kang L. Copper salts exhibited varying toxicity to skin cells. To be submitted.

4. Kathuria H, **Li H**, Pan J, Lim SH, Kochhar JS, Wu C, Kang L. Large size microneedle patch to deliver lidocaine through skin. Pharmaceutical Research, 2016, doi:10.1007/s11095-016-1991-4.

5. Lim SH, **Li H**, Pan J, Chiu NCG，Chui WK, Kang L. Introduction to pharmacy education in Singapore. Herald of Medicine, 2016, 35(2), 111-114. (In Chinese)

6. **Li H**, Bao H, Bok KX, Lee C-Y, Li B, Zin MT and Kang L. Durable antimicrobial coatings by quaternary ammonium silane copolymers with low toxicity. Biomaterials Science, 2016, 4(2), 299-309.

7. **Li H**, Low Y, Chong H, Zin MT, Lee C-Y, Li B, Leolukman M, Kang L. Microneedle-mediated delivery of copper peptide through skin. Pharmaceutical Research, 2015, 32(8), 2678-2689.

8. Nguyen D-V, Li F, **Li H**, Wong BS, Low CY, Liu X-Y, and Kang L. Drug permeation through skin is inversely correlated with carrier gel rigidity. Molecular Pharmaceutics. 2015, 12(2), 444-452. (**Co-first author**)

9. Kwan YH, Tung YK, Kochhar JS, **Li H**, Poh AL, Kang L. Sep 2014. Handbook of Cosmeceutical Excipients. Woodhead Publishing. **(Book)**

10. **Li H**, Yu Y, Dana SF, Li B, Li CY, Kang L. Novel engineered systems for oral, mucosal and transdermal drug delivery. Journal of Drug Targeting. 2013, 21(7): 611-629.

List of Patent

1. Antimicrobial Coating. Singapore filing date: 19 Apr 2016. Filing No.: 10201603107P.

List of Awards

1. Best Graduate Researcher Award (NUS), 2015

2. Excellent Safety Lead (Nomination), 2015

3. Innovation and Entrepreneurship Practicum Grant (SGD 10,000) by NUS under National Research Foundation's University Innovation Fund (UIF), 2014

4. EDB-IPP Scholarship, 2012- 2016

List of Tables

List of Figures

List of Abbreviations

AFM	Atomic force microscopy
AIBN	2,2'-Azobis(2-methylpropionitrile)
AMP	Antimicrobial protein
ANOVA	Analysis of variance
ATR	Attenuated total reflectance
BMP2	Bone morphogenetic protein 2
C. albicans	*Candida albicans*
CFL1	Cofilin 1
CFU	Colony forming unit
$Cu(OAc)_2$	Copper acetate
$CuCl_2$	Copper chloride
DMA	5-(N, N-dimethyl)-amiloride
DMA-C_{16}Br	[2-(methacryloyloxy)ethyl]dimethylhexadecylammonium bromide
DMEM	Dulbecco's modified Eagle's medium
DMSO	Dimethyl sulfoxide
DPRA	Direct peptide reactivity assay

DTPAC	Dimethyloctadecyl [3-(trimethoxysilyl)propyl] ammonium chloride
E. coli	*Escherichia coli*
ECVAM	European Center for the Validation of Alternative Methods
EDS	Energy dispersive X-ray spectrometer
ELISA	Enzyme-linked immunosorbent assay
FBS	Fetal bovine serum
FDA	Food and Drug Administration
FE-SEM	Field emission scanning electron microscopy
FOSL1	Human Fos-related antigen 1
FTIR	Fourier transform infrared
GHK	glycyl-L-histidyl-L-lysyl peptide
GHK-Cu	glycyl-L-histidyl-L-lysyl copper complex
GMPT	Guinea pig maximisation test
HaCaT	Human adult low calcium high temperature keratinocytes
HCl	hydrochloride
HDF	Human dermal fibroblasts
HEK293	Human embryonic kidney 293

HPLC	High performance liquid chromatography
HSP27	Heat shock protein 27
HSPA1A	Heat shock 70kDa protein 1A
IL-1α	Interleukin 1 alpha
IL-8	Interleukin 8
IUD	Intrauterine device
LC-MS	Liquid chromatography–mass spectrometry
LCP	Liquid crystal polymers
LLNA	Local lymph node assay
MAPTAC	[3-(methacryloylamino)propyl]trimethyl ammonium chloride
MBC	Minimum bactericidal concentration
MFC	Minimum fungicidal concentration
MIC	Minimum inhibitory concentration
MN	Microneedle
mRNA	Messenger ribonucleic acid
MSS	Microchannel Skin System
MTT	3-(4,5-dimethylthiazol-2-yl)-2,5-diphenyl tetrazolium bromide

PBS	Phosphate buffered saline
PCR	Polymerase chain reaction
QAC	Quaternary ammonium compound
QAS	Quaternary ammonium silane
S. aureus	*Staphylococcus aureus*
SOD1	Superoxide dismutase 1
TGA	Thermogravimetric analysis
TMSPMA	3-trimethylsilylpropyl methacrylate

Chapter 1 Background

1.1. Transdermal drug delivery

As the largest organ of the human body, skin provides a painless and compliant interface for systemic drug administration, which is referred to as transdermal drug delivery. Transdermal drug delivery has several advantages, including the bypassing of first-pass metabolism, avoidance of gastrointestinal side effects, possibility of extended therapy, ease of termination when needed, painless and friendly pediatric applications (1). Since the first transdermal patch was approved for use in 1979, there are 21 transdermal delivery systems approved by US Food and Drug Administration (FDA) (2).

However, the skin itself by nature, is to protect the human body from environment. Therefore, the molecules that passively diffuse though skin are quite limited. As a general rule, only hydrophobic drugs with a molecular weight less than 500 Da are able to passively diffuse through the skin (1).

1.2. Human skin structure and the barrier for cutaneous absorption

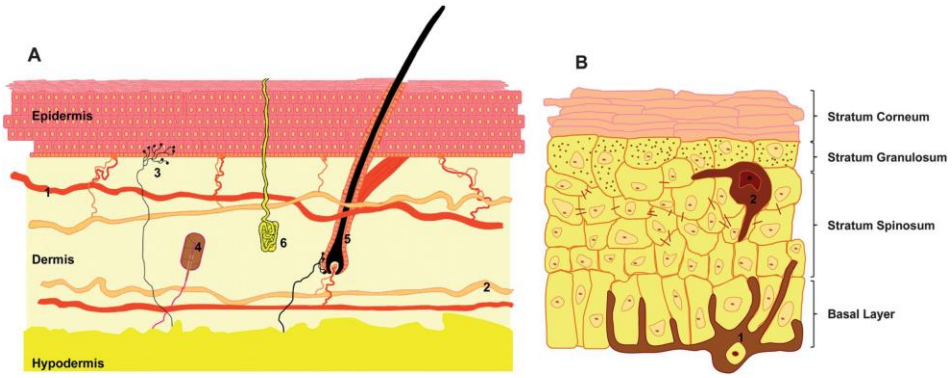

Figure 1.1 (A) Skin layers: hypodermis, dermis (containing blood vessels (1), lymph vessels (2), nerve endings (3), sense receptors (4), hair follicles (5), sebaceous glands and sweat glands (6)) and epidermis. (B) Layers of the epidermis: basal layer, *stratum spinosum*, *stratum granulosum* and the *stratum corneum*. The cells found in this layer of skin are keratinocytes with different levels of differentiation, Langerhans cells (1) and melanocytes (2). Adapted from (3).

Human skin comprises three basic layers, epidermis, dermis and the subcutaneous fat (**Figure 1.1A**). The stratified, avascular epidermis consists of five layers, *stratum corneum*, *stratum lucidum* (found in thick skin), *stratum granulosum*, *stratum spinosum* and *stratum basale* (**Figure 1.1B**). The five layers of epidermis have different morphology and varying levels of keratinocyte differentiation. *Stratum basale* contains the mitotically active keratinocytes. The cells of this layer divide and migrate upwards towards the outer layers. *Stratum corneum*, also known as horny layer, the outermost layer of epidermis, is the final stage of differentiation. It is made up of 10 to 30 continuous thin layers of highly keratinized dead cells (corneocytes) surrounding by tightly packed intercellular lipid multi-lamellae (4). The *stratum corneum* structure was described as 'brick and mortar' model, where the corneocytes represents the 'bricks' and the intercellular lipid bilayers represents the 'mortar' (5). The mechanically stiff structure presents a strong barrier to protect skin from infection, body water loss, chemicals and mechanical stress.

On the other hand, due to the existence of the *stratum corneum* barrier, most cosmetic and pharmacological agents are unable to be absorbed by the skin. Thus the number of cosmetic and drug candidates that can be successfully delivered through skin route is limited (6).

Drug absorption across skin can be subdivided into transappendageal pathway and transepidermal pathway. As sweat glands and follicles constitute only 0.1% of total skin area, drug absorption by the transappendageal pathway is limited (7). Transepidermal pathway can be further subcategorized into transcellular and intercellular routes. For transcellular routes, the drug molecules have to partition into hydrophilic corneocyte domain and diffuse across hydrophobic intercellular lipid lamellae, which is highly challenging for most molecules. Therefore, intercellular pathway is supposed to be the main route of drug absorption through *stratum corneum*, although this route is tortuous and

relatively small in surface area (8-10). As a general rule, only hydrophobic molecules with a molecular weight less than 500 Da are able to passively diffuse through the skin (1).

1.3. Enhancement of skin permeation

The highly impermeable nature of skin extensively limits cosmetics and drugs to be delivered via skin route. Hence, great efforts have been made to increase the permeability of the *stratum corneum* chemically or physically.

Conventional strategy to increase skin permeation for drug absorption involves the use of chemical enhancers. Chemical enhancers act by enhancing drug solubility in formulation, increasing partition in *stratum corneum*, or disrupting the intercelullar *stratum corneum* (11). The chemicals identified to increase the skin permeability include alcohols, dimethyl sulfoxide, sulfactants, amines, amides, azones, fatty acids and terpenes (8). Ideally, chemical enhancers should be nontoxic, nonirritant and nonallergenic and the skin barriers function should recover immediately after their removal. Unfortunately, many of these chemical enhancers have skin irritation issue (1). Meanwhile, this method is only applicable to the enhancement of small molecules and the amount of drug permeated though skin is limited (1).

Physical enhancers thus are developed as alternatives to disrupt the *stratum corneum* for the delivery of large molecules. These include iontophoresis, ultrasound, electroporation, thermal ablation, and microneedles. They have different mechanisms to increase the skin permeability and are currently in various clinical trials and FDA approval process for transdermal delivery of macromolecules and vaccines, including insulin, parathyroid hormone and influenza vaccine (12).

Iontophoresis acts by applying a small electric current to the skin ($< 500\ \mu A/cm^2$) for charged particles to diffuse across it. FDA has approved iontophoresis transdermal patch

of lidocaine hydrochloride and epinepherine bitartrate for dermal analgesia, fentanyl for on-demand systemic delivery, sumatriptan for the treatment of migraine (2). Iontophoresis was reported not suitable for the transdermal transport of molecules larger than 7000 Da (13). However, with the combination of chemical enhancers, liposomes systems or microneedles, iontophoresis was able to deliver larger molecules, such as insulin and bovine serum albumin (14, 15). It was regarded as one drawback of iontophoresis that the current penetrates mostly via the skin appendages. Thus the current in the hair follicle may be high enough to cause damage although the overall current per unit area was low (3).

Different from iontophoresis, electrophoresis utilizes a high voltage (≥ 100 V) for short duration (10 μs to 100 ms) thereby creating transient hydrophilic pores across skin. These pores allow the transport of a large range of molecules through skin, including small molecules, proteins and oligonucleotides (16). Although the electric field of electroporation is located at the *stratum corneum*, it may also affect the deeper tissues to cause pain (3). It was reported that only small region of skin would be affected, but more research should be done on the safety issue of the device.

Sonophoresis applies ultrasound in a continuous or pulsed mode to the skin surface after a topical formulation was applied. High-frequency sonophoresis (f > 1 MHz, noncavitational ultrasound) has been used since 1950s for topical drug delivery (17). Skin permeability enhancement of noncavitational ultrasound was usually limited to small, lipophilic molecules. Using more aggressive noncavitational ultrasound is limited since it will damage deeper tissue (1). Low-frequency sonophoresis (f < 100 kHz, cavitational ultrasound) was later found to be more effective in enhancing the transdermal drug delivery by disturbing the lipid packing in the *stratum corneum* via cavitation (17). Low-frequency sonophoresis was reported to be able to facilitate the transdermal delivery of hydrophilic drugs and high molecular weight drugs, including peptides, proteins, vaccines,

oligonucleotides, even nanoparticles and liposomes (18). One problem associated with ultrasound is miniaturizing the complicated system for home use and high cost of fabrication.

Thermal ablation applies localized heat for a short period of time to create micro-scale hydrophilic pores across the *stratum corneum* (19). The heat can be induced by various energy sources, such as radiofrequency (20), electrical heating elements (19) and lasers (21). *In vivo* study on animals demonstrated that human growth hormone and interferon alpha-2B can be delivered by skin with thermal ablation treatment (22, 23). The design of thermal ablation devices should precisely control the temperature (above 100 °C), duration (millisecond time scale or shorter), and localization of thermal energy applied to the skin, otherwise deeper skin tissue may get damaged.

Although the above mentioned physical enhancers have shown great promise for transdermal delivery of hydrophilic and large molecules, all of them require electrical power with sophisticated fabrication, which may render a high set-up and maintenance cost. They are also relatively large although efforts have been made to reduce their size. Furthermore, special training may be required to use such devices. The search for inexpensive and efficient transdermal drug delivery with convenient and safe properties leads to the development of microneedles.

1.4. Advantages of microneedles for drug delivery

Microneedles, an array of micron scale needles, are thought to be the hybrid of convenient and safe transdermal patches and efficient hypodermic injections. The idea of low-cost microneedles was first proposed in the 1970s (24), but microneedles were only made suitable for pharmaceutical application until the 1990s when microfabrication tools emerged (25). With the advancement in microfabrication, it is possible to fabricate

microneedles with various shapes, lengths and needle to needle spacing (26). They can be made long enough to breach the *stratum corneum* to increase the skin permeation, but short enough to avoid stimulating the nerves and blood vessels in the underlying dermis.

The advantages of microneedles can be

(1) Enhancement of the delivery of a large range of molecules, including hydrophilic drugs, peptides and proteins, to exert either topical effect or systemic effect (27-29);
(2) Targeted vaccine delivery to antigen-presenting cells (e.g., Langerhans cells and dermal dendritic cells) in skin, and possible self-administration of vaccines (30);
(3) Painless drug administration and increased patient compliance;
(4) No fear of needles to the patient;
(5) Avoidance of the risk of infection due to needle re-use with the use of dissolving microneedles;
(6) Faster healing of skin than that with hypodermic needles (31, 32);
(7) Avoidance of first-pass metabolism;
(8) Ease of termination of treatment by removing the microneedle patch;
(9) Dose reduction because of the enhanced drug delivery efficacy;
(10) Choice of complex release patterns (bolus/sustained) (33).

1.5. Materials of microneedles

Microneedles have been fabricated with various materials, such as silicon, glass, metals (stainless steel, titanium) and all kinds of polymers (34). Silicon and glass used to be attractive options to fabricate microneedles since they are common materials in the microelectronics industry and have good adaptability to many fabrication procedures. However, silicon and glass are expensive and silicon is not a FDA approved material (35). Furthermore, the production of silicon and glass microneedles is sophisticated and

relatively fragile (36). Compared with polymer microneedles, metallic microneedles are also less attractive, because of their high cost and the difficulties with mass production (37). Besides, silicon, glass and metals are non-biodegradable and thus safety issues arise when breakage in the skin happens. Polymeric microneedles overcome the limitations of silicon, glass and metal microneedles. They provide advantages like low cost, improved resistance to shear-induced breakage due to their viscoelastic property, and safety in case of accidental breakage in the skin tissue (37).

Various biocompatible polymers have been used to produce microneedles. Natural polymers and sugars, such as thermoplastic starch (38, 39), carboxymethylcellulose (33), amylopectin (33), dextran (40), maltose (41, 42) and galactose (43) have been studied for microneedle fabrication. Microneedles made from carbohydrates provided rapid drug delivery due to their rapid dissolving nature in the skin. Dextrin was used to fabricate microneedles without any special equipment (33). However, they have processing issues such as caramelization and difficulties in handling of molten sugar. Besides, sugar microneedles tend to be hygroscopic, which would be a problem for storage (43). A high Young's modulus of the material is required to ensure sufficient mechanical strength of the microneedles fabricated (44).

A lot of studies demonstrated the fabrication of microneedles from synthetic polymers, such as polyvinyl acetate (45), carbomer (45), polyetherimide (46), polycarbonate (29), polyethylene glycol (47), polylactide-co-glycolic acid (48), polyvinylpyrrolidone (49), and poly(methylvinylether maleic anhydride) (50). Kochhar *et al.* reported a single-step photolithographical method to fabricate polyethylene glycol microneedles by exposing macromer poly(ethylene glycol) diacrylate solution to UV light through a patterned photomask for a few seconds. Drug can be premixed with the macromer solution and encapsulated into both the microneedles and the backing layer, which acted as reservoir for

sustained release (47). Bovine serum albumin was also successfully incorporated into the microneedles without compromising the structures of the protein (51). A polycarbonate hollow microneedle array was integrated into a device with a drug reservoir and springs for self-application of drug. Animal studies demonstrated that the device can be used to effectively deliver small molecules and proteins (29). Dissolving microneedles loaded with insulin were prepared from poly(methylvinylether maleic anhydride) solution using laser-engineered molds (50). Dissolving polyvinylpyrrolidone microneedles for influenza vaccination was fabricated by photopolymerization of the monomer N-vinylpyrrolidone solution mixed with the lyophilized vaccine in a microneedle mold. Fast dissolution of microneedles was observed when inserted into pig skin. *In vivo* study demonstrated that this microneedle vaccine patch achieved more efficient lung virus clearance and better immune responses than intramuscular vaccination (49). Needle-free vaccination can be useful in case of outbreak of a pandemic. It may also prevent the potential risk from hypodermic needles reuse in third world countries. To get these products commercialized, however, they must be efficient and cost-effective (52).

1.6. Modes of drug delivery by microneedles

Generally, there are four modes of transdermal drug delivery by microneedles dependent on the design of microneedles (**Figure 1.2**).

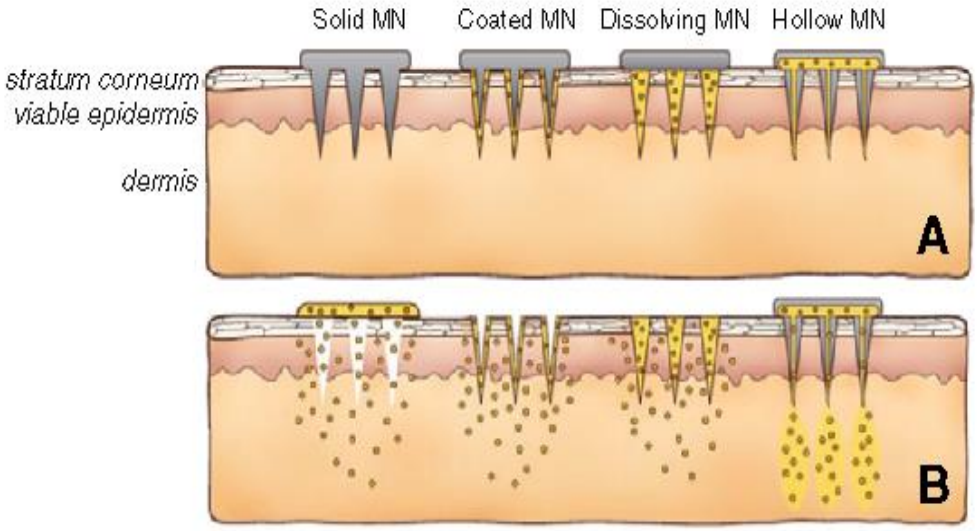

Figure 1.2 Methods of drug delivery to the skin using microneedles (MN). Adapted from (53).

(1) Solid microneedles can be used as pretreatment of skin before application of topical formulations, which is also called "poke and patch" approach (54). Once the microneedles were removed from the skin, a drug-loaded patch or a semi-solid topical formulation (e.g., cream, gel, lotion, or ointment) was applied to the treated area. Then the drug can diffuse into the skin through the formed micro-sized channels. This two-step administration approach is technically simple. We do not have to consider whether or not the fabrication process of microneedles will compromise the drug stability. Current available topical formulations may be directly used for this approach, so reformulation of the drug may not be needed (55). The first microneedle paper on drug delivery adopted this approach for *in vitro* delivery of a model molecule, calcein, and the skin permeability increased by up to four orders (25). This approach has been studied for sustained delivery of drugs. However, the dosing of drug delivery into skin is not precise. Only part of drug in the formulation can be delivered.

(2) Solid microneedles can also be coated with drug-loaded water-soluble formulations. After insertion into skin, the coating can dissolve from the microneedles into the skin, and then the microneedles can be removed. This approach is referred as "coat and poke" (54). This approach is attractive for a rapid bolus delivery of drug into skin. The coating process can be conducted at ambient conditions and the solid state of coated drug is more suitable for long-term storage even at room temperature (56). A large range of compounds have been coated on microneedles, including molecules with small molecular weight, proteins, vaccines, DNA and microparticles (27, 56-58). For this approach, an efficient coating procedure and a suitable coating formulation are required (59). Since the limited available area of microneedles tips, the quantities of drugs that can be coated are low. Thick coating can increase the coating amount, but the sharpness of microneedles may get compromised, thus the microneedle penetration ability is affected (55). Therefore, this approach is more suitable for very potent drugs, such as vaccines (57, 58).

(3) Dissolving microneedles are made of biodegradable or water-soluble polymers/sugars with drugs encapsulated inside. Microneedles get degraded/dissolved inside skin and the drugs get released (33). This approach is also called "poke and release". Since the needles disappear eventually, no bio-hazardous waste is left after use (49). The release rate of drug is dependent on the dissolving rate of the polymer. Sullivan *et al.* developed an influenza vaccine microneedle patch out of vinylpyrrolidone monomer, the microneedles dissolved within minutes (49). Lee *et al.* showed that bolus delivery was achieved by encapsulating drug inside microneedles only, while sustained release over hours to days was possible by incorporating drug in the backing of microneedles (33). Polylactide-co-glycolide microneedles were shown to provide controlled release of encapsulated drug in skin for hours to months (48). Because of the elasticity of skin,

microneedles usually cannot be fully inserted into skin. So to ensure an accurate dose of drug delivered into skin, it is desirable to load drug in the tips of microneedles only. Two-layered dissolving microneedles were developed to encapsulate sumatriptan in the microneedles tips (60). Chu *et al.* located drug at the microneedle tips by introducing a bubble at the base of microneedles and prevented drug diffuse to the backing layer of microneedles (61). Polymer particle-based micromolding was possible to locate compounds in different regions of the microneedles (62). However, microneedle fabrication process often involves the use of UV irradiation, elevated temperature or organic solvents, which could impair the stability of fragile compounds, such as proteins and DNA (33, 48, 61). Similar to coated microneedles, the amount of drug that can be encapsulated inside the microneedles is also limited. Besides, high loading of drug might compromise the strength of microneedles.

For certain polymeric microneedles with drug incorporated inside, the drug can be released from the microneedles after microneedles are inserted into skin. However, the microneedles do not completely dissolve over time (63). This is another scenario of "poke and release". Hybrid microneedles have also adopted "poke and release" approach to delivery drug into skin, e.g., solid silicon microneedles with biodegradable tips (64) or stainless steel electrode pillar with water dissolvable tips (65).

(4) Hollow microneedles can be used to deliver liquid formulations into skin through the needle bore actively or passively. This approach is also known as "poke and flow". Similar to hypodermic injection, hollow microneedles can be used together with a driven force such as pressure, thus allow faster rates of delivery. This is an important advantage over solid microneedles (53, 55, 66). Hollow microneedles are commonly used with a syringe to inject liquid solutions into skin. A reservoir filled with drug solution can be attached to hollow microneedles thus allow a higher amount of

injection (67, 68). Rates of delivery can be modulated by a syringe (68), pressurized gas (69), a syringe pump (70), a spring (29), and a micropump (71, 72). Furthermore, a lab-on-a-chip system can be integrated with hollow microneedles to deliver the drug into skin in a controlled way (73). Moreover, hollow microneedles require not only the control of microneedle insertion process but also the fluid infusion into skin (53). Experimental data and numerical simulations showed that although geometry of microneedle tips largely controlled pressure drop for fluid infusion through the microneedles, the pressure were much less than those required for injection into skin. It indicated that the primary resistance to fluid flow was associated with infusion into the skin and not through the microneedles (74). It was reported that the fluid flow rate into skin was optimized by inserting partially retracting microneedles after insertion, infusing at high pressure, using microneedles with a beveled tip, and adding hyaluronidase to the infusion solution. Hyaluronidase was used to reduce resistance in the skin during microneedle insertion by rapidly breaking down hyaluronan within skin collagen fibers. Seven fold increase of flow rate was observed with addition of hyaluronidase (69).

Current existing injectable formulations can be used directly in hollow microneedles. However, this loses the advantage of solid microneedle delivery methods to deliver dry-state drug formulations without reconstitution to improve drug stability and the patient convenience of a patch-based delivery method (53). Besides, hollow microneedles have the risk of clogging at tip opening. The hollow nature impairs the strength of microneedles. Thus fabrication of microneedles from polymers is restricted by the mechanical weakness of polymers and the simplicity of the micromolding process (37, 75).

The comparison of different drug delivery modes by microneedles are further summarized in **Table 1.1**. Although there are different microneedle designs and drug delivery strategies developed, each of them has advantages as well as disadvantages. For a given application, it is necessary to find the best microneedle design and drug delivery approach from these options. Poke and patch approach is the simplest design for microneedle-assisted delivery, since microneedles only need to be designed for biomechanical function (53). Most of the currently approved microneedle products are drug-free microneedles for cosmetic and other purposes. They can be adapted for drug delivery purpose by using poke and patch approach, which will be the focus of my thesis.

Table 1.1 Advantages and disadvantages of different drug delivery modes by microneedles.

Drug delivery mode	Advantages	Disadvantages
Poke and patch	No or limited reformulation needed Technically simple No pump or encapsulation/coating process required Sustained release Combination with other delivery methods, such as iontophoresis	Two-step administration step No precise dosing
Coat and poke	Needle strength is retained after coating No patch or pump required Precise dosing	An efficient coating procedure needed Reformulation of drug needed Small dose Reduction of needle sharpness/ penetration ability
Poke and release	No patch or pump required Precise dosing No sharp waste	Reformulation of drug needed Small dose Impaired needle strength
Poke and flow	Adjustable rate of drug delivery Delivery of high volumes Integration into lab-on-a-chip systems possible Precise dosing	Risk of clogging Impaired needle strength More complex device

1.7. Current issues with the use of microneedles

Since the microneedle-based drug delivery paper was first published in 1998, there has been an exponential increase of research in this area (53). Most of these papers focus on fabrication technology of microneedles and application of microneedles in drug and vaccine delivery. However, there are still a lot of unsettled issues.

1.7.1. Microneedle application method and skin models used to study the microneedle-assisted system

To achieve painless application, microneedles were usually fabricated in a range of 50 μm to 1000 μm in length. Because of the elasticity of skin, the depth of microneedle penetration into skin is less than the needle length itself. Certain force or speed are needed for successful penetration (76). A number of studies have been done on the effect of microneedle geometries, force of insertion, velocity of insertion and density of microneedles arrays on drug delivery (77-80). Oh *et al.* reported that microneedles with a longer length and more needles per array had a better enhancement in calcein delivery (77). However, Verbaan *et al.* found that increasing the number of microneedles per array did not result in a significant increase of drug transport (78), while Wu *et al.* found that beyond a certain number of microneedles there was only little increase in flux, as the relative reduction in skin resistance for diffusing molecules after each additional microneedle piercing was decreased (79). In another study, Yan *et al.* observed that with a same force (44.5 N) applied on microneedle array, further increase of needle length beyond 600 μm did not show a significant increase in drug flux. In addition, lower needle density arrays were more effective in enhancing drug flux (80). This may be explained by another paper that there was an increase in percentage penetration with an increase in needle spacing, which indicated that the increase of needle numbers per array doesn't necessarily increase the pores created by microneedles (81). Regarding the application method of microneedles,

Verbaan *et al*. reported that piercing was not successful for microneedles with a length of 300 μm, while it was possible with microneedle lengths of 550 μm and longer with manual application (82). In a further study, it was found that with the use of an electrically driven applicator, the piercing was more effective than manual application. A higher velocity resulted in a higher transport rate (78).

These studies were conducted to explore the effect of microneedle application methods, microneedle length and needle density on drug delivery because it was supposed that the inherent factors that would influence drug delivery were depth of penetration and numbers of penetration after microneedle treatment. However, the inherent factors, the depth of penetration and numbers of penetration were not quantified directly in these studies, which may partly explain the above contradicting results. Therefore, it is important to directly quantify the depth of penetration and numbers of penetration and relate with the performance of microneedle-mediated delivery system. For a given microneedle array, it is necessary to study the effects of application method and application force on drug transport, to ensure consistent delivery of drug.

Besides, different kinds of skin models were used in the above *in vitro* studies, ranging from animal skins, human dermatomed skin and human epidermis (77-82). The skin model chosen may also affect the performance of a microneedle system. For passive diffusion through skin, it was found that the thickness and components of the *stratum corneum* was important to compare the different skin models. For microneedle-assisted drug delivery, the *stratum corneum* is breached by microneedles. The permeation rate-limiting step may transfer from the *stratum corneum* to the viable layers. However, limited studies have been done to compare different skin models for microneedle-based drug delivery.

1.7.2. Formulation of drugs to be delivered

When comparing different approaches of microneedles, it was usually mentioned that one advantage for "poke and patch" approach is no or limited need of reformulation (55). However, the passages created by microneedles altered the permeation properties of skin, i.e., drug can now penetrate skin in a much faster mass transfer rate than normal diffusion through the intact skin. This fundamental difference may potentially change the principles of dosage form design, which traditionally is based on the understanding that drugs diffuse through the tortuous fissures inside *stratum corneum.* However, there are only limited studies to show the effect of formulation on drug delivery with microneedle assistance currently. The charge of a drug can affect its permeation through skin. Banks *et al.* evaluated the effect of drug ionization on skin permeation of naltrexone, and its active metabolite, naltrexol, through microneedle-treated and untreated guinea pig skin by comparing different pH values of aqueous formulation. Naltrexol in its poorly soluble unionized form (at pH 8.5) showed only limited flux enhancement after microneedle-treatment. However, in the highly-soluble charged state (at pH 4.5), naltrexol not only permeated across untreated skin much faster, but also showed a greater flux improvement post microneedle-treatment (83). Besides, it was also reported that the effect of co-solvents/excipients on the percutaneous transport rates through microneedle-treated skin in a fashion different from that of intact skin (84). Due to the low diffusional resistance of microneedle treated skin, the skin permeation rate-limiting step may shift from skin to drug delivery systems (84). Thus, even for "poke and press" approach, it is equally important to study the formulation (including drug format, pH, solvent, concentration, and excipient) to be delivered to optimize the microneedle-assisted delivery system.

1.7.3. Safety issue related with microneedle application

Microneedles may cause mild, transient skin irritation. The length of microneedles was found to be closely related with skin irritation. Microneedles with 400 μm length induced greater erythema and blood flow than microneedles with 200 μm length (85). Similar mild erythema was also found with other solid microneedles. They usually disappear within hours (85, 86). These studies showed that microneedles generally are safe to use. However, one should keep in mind that when microneedles were associated with the formulation to be delivered, enhanced delivery of drug and excipients might also raise safety issues, for example, causing irritation to skin. So for a given microneedle-mediated drug delivery system, it is important to evaluate whether the enhanced delivery of drugs/excipients would cause any toxicity to human body.

Besides, it is also important to consider whether the pathway created by microneedles in the skin might be sites for infection. An *in vitro* study was conducted to assess the ability of microorganisms to traverse microneedle-induced holes. It was found that microneedle puncture resulted in significantly less microbial penetration than that induced by hypodermic needle puncture and that no microorganisms crossed the viable epidermis in microneedle-punctured skin (87). In another study, the risk of bacterial infection associated with microneedle treatment was found no greater than that with a hypodermic injection (88). Furthermore, studies in animals and humans generally demonstrated no infection associated with the microneedle use. However, these studies were conducted on healthy subjects and the microneedle application sites were usually cleansed before application of sterile microneedles. Therefore, the infection risk of microneedle application is unknown in immune-compromised patients (89). Besides, microorganisms were shown to adhere to microneedles after its application (87). Different from hypodermic injections, microneedles are prone to be designed for self-administration at home. As such, reuse of

microneedles is quite possible and inappropriate reuse of microneedles will increase the risk of infection.

1.8. Hypotheses

From above review, it was found that there are still a number of issues that limit the widespread use of microneedles in pharmaceutical and cosmetic fields, although increasing studies have been carried out on microneedles for transdermal drug delivery in recent years. My thesis will target at these issues related with microneedle mediated drug delivery systems with 3M™ Microchannel Skin System (MSS) used as the model microneedles. 3M MSS comprises a microneedle array and a reusable handle, which is illustrated in **Figure 1.3**. The plastic microneedle array is injection molded from liquid crystal polymers (LCP) and comprises of a rectangular grid of needles (13 by 27 per array, or 351 needles) centered on an oval array. The microneedles have square pyramidal shape with a needle height of about 700 μm and a tip-to-tip needle spacing of 500μm.

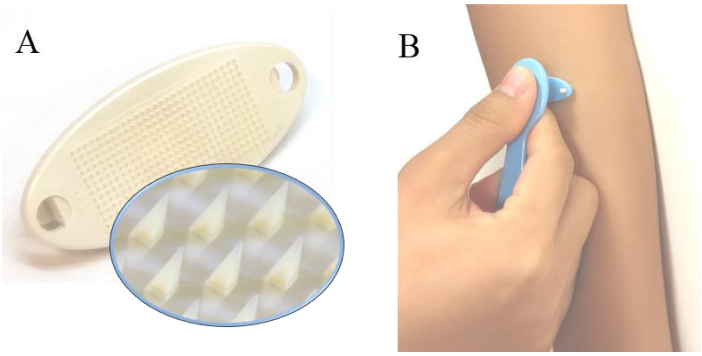

Figure 1.3 (A) 3M™ MSS microneedle array and the individual needles. (B) Illustration of microneedle application with an applicator.

Here are the hypotheses for the studies in the thesis:

- The efficacy and safety of MN mediated transdermal drug delivery systems can be influenced by MN application methods and drug formulation used.

- Antimicrobial property of microneedles can be achieved by an antimicrobial coating to reduce the potential risk of infection related with the use of microneedles.
- An adhesive and solvent free lidocaine HCl patch with low drug loading can achieve effective and fast anesthetic effect with microneedle pretreatment.

1.9. Specific aims and objectives

The specific aims and objectives of the studies are outlined below to prove the hypotheses:

1. To study the influence of microneedle application force on drug delivery efficacy by influencing the depth and numbers of passages created.
2. To investigate the difference of various skin models used in *in vitro* skin permeation study.
3. To study the skin irritancy potential of enhanced delivery of drug (copper peptide).
4. To develop antimicrobial microneedles to reduce the infection risk related with the use of microneedles.
5. To study the influence of formulation factors, such as drug format and dosage form on microneedle-mediated delivery.
6. To fabricate an adhesive-free lidocaine patch, specifically for microneedle mediated drug delivery system.

To address these specific aims and objectives, the thesis is presented in five parts as discussed below. For each part, an individual introduction part would be included to clarify the specific background and purpose of study.

In **Chapter 2**, we investigated the transdermal delivery of a tripeptide complex, glycyl-L-histidyl-L-lysyl copper complex (GHK-Cu, copper peptide) with the assistance of microneedles. GHK-Cu is a widely used cosmetic ingredient, but has the issues of limited skin absorption and fast degradation inside skin. In this chapter, we investigated the

influence of microneedle application force on the characteristics of transport pathway created and the performance of skin permeation of copper peptide. We also investigated the difference of skin models used in microneedle-assisted transdermal drug delivery. The three skin models, i.e., human dermatomed skin, human epidermis and rat skin are commonly used in conventional transdermal drug delivery. The work was intended to provide insight on which skin model is suitable for assessing a microneedle assisted delivery system.

In **Chapter 2**, it was demonstrated that the microneedles can enhance the delivery of copper peptide and make the delivery of copper supplement possible by skin route. However, the enhanced delivery of copper may present issues of skin toxicity. Thus, **Chapter 3**, we further investigated the skin toxicity potential of copper peptide (GHK-Cu) and compared it with two other copper compounds, copper chloride ($CuCl_2$) and copper acetate ($Cu(OAc)_2$) using an *in vitro* skin irritation test by using multiple biomarkers. Based on the mechanism of skin irritation, we examined and proposed a paradigm to assess the skin irritation potential of copper compounds using cytotoxicity assay, gene and protein expression levels of cytokines and other newer biomarkers. To our knowledge, this is a first study evaluating the irritancy of different types of copper compounds at the cellular, genomic and proteomic levels using keratinocyte cell line. This approach may also be useful to assess the irritancy potential of other similar inorganic compounds or minerals through the skin, which is potentially a valuable tool in the cosmetological, dermatological and pharmaceutical fields.

In **Chapter 4**, we fabricated novel quaternary ammonium silane (QAS) based antimicrobial copolymers with low toxicity which can form effective and durable coating. Subsequently in **Chapter 5**, one of the synthesized QAS copolymer, PDT-10%, was used to coat microneedles to confer the microneedles with an antimicrobial property to reduce

the potential infection issue associated with microneedle usage. The biocompatibility of the coating was investigated as well.

In **Chapter 6**, we hypothesized that microneedles would create an alternative pathway for drug permeation though skin and it should have a preference of drug molecules different from conventional passive percutaneous drug delivery. The percutaneous delivery of lidocaine and lidocaine hydrochloride (HCl) was compared with microneedle pretreatment. Furthermore, the drugs were fabricated into an adhesive and solvent free patch, named "dry patch" by spraying coating with limited excipients incorporated inside. The efficacy of the resulted dry patch together with microneedle pretreatment was investigated by both *in vitro* skin permeation study and *in vivo* pig study.

Chapter 2 Microneedle-mediated delivery of copper peptide through skin

(Adapted from Pharmaceutical Research. 2015, 32(8):2678-2689)

2.1. Introduction

Glycyl-L-histidyl-L-lysyl (GHK) is a naturally occurring carrier tripeptide with high affinity for copper ions (**Figure 2.1**). GHK was first isolated from human plasma by Dr L. Pickart because of its activity to prolong survival of normal liver cells (90). Subsequently, researchers found that GHK-Cu can stimulate the synthesis of extracellular matrix macromolecules, such as collagen and glycosaminoglycan (91-93). It can activate the production of metalloproteinases and anti-proteases that remove damaged proteins from the extracellular matrix macromolecules (94). GHK-Cu was also found to increase decrorin expression and decrease TGF-beta expression, which is beneficial for a scar-free healing (95, 96). The increased expression of p63 of keratinocytes by both GHK-Cu and GHK suggests that GHK and its copper complex can promote the survival of basal stem cells in skin (97, 98). These contribute to the wound-healing and skin remodeling effects of GHK-Cu (91, 99-103). The biochemical action of GHK and GHK-Cu on skin cells were summarized in **Table 1.1**. Recent genomic studies revealed that GHK can directly modulate the expression of a large number of human genes and reverse gene expression to a healthier state, which may explain the diversity of its biological actions (104-106). Furthermore, *in vivo* studies showed that GHK-Cu can improve hair growth, skin regeneration and wound healing (99).

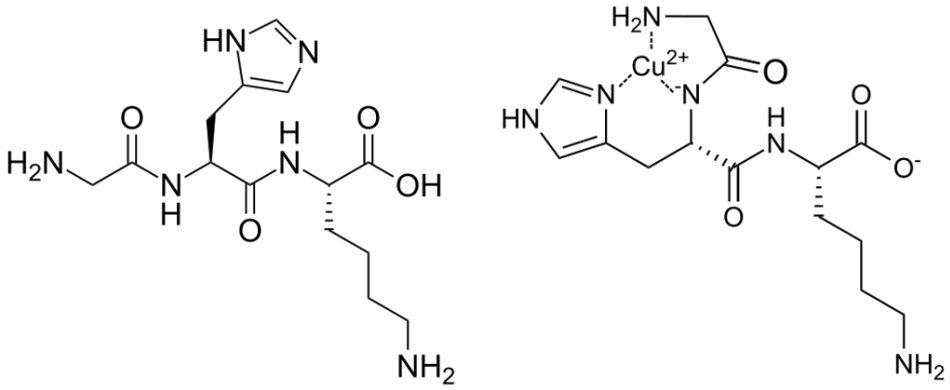

Figure 2.1 Chemical structures of GHK peptide and its copper complex.

Table 2.1 Biological effect of GHK-Cu on skin cells.

Factor studied	**Cells**	**Effective or tested concentration**	**Result**	**Note**	**Ref**
Collagen	Fibroblasts from human foreskins	10^{-12} M to 10^{-8} M	Increased procollagen synthesis at mRNA level with a maximal stimulation at 10^{-9} M	1. The stimulation is independent of any change in cell number and viability. 2. The effect was reproduced by GHK alone but not by copper ions	(91)
1. Cell growth 2. Collagen	Human dermal fibroblast cell line, HS68	10^{-12} M	1. Increased cell viability 2. Increased type-1 collagen expression at mRNA level but not at protein level 3. Combination of red LED light and GHK-Cu treatment increased cell viability 12.5 fold, beta-FGF 2.3 fold, and also collagen production	Cultured in Low-serum-contained medium	(107)
MMP-2, TIMP-1, TIMP-2	Fibroblasts from rat dermis	10^{-10} M to 10^{-8} M	1. Increased proMMP-2 expression at both protein mRNA level with a maximal stimulation at 10^{-9} M 2. Increase TIMP-1 and TIMP-2 expression	1. Cultured in Low-serum-contained medium 2. This effect of MMP-2 regulation was reproduced by copper ions but not by GHK alone	(94)

1. Cell growth 2. bFGF and VEGF	Human dermal fibroblasts (normal and irradiated)	10^{-9} M	1. Enhanced cell growth of both cell types 2. Increase the expression of bFGF and VEGF in irradiated human dermal fibroblasts	Serum free culture	(108)
Glycosaminoglycan	Human dermal fibroblasts	10^{-9} M to 10^{-7} M	1.Increased expression of Glycosaminaoglycan with a maximal stimulation at 10^{-8} M 2. Preferential accumulation of heparin sulphate in the cell layer and dermatan sulphate in the culture medium.		
Decorin	Rat dermal fibroblasts	10^{-9} M	Increased decorin expression at both mRNA and protein level.	1. Cultured in Low-serum-contained medium 2. Decorins functions by regulating assembly of collagen fibrils, preventing scar formation and decreasing the level of TGF-beta, which is known to increase scarring.	(95)
TGF-beta	Normal and keloid-producing dermal fibroblasts	10^{-9} M	Decreased TGF-beta expression in both cells.	1.Serum free culture 2. Possibility of decreasing excessive scar formation.	(96)
1. cell growth 2. integrins 3. p63 4. PCNA	Human keratinocytes and skin equivalent models	1–100µM in monolayer culture 1µM in skin equivalent culture	1. Stimulatory effect on keratinocyte growth 2. Increased expression integrin alpha6, integrin beta1, PCNA and p63.	P63 is putative stem cell marker of the skin, so it suggests that GHK-Cu promotes the survival of basal stem cells in the skin.	(97)
1. cell growth 2. integrins 3. p63 4. PCNA	Human keratinocytes and skin equivalent models	1–100µM GHK in monolayer culture and 1µM GHK in skin equivalent culture	1. Stimulatory effect on keratinocyte growth 2. Increased expression integrin alpha6, integrin beta1, PCNA and p63.	Copper-free GHK showed similar effects with copper-GHK.	(97)

Minerals are essential for human health and mineral supplementation is recommended to complement dietary intake. Supplementation of minerals via oral route is the most common way. However, oral mineral absorption is affected by many factors including interactions with other dietary components in the gastrointestinal tract (109). Gastrointestinal side effects have also been reported with oral ingestion of some minerals, such as copper and iron. In addition, oral liquid forms of iron supplementation may cause teeth stains (110). To this end, transdermal delivery of minerals may be a useful alternative but remains largely unexplored. Copper as an essential trace element plays a critical role in diverse biological processes, such as haemoglobin synthesis and the stimulation of skin biomarkers including collagen and elastin (111). Copper also has an important role in the activation of key enzymes specific to tissue repair and in the cross-linking and maturation of collagen in healing wounds (110). Because of the gastrointestinal irritation that oral intake of copper can cause, transdermal delivery of copper can act as a good alternative, although skin absorption of charged ions is very low (112, 113). It was found that when GHK is coupled with copper, the peptide blocks the redox activity of copper, hence permitting the delivery of copper in a non-toxic form that can be subsequently utilized by the cells (97, 114).

Although its biological actions start at picomole level, far higher dosages have been used in clinical trials, since the GHK-Cu uptake levels are very low through skin. On the other hand, if GHK-Cu is injected intradermally, GHK is rapidly cleared (95% clearance in 1 min). The fragility and rapid breakdown of GHK is the major obstacle for clinical and cosmetic applications (115). In clinical trials involving GHK-Cu, large variations were observed and its efficacy towards the healing of indolent human wounds or skin ulcers were not found (99, 116, 117). To address the concerns, a variety of chemical modification to GHK has been carried out to produce breakdown-resistant copper complexes, e.g., replacement of histidine residue with either a synthetic amino acid, L-spinacine, or L-

1,2,3,4-tetrahydro-isoquinoline-3-carboxylic acid, but none were found better than GHK-Cu (115).

The low uptake of GHK-Cu by skin is a common problem associated with many other peptides and molecules. This is because skin itself in nature is to protect human body from environment. So the molecules that can be delivered though skin are quite limited. As a general rule, only hydrophobic molecules with a molecular weight less than 500 Da are able to passively diffuse through the skin (1). GHK-Cu with a log P of -4.5 can represent hydrophilic peptides that have difficulty in penetrating into skin (11). Because of the diverse biological effects of GHK-Cu, along with its potential as a source of copper supplementation, it is of interest to find out a method to enhance its skin absorption.

As an alternative, we propose the use of microneedles, a minimally invasive but effective skin permeation enhancement method, to facilitate the effective and sustained delivery of GHK-Cu through skin. If an effective skin uptake of GHK-Cu is possible in a sustained manner with microneedle pretreatment, GHK-Cu is expected to better fulfil its biological effects.

Microneedles with length in micron range can enhance skin permeability with no pain by breaching the *stratum corneum* layer of skin with self-administration (35). It has been shown that microneedles are associated with a lower risk of microbial infection than hypodermal needles (87). There are different methods of drug delivery to skin with microneedles, and microneedle pretreatment followed by a topical formulation have the advantages of possible extended release (53). Studies have shown that pretreatment of skin with microneedles can enhance delivery of topically applied formulations (28, 118), including peptides (119).

In this study, we investigate the effectiveness of a commercial microneedle product, 3M MSS, in enhancing the skin permeability of copper peptide, using both rat and human skin models. Since MSS is hand-applied by using an applicator, the effect of different thumb forces was studied. In addition, we also carried out cell and animal testing to verify its safety.

2.2. Materials and methods

2.2.1. Materials

GHK-Cu and GHK were purchased from McBiotec, Nanjing, China. The ratio of GHK to Cu is 2:1 (manufacturer data). Copper standard solution (1 g/L), and trypan blue solution (0.4%) were purchased from Sigma-Aldrich, Singapore. Concentrated nitric acid (69% w/w) was purchased from VWR International S.A.S, Singapore. Rhodamine B was purchased from Alfa Aesar (Lancaster, UK). Phosphate buffered saline (PBS) (pH 7.4, 10×) was obtained from Vivantis, Malaysia. PDMS (Sylgard® 184 Silicone Elastomer Kit) was purchased from Dow Corning (Midlan, MI, USA). Solvable™, an aqueous based tissue solubilizer, was purchased from PerkinElmer (Watham, MA, USA). Pierce® BCA protein assay kit was purchased from Thermo Scientific (Rockford, IL, USA). 3-(4,5-dimethylthiazol-2-yl)-2,5-diphenyl tetrazolium bromide (MTT) and dimethyl sulfoxide (DMSO) were purchased from MP Biomedicals, Singapore. Dulbecco's modified Eagle's medium (DMEM) and fetal bovine serum (FBS) were purchased from Life Technology, Singapore. Penicillin streptomycin solution was purchased from PAN-Biotech GmbH, Germany. All chemicals were used as supplied.

2.2.2. Skin and microneedle application

Human dermatomed skin (referred as human skin) was obtained from Science Care (Phoenix, AZ, USA). The skin tissues were excised from the thighs of Caucasian female cadaver, who died at the age of 92. Human epidermis was separated from the human dermatomed skin after the skin was immersed in 60°C water bath for 1 min.

Besides human skin, rat skin was also chosen for the *in vitro* skin permeation and penetration study. Skin of rodents, including rats, is the most commonly used in *vitro* percutaneous permeation studies because of its availability (120). Rat abdominal skins were obtained from National University of Singapore Comparative Medicine through the tissue sharing program. The hair on rat skin was removed by an electrical shaver followed by hair removal cream (Veet^{TM}) application and removal after 2 min. Subcutaneous fat and connective tissues were also trimmed off (121).

A 6 mm thick PDMS substrate was used to support the skin for microneedle application as reported (81). The skin was spread over the PDMS substrate mounted on a Styrofoam board with epidermis side up. A microneedle array was then put on the skin sample. Four different forces were applied through an applicator at 4.5 N, 10.0 N, 13.3 N and 22.2 N for 10 seconds, respectively, using a force gauge (HF-10, JISC, Japan).

The use of animal skin was approved by the National University of Singapore Institutional Animal Care and Use Committee. The use of human skin was approved by the National University of Singapore Institutional Review Board.

2.2.3. Depth of microneedle penetration measurement

Microneedles were first primed with oxygen plasma in a plasma cleaner (Harrick Plasma, US) for 3 min to render them hydrophilic. The arrays were then flood-coated with 70 µl of

0.1% w/w rhodamine B solution and dried at 35 °C for 1 h. The rhodamine B coated arrays were then applied with a force of 4.5 N, 10.0 N, 13.3 N and 22.2 N for 10 seconds respectively on rat and human dermatomed skin samples. The depth of penetration was measured indirectly by recording the distance from the tip of the microneedles to the boundary where the rhodamine B coating was wiped off after skin insertion (28). To analyze the penetration depth of the microneedles, the microneedles were imaged using a stereoscopic microscope (Nikon SMZ25, Japan). The depth of penetration for each array was then determined by measuring 35 out of the total 351 microneedles per array. Three arrays were tested for each force.

Confocal laser scanning microscopy was used to visualize the micro-conduits created in rat skin placed on a piece of glass slide. The scanning started from the *stratum corneum* side, through the z-axis of the microscope (A1R+si, Nikon, Japan) at 10× magnification. The excitation wavelength was 562 nm and fluorescence emission was at 570-620 nm for rhodamine B.

2.2.4. Histological examination

Histological examination of rat skin was carried out by cutting the microneedle treated skin samples into 10 μm sections using a Microcryostat (Leica, Germany). The histological sections were stained with hematoxylin and eosin and imaged using a microscope (Olympus, Japan).

2.2.5. Field emission scanning electron microscopy (FE-SEM)

After human dermatomed skin and human epidermis were treated with microneedles, the skins were immediately immersed in 2.5% glutaraldehyde (Sigma-Aldrich, Singapore) solution overnight, followed by ethanol dehydration and vacuum drying. Then the skin

sample was attached to a SEM stub by a carbon tape (NEM tape, Nisshin EM. Co. Ltd.), and platinum sputter-coated using a JFC-1600 autofine coater (JeOL, Japan) at a current of 10 mA for 80 s. The images of the skin were then taken using a JSM-6700F field emission scanning electron microscope (JEOL, Japan).

2.2.6. Percentage of penetration measurement

The percentage of penetration was tested using trypan blue coated microneedles. Microneedle arrays were first treated with oxygen plasma for 3 min, flood-coated with 70 µl of trypan blue solution and then dried at 35 °C for 1 h. After application of a microneedle array with the specified force on skin, the skin was cleansed with water. Application sites were then imaged by using the stereoscopic microscope. The visible insertions were counted and the percentage of penetration (the number of stained dots divided by the total number of array microneedles) was calculated. At least 3 replicates were performed at each force.

2.2.7. *In vitro* skin permeation study

Vertical Franz diffusion cells with an effective exposed area of 1 cm^2 were used. The pretreated skin samples were mounted onto Franz diffusion cells with epidermis facing up. The intact skin was used as control. The donor cell contained 2 ml of 5.8 mM $(GHK)_2Cu$ (the molar ratio of GHK to Cu in the raw material was 2 to 1) solution while the receptor cell contained 4.8 ml of 1× PBS. The cells were placed inside a chamber with temperature controlled at 32 °C (comparable to the physiological temperature of the skin surface). Magnetic stirrers in the receptor cells stirred at a speed of 100 rpm. The receptor solutions were withdrawn at pre-set time intervals and replaced with fresh ones. The receptor solutions were subjected to the measurement of copper permeated through the skin by atomic absorption spectroscopy (AAS) and the measurement of peptide permeated by high

performance liquid chromatography (HPLC). At completion, the skin surface was washed by rinsing the donor and receptor compartments with 1 ml water 3 times respectively. The skin was then removed from the diffusion cells, dried with Kimwipes and collected into Falcon tubes for the measurement of copper retained in skin by AAS (122). Three replicates were conducted for each group.

2.2.8. AAS method

Copper concentrations were determined by using an atomic absorption spectrometer (PinAAcle 900T, PerkinElmer) with acetylene flow rate of 2.5 L/min and compressed air flow rate of 10 L/min. The instrument was calibrated with Cu working standards (1.57 - 62.95 µM) made from Cu stock standard solution (1 g/L) with 2% nitric acid as diluent. Diluted permeation samples collected from receptor solutions were then aspirated into the air/acetylene flame where Cu atoms absorb light of 324.75 nm. All readings of standards and samples were conducted with the instrument in the absorbance mode. To digest skin tissues prior to analysis, concentrated nitric acid was used as previous studies have shown that it quantitatively releases trace elements from biological tissues (123). Nitric acid of 2.5 ml was added to each of the Falcon tubes containing skin samples and heated at 80 °C using a thermostatic water bath until complete digestion of the skin samples (123). After that, they were topped up to 10 ml using deionized water and filtered using 0.22 µm polytetrafluoroethylene membrane. The filtered solution was used for the measurement of copper retained in skin.

2.2.9. HPLC method

The amount of GHK permeated was determined by using Hitachi L2000 LaChrome Elite HPLC system with Agilent Bio SCX NP3 column (50 mm x 4.6 mm, 3 µm). The mobile phase consisted of Mobile A (Millipore water) and Mobile B (10 mM NaH_2PO_4 with 0.5

M NaCl) with a gradient elution program with a mixture of solvents A and B as follows: 0% B for 1 min, 1 – 100% B for 1 – 5 min, 100% B for 5- 8 min, 100 – 0% B for 8 – 8.1 min, and 0% B for 8.1- 11 min. The flow rate was set at 0.5 ml/min. The injection volume was 20 µl for each sampling and ultraviolet detection was performed at a wavelength of 218 nm. A calibration curve was conducted using GHK standard solution from 1.18 µM to 587.58 µM.

2.2.10. Skin total protein determination

Skin samples were put into a 2 ml tube with 1.5 ml Solvable™ added. Then the tube was heated at 60 °C for 4 hours to allow the completely dissolution of skin. The total protein level of skin was determined by using a Pierce BCA protein assay kit after the skin digestion solution was diluted appropriately with water.

2.2.11. Cytotoxicity assay of GHK-Cu on skin cells

The cytotoxicity of different concentrations of GHK-Cu against human adult low calcium high temperature (HaCaT) keratinocytes and human dermal fibroblasts (HDF) were studied by MTT assay in 6 replicates. Briefly, 5,000 cells in 200 µl culture medium (DMEM supplemented with 10% FBS and 1% penicillin-streptomycin solution) per well were seeded into 96-well plates and incubated for 24h. The culture medium was then removed. Subsequently, 180 µl fresh culture medium and 20 µl of GHK-Cu samples (0.058 - 58000 µM $(GHK)_2Cu$ in PBS) were added per well and incubated for 24 , 48 and 72 hours, respectively. For control group, 180 µl fresh culture medium and 20 µl of PBS were added. At the respective analysis point, the medium was removed. The wells are washed with 200 µl PBS and replenished with 200 µl fresh medium per well. Twenty µl MTT solution (5 mg/ml in PBS) was added to each well, after which the plates were incubated for an additional 4 h. The supernatant was then removed and formazan crystals were solubilized

in 150 µl DMSO. Absorbance was recorded at 595 nm with a microplate reader (Tecan, Switzerland). Wells containing DMSO alone were used as the blank. Percentage of cell viability was expressed as $(A_{sample} - A_{DMSO})/ (A_{control} - A_{DMSO}) \times 100\%$.

2.2.12. *In vivo* irritation test on pigs

Young adult swine (Yorkshire X), ranging from 10 to 40 kg were used for the study. The animals were first sedated with ketamine (10 mg/kg) and then anesthetized with isoflurane gas. Atropine was administered to reduce salivary, tracheobronchial, and pharyngeal secretions. The ham area of pigs was shaved with an electrical shaver followed by a disposable shaver. The microneedles were applied on the skin with a hand force of around 20 N (estimated by using the force gauge) for 10 s. Then the skin was observed for irritation and imaged with time. In another testing, immediately after microneedle treatment, the application site was covered by gauze saturated with GHK-Cu solution, then fixed with plaster. After 8 hours, the gauze was removed and the skin was imaged. The studies were repeated on 3 to 4 pigs. The pigs were later recovered. The procedure for animal testing was approved by the National University of Singapore Institutional Animal Care and Use Committee.

2.2.13. Statistical analysis

All results were presented as mean ± standard deviation. Statistical analysis was performed by one-way analysis of variance (ANOVA) followed by Tukey *post hoc* test using IBM SPSS Statistics 19. A probability value of $p < 0.05$ was considered statistically significant.

2.3. Results

2.3.1. Depth of microneedle penetration

In **Figure 2.2A**, the yellow line indicated the distance from the tip of the microneedles to the boundary where the rhodamine B coating has been wiped off after skin insertion. The value of the distance was taken as depth of penetration of microneedles. **Figure 2.2B** showed the direct measurement of the depth of penetration using confocal laser scanning microscopy by measuring the depth of the microneedle fluorescence pattern inside the skin. The depth of penetration associated with an application force of 13.3 N on rat skin was measured to be 130 μm with direct measurement and 146 μm using indirect measurement. It was found that the results obtained from indirect depth of penetration measurement method had no difference from those obtained by direct measurement method ($p > 0.05$). Hence, the indirect method was used for this study for its convenience. Furthermore, **Figure 2.2C** further ascertained the presence of microscale passages created by microneedles inside the rat skin. **Figure 2.2D** showed that the depth of penetration of microneedles increased linearly with application force both on rat ($r^2 = 0.9977$) and human ($r^2 = 0.9758$) skin samples in the tested force range from 4.5 N to 22.2 N. At 22.2 N, the depth of penetration on human skin is significantly higher than that on rat skin.

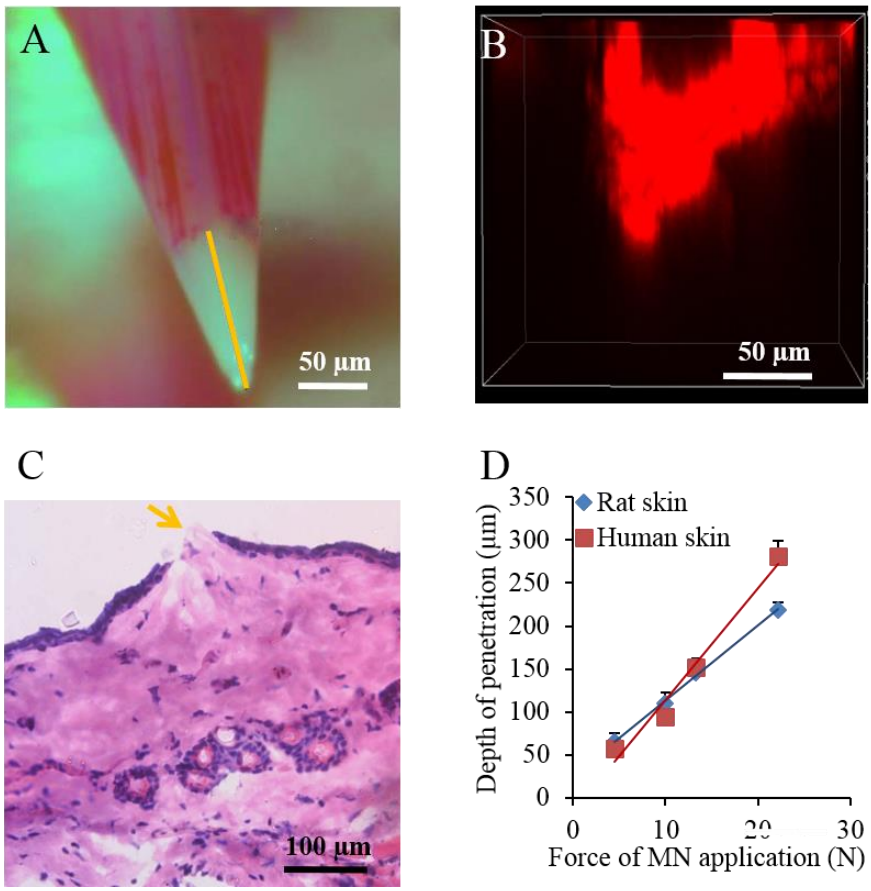

Figure 2.2 Depth of microneedle penetration measurement. (A) Indirect measurement of depth of penetration using rhodamine B-coated microneedles. The yellow line shows the depth of penetration. (B) Confocal image showing the fluorescent pattern of a single microchannel after microneedle application. (C) Histological section of rat skin stained with hematoxylin and eosin after microneedle application. The yellow arrow shows the breach of epidermis. (D) Depth of penetration against force of microneedle (MN) application.

2.3.2. Percentage of penetration

The percentage of microneedle penetration in rat skin was measured using trypan blue coated microneedles. **Figure 2.3A** and **B** shows the representative image of rat skin, human dermatomed skin after application of trypan blue-coated microneedles at 22.2 N, respectively. The blue dots that remained on the skin indicated the successful penetration of microneedles into skin. The number of the blue dots was used to calculate the percentage of penetration per microneedle array. **Figure 2.3C** showed that a higher force of

microneedle application resulted in a higher percentage of penetration. The increase in force of microneedle application on rat skin resulted in a sharper increase in the percentage of penetration as compared to that on human dermatomed skin. The highest force of 22.2 N made the percentage of penetration to be almost 100% on rat skin and 30% on human dermatomed skin.

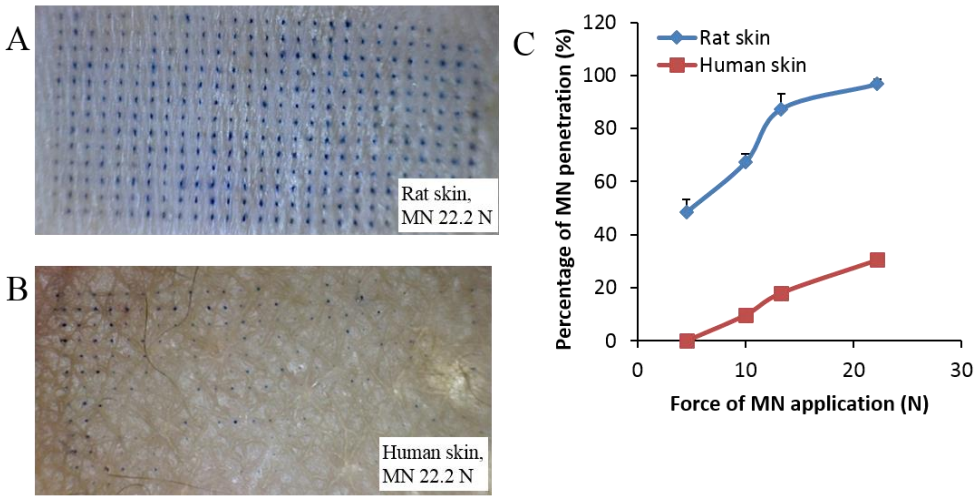

Figure 2.3 Percentage of penetration. Representative images of 22.2 N MN application force on rat skin (A) and human dermatomed skin (B). (C) Percentage of penetration against force.

2.3.3. *In vitro* skin permeation study

To assess the enhancing effects of the microneedles for GHK-Cu to permeate through skin at different forces of application, we performed *in vitro* drug permeation study. Upon topical administration, the copper ions are subjected to dynamic ligand exchange inside skin (122). Therefore, quantitative assessment of skin penetration of GHK-Cu is challenging. Hence, we analyzed the permeation of copper and GHK separately by using AAS and HPLC. **Figure 2.4A** and **B** showed that the amounts of copper and peptide permeated through rat skin were significantly increased after microneedle pretreatment. **Figure 2.4C** and **D** showed that for non-treated human dermatomed skin, there was no peptide detected in the receptor solution, while only trace amount of copper was detected,

which may be from the skin itself (data not shown). With the microneedle pretreatment, copper and peptide were detected in the receptor solution. However, substantial high amounts of copper and peptide were detected only when a high force (22.2 N) was used.

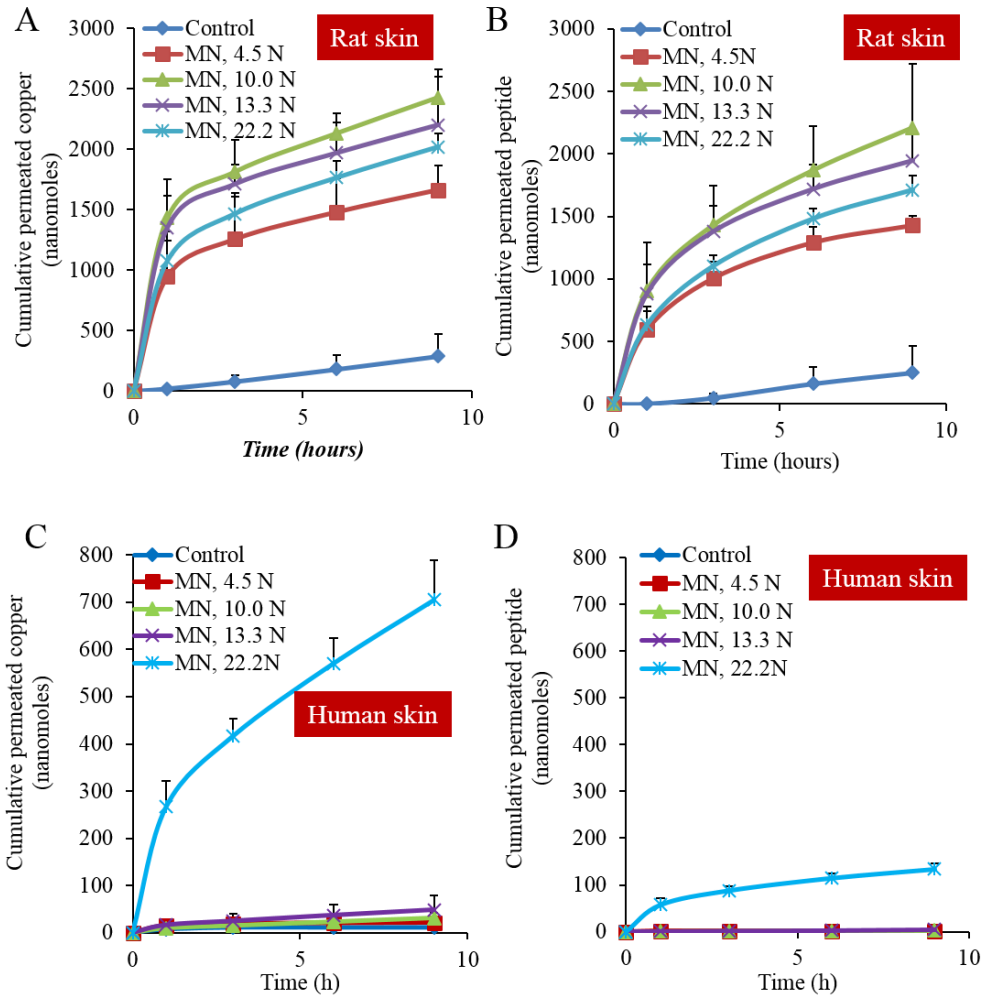

Figure 2.4 *In vitro* skin permeation study. The cumulative amount of copper (A) and peptide (B) permeated through rat skin pretreated with varying application forces. The cumulative amounts of copper (C) and peptide (D) permeated through human dermatomed skin pretreated with varying application forces.

Figure 2.5 showed that there was no significant difference in the amount of copper retained in skins after 9 hours' permeation study among the microneedle pretreated skin and the control at various forces. However, significant difference was found between rat and human skin.

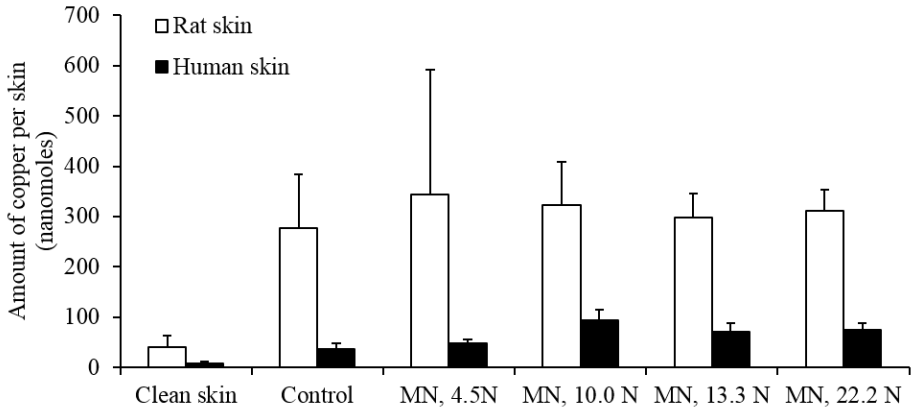

Figure 2.5 Cumulative amount of copper retained in skin after 9 h permeation study. The 'Clean skin' refers to the skin that was not used in permeation study.

2.3.4. Cytotoxicity assay of GHK-Cu on cells

Figure 2.6 showed that $(GHK)_2Cu$ was not toxic to either HaCaT keratinocytes or HDF cells in the range of 0.0058 – 5800 µM. Besides, GHK-Cu at 5800 µM showed certain stimulatory effect on HDF proliferation. Other research groups have also shown that GHK-Cu can stimulate the growth of dermal fibroblasts (107, 108).

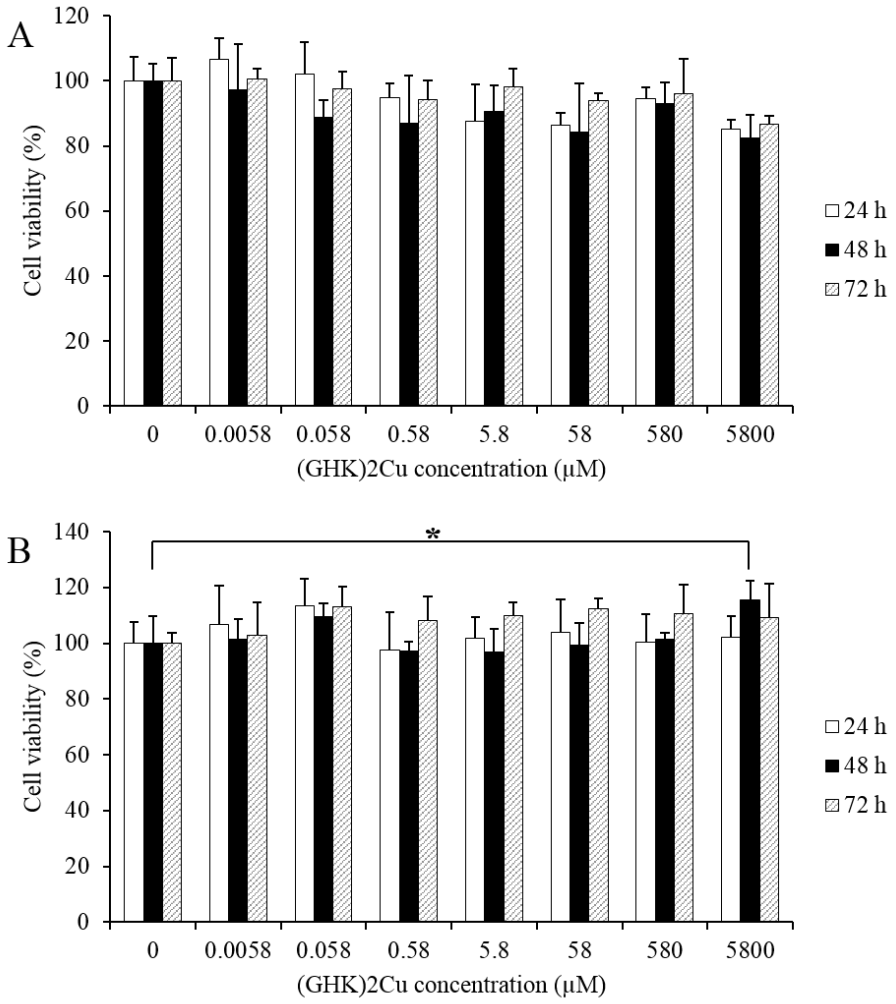

Figure 2.6 Cytotoxicity study. Viability of HaCaT keratinocytes (A) and HDF (B) after incubation with $(GHK)_2Cu$ for 24, 48 and 72 h.

2.3.5. *In vivo* irritation test on pig skin

For blank microneedles, minimal erythema was observed immediately after removal of microneedles. Mild erythema was observed at 5 minutes but almost not visible after 25 minutes (**Figure 2.7A**). For GHK-Cu application immediately after microneedle pretreatment, no erythema or edema was observed for 8 h (**Figure 2.7B)**.

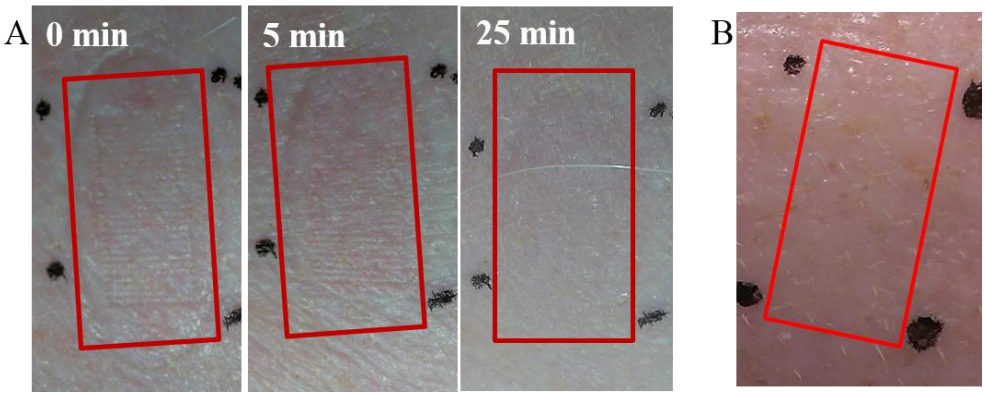

Figure 2.7 Representative images of *in vivo* irritation test on pig skin. (A) The skin conditions after microneedle application. (B) The condition of microneedle pre-treated skin, followed by application of 5.8 mM copper peptide for 8 h. The black marker dot and the marked rectangle area indicated the microneedle treated area.

2.3.6. Test on human epidermis

Apart from full skin and human dermatomed skin, human epidermis was also tested. From the SEM images of microneedle treated skin in **Figure 2.8**, we observed more and larger holes in human epidermis other than human dermatomed skin with the same microneedle force used. The epidermis was penetrated through and the carbon tape on the stub was observed as shown in the zoom in figure of single penetration in **Figure 2.8B**.

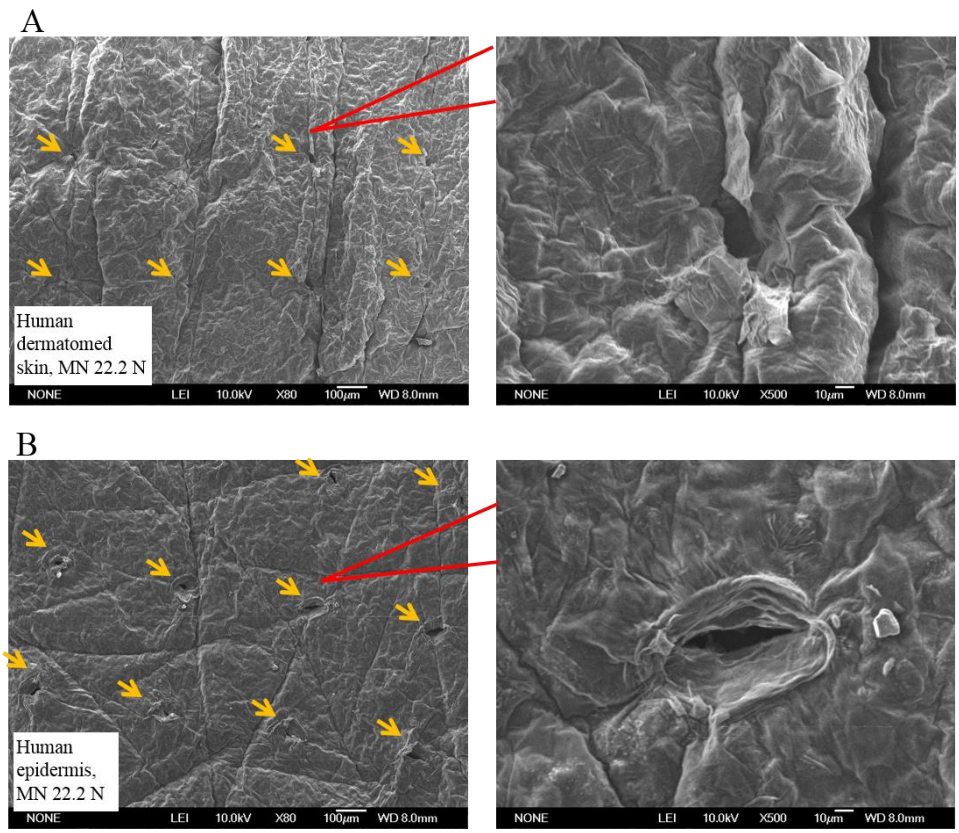

Figure 2.8 SEM images of skin after microneedle treatment with application force of 22.2 N. The yellow arrows indicate the breach of the skin surface by the microneedles. (A) Human dermatomed skin. (B) Human epidermis.

Skin penetration test with trypan blue coated microneedles and *in vitro* permeation study were also conducted on human epidermis.

As shown in **Figure 2.9A and B**, the increase in force of microneedle application on human epidermis resulted a sharper increase in the percentage of penetration as compared to human dermatomed skin. The percentage of penetration on human epidermis approached 100% at forces of 13.3 N and 22.2 N.

As shown in **Figure 2.9C and D**, the permeation behaviour of GHK-Cu across intact epidermis was quite similar with that across intact human dermatomed skin as shown in Figure 3C and 3D. It indicated that epidermis is the main barrier for GHK-Cu to be delivered through intact skin. Different from the result of dermatomed skin, even with a

mild force of microneedle application (4.5 N), there is a sharp increase in the GHK-Cu permeating through the human epidermis. When the epidermis was treated with a higher force, 13.3 N and 22.2 N, leakage of the donor solution was observed during the permeation experiment preparation despite repeating the experiment for three to four times, which made it impossible to continue the permeation study. This phenomenon could be explained by the differences in the percentage of penetration between human dermatomed skin and human epidermis. A microneedle application force of 13.3 N and 22.2 N resulted in close to 100% penetration of microneedles on the epidermis, while the proportion of microneedles that penetrated the dermatomed skin were around 18% and 30% respectively. Furthermore, **Figure 2.8** showed that large holes were observed in human epidermis than that in human dermatomed skin at the same microneedle application force and the epidermis were penetrated through at force of 22.2 N. Due to the presences of many holes created in the epidermis within a small area treated by the microneedles of high forces, coupled with the already thin epidermal layer, the treated epidermis was unable to contain the weight of the donor solution. The loss of structural integrity of the microneedle treated epidermis could have resulted in the leakage of the donor solution into the receptor compartment when preparing for the permeation study.

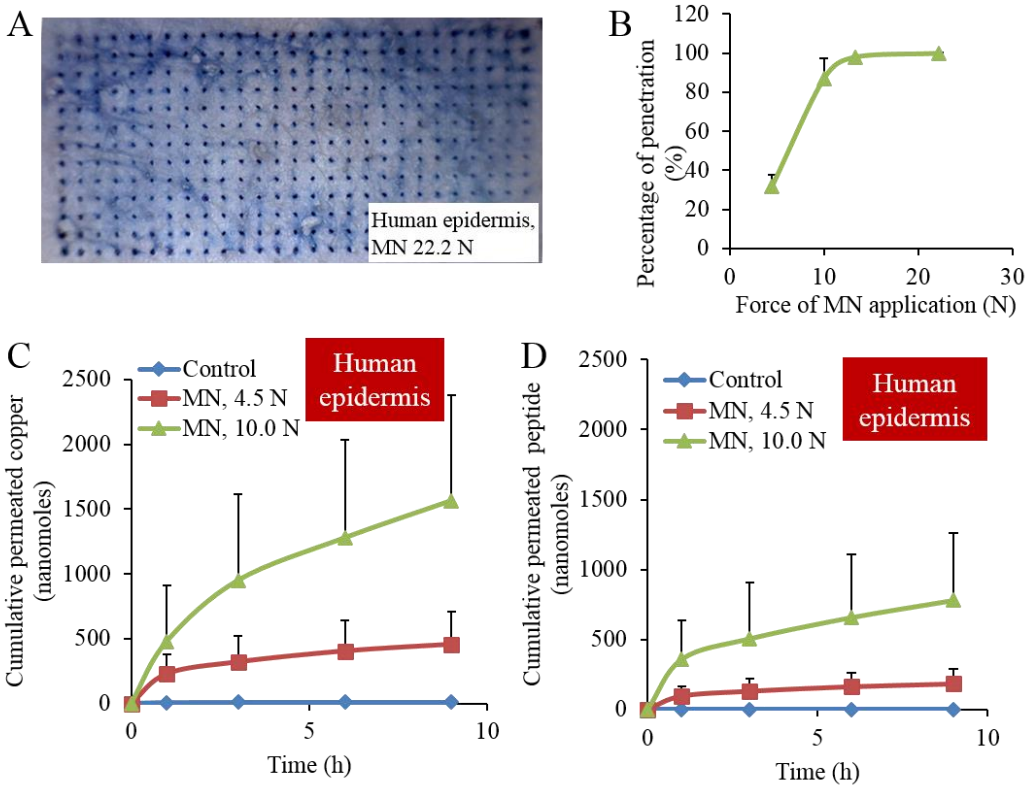

Figure 2.9 Microneedle penetration and permeation test on human epidermis. (A) Representative images of 22.2 N MN application force on human epidermis. (B) Percentage of penetration against force of MN application on human epidermis. (C) and (D) were cumulative amount of copper and peptide permeated through human epidermis treated with varying application force of microneedles, respectively.

2.3.7. The effect of different donor concentration on skin permeation

Besides the of 5.8 mM $(GHK)_2Cu$ solution used in the donor compartment, a higher concentration of $(GHK)_2Cu$ solution, 29.0 mM was also tried in the donor compartment to differentiate the donor concentration effect. The data was shown in **Figure 2.10**. When test was done on intact human dermatomed skin, no permeation of GHK-Cu was observed even when donor GHK-Cu concentration was as high as 29.0 mM. With the pretreatment of microneedles on human dermatomed skin, significantly higher skin permeation of GHK-Cu was observed with the use of a higher concentration of GHK-Cu solution.

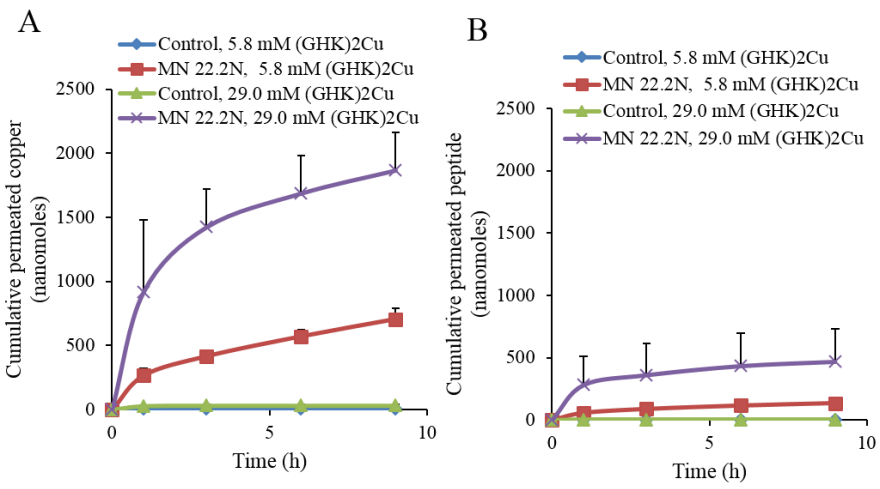

Figure 2.10 *In vitro* permeation study of GHK-Cu solution with different concentrations on human skin. (A) and (B) are cumulative amount of copper and peptide permeated respectively.

2.3.8. The effect of complexation on GHK delivery

The permeation study was conducted with 11.6 mM GHK solution in the donor compartment as well, with the result shown in **Figure 2.11**. GHK-Cu permeation through intact skin was not observed, while significantly high amount of GHK-Cu permeated the skin with microneedle pretreatment. On the other hand, microneedle pretreatment did not show much influence on the skin delivery of GHK.

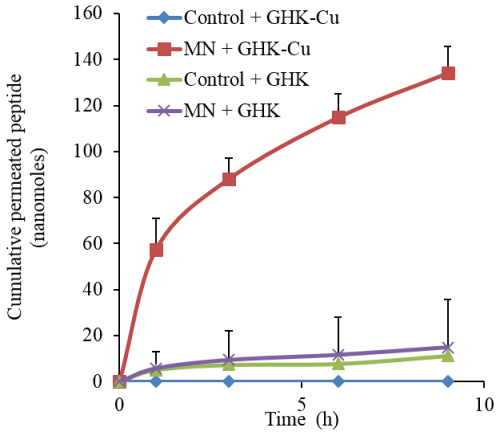

Figure 2.11 Cumulative permeated peptide through human dermatomed skin in i*n vitro* permeation study when either GHK-Cu or GHK solution was used in the donor solution.

2.4. Discussion

Microneedles can painlessly enhance the skin permeation of a wide range of therapeutic compounds which can barely penetrate human skin (53). It has been reported that the microneedle application force and velocity can influence its enhancing effect (77-80). In this study we evaluated the skin permeation of topical GHK-Cu *in vitro* using a microneedle array from 3M Company. The 3M MSS is designed for manual application with a plastic applicator. The thumb forces tested were: 4.5 N (low), 10 N (medium), 13.3 N (medium) and 22.2 N (high).

To study the depth of needle penetration, two approaches have been used. One is the direct measurement of the microchannels inside skin by confocal laser scanning microscopy and the other is the indirect measurement. In the indirect measurement, the depth of penetration was obtained by measuring the length of needle tip where rhodamine B dye was wiped off (28). But the coating rhodamine B onto the microneedles was complicated. To simplify the microneedle coating procedure, we treated the microneedles with oxygen plasma, which was found to be very effective for rhodamine B coating.

The linear relationship between depth of penetration and microneedle application force indicates that these two factors are strongly correlated. However, we cannot assume that the linearity will be the same when the force is out of the range (< 4.5 N or > 22.2 N)(124). The force range would be from 13 to 63 mN/needle in our study if converted to force per needle. Some of these forces are even lower than the insertion forces of reported microneedles. For example, Park *et al.* reports measured microneedle insertion force of 37 mN with a tip 20 μm in diameter (125). It indicated that our microneedle array has a high efficiency for skin insertion.

To study the percentage of penetration, trypan blue coated microneedles were used. Trypan blue is known to specifically stain the sites of the *stratum corneum* perforation (47). A common procedure is to treat the skin first with microneedles, and then transfer trypan blue solution on the treated area for targeted staining (47, 78). However, we found that wrinkles and hair follicles can also be easily stained. Besides, trypan blue solution has limited contact with skin surfaces to ensure staining of all the microchannels because of the hydrophobic nature of skin surfaces. To solve this problem, we coated trypan blue directly onto the microneedles and then conducted the penetration test on skin. The false staining on the skin surface was then wiped off with water. With the new method, we can easily get clear staining images indicating the successful penetration of microneedles.

The results showed that with a higher force, the percentage of penetration increased. However, the effects are different on rat and human skins. Rat skin was much easier to be stained than human dermatomed skin. Trypan blue stains damaged cells selectively because the damaged cell membranes allow trypan blue to enter and stain the nuclei and cytoplasm (126). Since the *stratum corneum* is made up of layers of highly keratinized cells thus it will not be stained by trypan blue. Trypan blue can stain the epidermis at the sites of the *stratum corneum* perforation (81). Although rat full skin and human dermatomed skin samples had the similar thickness, around 500 μm, rat skin has a much thinner layer of epidermis (~15 μm, **Figure 2.2C**) than human skin (~200 μm). After the *stratum corneum* of rat skin is penetrated by microneedles, the viable epidermis below may be easily stained. On the other hand, the human skin has a more complicated structure. The layer below the *stratum corneum* is the *stratum granulosum*. Since the *stratum granulosum* is made up of partially keratinized cells without nuclei, it is more difficult to stain (127).

In general, microneedle pretreatment can increase skin delivery of GHK-Cu, although the results were quite different on rat and human skin. The permeation of copper peptide was

observed for non-treated rat skin, but almost none for intact human dermatomed skin. With microneedle pretreatment, the permeated amount of copper and peptide increased significantly than those through non-treated rat skin (**Figure 2.4A** and **B**). For human skin, microneedle pretreatment made permeated copper and peptide detectable. But substantial increase in the skin permeation was only observed at 22.2 N (**Figure 2.4C** and **D**).

We noticed that the depth of penetration was proportional to application forces in both rat skin and human dermatomed skin models. For the rat skin, however, the microneedles can easily penetrate the entire epidermis at all the forces, as the thickness of epidermis of rat skin is ~15 µm (**Figure 2.2C**). Epidermis, especially, its outermost layer, i.e., the *stratum corneum*, is the main barrier. Thus, the permeation of copper peptide through rat skin was independent of depth of penetration in rat skin model, similar to another finding (81). Bachhav *et al.* also found the transport of lidocaine was independent of the depth of the microchannels created by laser after removal of the *stratum corneum* (21).

In the case of human dermatomed skin model, when microneedle application forces were less than or equals to 13.3 N, increase in skin permeation was observed because the *stratum corneum* was penetrated, while the distinct increase in the skin permeation at 22.2 N may mainly be due to the penetration of whole epidermis layer (the epidermis layer of the human skin is ~200 µm). It indicated that viable epidermis layers are also significant permeation barriers *(128).*

Apart from the two types of skin models (rat full skin and human dermatomed skin), we also tested human epidermis. Human epidermis has been widely used in *in vitro* skin permeation experiment to study the conventional transdermal drug delivery (129). Human epidermis has also been used to study microneedle assisted transdermal drug delivery (36, 80). However, in our study, it was shown that human epidermis, without the dermis layer,

showed a much higher percentage of penetration with microneedles as compared to human dermatomed skin (**Figure 2.8** and **Figure 2.9**). It may be because the thick dermis in the dermatomed skin could provide cushion effect and have absorbed some of the force applied onto the epidermal layer. Furthermore, a sharp increase in skin permeation of copper peptide was observed even with a mild microneedle application force on human epidermis (**Figure 2.9**). As such rat skin and human epidermis may have their limitations as models to study the physical enhancement of skin by using microneedles.

Furthermore, higher skin permeation of GHK-Cu can be obtained with the use of a higher concentration of GHK-Cu solution with microneedle treatment. However, no permeation of GHK-Cu was observed through intact human dermatomed skin even when the GHK-Cu concentration increased (**Figure 2.10**). It suggested that increasing GHK-Cu concentration alone in topical formulations might not be a good choice to improve the effect of the GHK-Cu creams/gels.

The ratio of copper to peptide permeated though rat skin was around 1:1, while when human skin models were used, the ratio was much higher. It may be partly due to the fact that more copper was retained in rat skin than in human skin. Moreover, GHK-Cu complex can permeate at faster rate than GHK alone (**Figure 2.11**Error! Reference source not found.), which suggested a potentially useful approach to deliver minerals through skin.

Although it was found that application force was correlated with copper permeation through skin, no correlation was found between application force and copper retention inside skin. Partitioning of copper can be influenced by complexation with proteins in the skin (130). In this case, the skin proteins were probably saturated with copper at the end of the permeation study, thus no difference of copper was found inside the skin samples. On the other hand, the difference between rat skin and human dermatomed skin may be due to

the difference of protein content in the two types of skin. The weight of skin was around 0.40 g and 0.10 g while the protein content was around 36 mg and 10 mg for one piece of rat skin and human dermatomed skin used in permeation study, respectively. The retained peptide in skin was not studied in this *in vitro* model since GHK peptide would degrade rapidly because of the existence of enzymes *in vivo* (131).

Besides its efficacy, the skin irritancy potential of the microneedle array was also tested, using MTT assay to monitor the metabolic activity of keratinocytes and fibroblasts (132). The cytotoxicity assay showed that GHK-Cu was not toxic to HaCaT keratinocytes and human dermal fibroblasts in the range of 0.0058 – 5800 μM (**Figure 2.6**). From the *in vitro* permeation study, the highest amount of copper retained in skin was around 600 nanomoles (**Figure 2.6**). The weight of skin was ~0.4 g. So the retained copper can reach a concentration of ~150 μM by calculation, which is less than 5800 μM. Thus it is not expected to cause any skin side effects. Furthermore, irritation test on pig skin confirmed that the skin recovered quickly after microneedle application and the combination of microneedles and topical GHK-Cu formulation did not cause any skin irritation. The skin of the domestic pig is widely accepted as a suitable model for human skin for dermatological research and for percutaneous permeation studies because pig skin is usually considered as the closest in structure to human skin among different animal species (133). Pigs have also been used in the studies of microneedle assisted topical drug delivery (27, 28). Nevertheless, it is still necessary to further confirm the safety of microneedle assisted GHK-Cu application on human subjects.

The recommended intake of copper for healthy adults is 0.9 and 1.3mg/day by American Food and Nutrition Board and World Health Organization, respectively (134, 135). In our study, about 705 nanomoles/cm^2 of copper can permeate through human skin with the assistance of microneedles in 9 hours. A steady flux of 48.1 nanomoles/h/cm^2 was

calculated from the permeation curve (**Figure 2.4C**). So about 721 nanomoles/cm^2 of copper was expected to permeate through the skin in the next 15 hours. Altogether there would be about 1426 nanomoles/cm^2 (which is about 0.091 mg/ cm^2) of copper permeating through human skin in 24 hours with the assistance of microneedles. So a patch size of 9 to 15 cm^2 may be designed to meet the daily intake requirement of copper.

2.5. Conclusion

The application force was found to affect the percutaneous delivery efficiency of copper peptide by influencing the depth and percentage of microneedle penetration through skin. The skin permeation of copper peptide can be enhanced by microneedle pretreatment at a high thumb force with minimal skin disturbance. In 9 hours, 134 ± 12 nanomoles of peptide and 705 ± 84 nanomoles of copper can permeate though the pretreated human skin. It indicates that microneedles may be useful to deliver similar peptides or minerals through skin. Besides, human epidermis and rat skin may not be suitable models for *in vitro* skin permeation study when microneedles are used.

Chapter 3 Selected biomarkers revealed potential skin toxicity caused by certain copper compounds

3.1. Introduction

Copper is an essential trace element critical for normal human metabolism and copper deficiency can occur with insufficient copper intake. However, excess copper intake may also cause toxicity to human. Copper and its alloys are present in numerous articles of everyday use, such as coinage, tools, jewelry, and dental materials, thus it comes in regular, sometimes extended and intimate contact with skin. For medical applications, copper intrauterine devices (IUD) are a type of long-acting reversible contraception because copper (II) ions released from the devices are deleterious to sperm cells (136). Direct and prolonged contact of copper with skin/mucosa may result in electrochemical reactions that release copper ions, which become diffusible through skin (130). Copper in its metallic state has no effect on the skin and it becomes a potential irritant or allergen only when it is corroded and thus become soluble through the action of exudates encountered on the skin surface, or in a relatively corrosive physiological environment such as the oral cavity or the uterus (137).

Copper compounds have been used as paint pigments, as wood preservative and pesticides historically (138). Copper complex and compounds are also active ingredients/excipients in cosmetic and pharmaceutical industries, e.g., copper peptide for skin regeneration purpose, cupric aspirinate and cupric salicylate for rheumatoid arthritis treatment, copper conjugated dendrimer with antitumoral activity, and copper liposome for an enhanced stability of doxorubicin (139-143). Copper can also act as a delivery vehicle, where it is used in photothermal nanoparticles. These copper nanoparticles-mediated drug delivery can significantly increases the permeability of drug and enables sustained and controlled

transdermal drug delivery (144). With the developments of novel skin permeation enhancement methods such as microneedles and laser, copper compounds can be potentially used on skin for cosmeceutical or medicinal purposes (35, 139, 145). Efficacy studies and safety studies are equally important for a successful development of a drug delivery system. However, many current studies are mainly focused on improving the pharmacodynamics and pharmacokinetics properties of copper, data on dermal toxicity by copper and its compounds is limited and their toxicity potential has not been well established.

Furthermore, along with wide exposure of copper on the skin or mucosa, cases of contact dermatitis have been reported, although not frequent. A woman had a 5-year history of painful lichenoid lesions on the left mucosa and the left side of the tongue adjacent to a dental metal prosthesis containing copper. The symptoms relieved almost immediately and the lichen disappeared after the prosthsis had been changed to one without copper. Dermatitis and eczematous rash was reported with people with IUD. Hand eczema was reported with cashiers and other professionals handing coins which may be caused or aggravated by the release of metal including copper (137). Irritant effects have been frequently found from occupational exposures to copper-based pesticides, including allergic reactions, itching, and eczema (146).

Considering the wide contact of coppers and its compounds in our daily life, data on dermal irritation by copper and its compounds is scant and the role of copper as an irritant/sensitizer remains controversial (137). A recent review paper on copper hypersensitivity concluded that copper is a weak sensitizer as compared with other metal compounds (147). However, with the prevalence of skin permeation enhancement methods (such as microneedles and laser) used in cosmetic and pharmaceutical industry (1), copper

compounds may pose a higher risk on the disrupted skin, which necessitate thorough skin toxicity testing of the copper and its compounds.

Animal tests for acute skin irritation assessment usually follows Draize rabbit test while the well accepted assays for skin sensitization include local lymph node assay (LLNA) and guinea pig maximisation test (GPMT). However, there is indication that the LLNA is deficient in detecting metals and organometallic compounds (148). Furthermore, because of questionable significance of animal data and ethical opposition to animal test, efforts have been made to find alternative testing methods to identify the skin toxicity chemicals (149-151). Most considerations of non-animal alternatives for skin irritation/sensitization tend to examine a single aspect of the process of induction (e.g. chemical reactivity, epidermal bioavailability, dendritic cell responses). However, experts in the area generally conclude that it will require a combination of data from multiple endpoints to truly discriminate and classify sensitizing and/or irritant substances *in vitro*. Besides, direct peptide reactivity assay (DPRA) is a kind of chemical reactivity assay recommended by the European Center for the Validation of Alternative Methods (ECVAM) for skin sensitization testing. However, DPRA is not suitable for metal compounds, because they may form bonds with nucleophilic residues in histidine (152).

In Chapter 2, we demonstrated that the use of microneedle pretreatment can enhance the delivery of copper peptide and the safety of the combination was demonstrated by MTT cytotoxicity assay and *in vivo* pig study. In this chapter, we further investigate the safety of the skin toxicity potential of copper peptide (GHK-Cu) as well as two other copper compounds, copper chloride ($CuCl_2$) and copper acetate ($Cu(OAc)_2$) using an *in vitro* skin irritation test by using multiple biomarkers. Based on the mechanism of skin irritation, we examined and proposed a paradigm to assess the skin irritation potential of copper compounds using cytotoxicity assay, gene and protein expression levels of cytokines and

other newer biomarkers. To our knowledge, this is the first study evaluating the irritancy of different types of copper compounds at the cellular, genomic and proteomic levels using keratinocyte cell line. This approach may also be useful to assess the irritancy potential of other inorganic compounds or minerals through the skin, which is a critical tool in the cosmetological, dermatological and pharmaceutical applications.

3.2. Materials and methods

3.2.1. Materials

GHK and GHK-Cu were purchased from McBiotec (Nanjing, China). The ratio of GHK to Cu is 2:1 according to manufacturer data. Copper (II) chloride (99%) and copper (II) acetate monohydrate (≥ 98%) were purchased from Sigma-Aldrich (St. Louis, USA). Random primers and SYBR safe DNA gel stain were supplied by Invitrogen, Life Technologies (USA). RNeasy Mini Kit and QuantiFast SYBR Green PCR kit were purchased from Qiagen (Germany). Random primers and avian myeloblastosis virus reverse transcriptase were purchased from Promega (Madison, Wisconsin, USA). Human interleukin 1 alpha and interleukin 8 enzyme-linked immunosorbent assay (ELISA) kits were purchased from Biolegend (San Diego, CA, USA). Human Fos-related antigen 1 (FOSL1) and Heat shock 70kDa protein 1A (HSPA1A) ELISA kits were purchased prom MyBioSource (San Diego, CA, USA). Reagents used for cytotoxicity assay was the same with that used in Chapter 2.

3.2.2. Cytotoxicity assay

The cytotoxicity of different concentrations of GHK, GHK-Cu, $Cu(OAc)_2$ and $CuCl_2$ against HaCaT keratinocytes were studied by MTT assay in 6 replicates. Cells were seeded at a density of 5000 cells per well in 200 µl fresh culture medium (DMEM supplemented

with 10% FBS and 1% penicillin/streptomycin solution) into 96-well flat-bottomed microtiter plates (Costar, Corning, USA) and incubated at 37 °C in humidified 5% CO_2 using AutoFlow NU-5510 Direct Heat CO_2 Incubator (NuAire, USA) for 24 hours before treatment. The culture medium was then removed after 24 hours of incubation. Subsequently, 180 µl fresh culture medium and 20 µl of samples (0.058 - 58000 µM in sterile water) were added per well and incubated for 24, 48 and 72 hours. For control group, 180 µl fresh culture medium and 20 µl of sterile water were added. At the respective analysis point, the medium was removed, washed with 200 µl PBS and replenished with 200 µl fresh medium per well. Twenty µl of filtered MTT solution (5 mg/ml in PBS) was added to each well, after which the plates were incubated for an additional 4 h. The supernatant was then removed and resultant formazan crystals were solubilized in 150 µl DMSO. Absorbance was recorded at 595 nm with a microplate reader (Tecan, Switzerland). Wells containing DMSO alone were used as blank. Percentage of cell viability was expressed as $(A_{Sample} - A_{DMSO}) / (A_{Control} - A_{DMSO}) \times 100$ %.

3.2.3. *In vitro* skin irritation test

HaCaT keratinocytes were cultured in DMEM containing 10% FBS and 1% penicillin/streptomycin and were maintained under 37 °C with humidified 5 % CO_2. When the cells reached approximately 80% confluency, cells were harvested with trypsin and seeded at a density of 2.9×10^5 cells per well in 2.5 ml of culture medium into 6 well flat-bottomed plates (Costar, Corning, USA) and incubated for 24 hr.

GHK, GHK-Cu, $CuCl_2$ and $Cu(OAc)_2$ were used at a final concentration of 58 µM and 580 µM. Sterile water was used as a control. All the chemicals were diluted with sterile water to appropriate concentrations before the start of each experiment.

Then, 250 µl sample solution (580 and 5800 µM in sterile water) and 2.25 ml of culture medium were added into each well in triplicates. For control group, 250 µl sterile water and 2.25 ml culture medium were added. Cells were subjected to treatment in incubator for 24 hours. Following treatment, the culture medium was recovered and used for protein quantification using ELISA. The cells in the appropriately labelled wells were used subsequently for messenger ribonucleic acid (mRNA) extraction.

3.2.4. mRNA extraction

mRNA was extracted from cells using the RNeasy Mini Kit in accordance with the manufacturer's instructions. The concentration of mRNA were determined using NanoDrop 1000 Spectrophotometer (Thermo Scientific, USA). Reverse transcription of total mRNA were performed at 1 µg of total mRNA in 25 µl final volume using random primers and avian myeloblastosis virus reverse transcriptase. The concentration of complementary deoxyribonucleic acid (cDNA) after reverse transcription were also determined using NanoDrop Spectrophotometer.

3.2.5. Quantitative real-time polymerase chain reaction (PCR)

Quantitative real-time PCR reaction was performed using Rotor-Gene Q real time PCR cycler (Qiagen, Germany). Primers (Integrated DNA technologies, Singapore) used for PCR reactions were listed **Table 3.1**. Primers sequence for beta actin (ACTB), interleukin 1 alpha (IL-1α), FOS-like antigen 1 (FOSL1), cofilin 1 (CFL1), bone morphogenetic protein 2 (BMP2) and heat shock protein 70 kDa 1A (HSPA1) were synthesized as previously described (153-155). While primer sequence for interleukin 8 (IL8), heat shock protein 27 (HSP27) and superoxide dismutase 1 (SOD1) were designed using Primer3 (http://frodo.wi.mit.edu/) and Primer-BLAST (http://www.ncbi.nlm.nih.gov/tools/primer-blast/). Primer specificity was verified by running PCR for 40 cycles at 95 °C for 10

seconds and 60 °C for 60 seconds, followed by gel electrophoresis on a 3% agarose gel stained with SYBR safe DNA gel stain.

Table 3.1 DNA sequence of primer pairs used for quantitative real time PCR.

Gene symbol	Gene name	Accession Number	Product length (bp)	Forward Primer (5' to 3')	Reverse Primer (5' to 3')
IL1A	Interleukin 1 alpha	NM_000575	89	ggttgagtttaagccaatcca	tgctgacctaggcttgatga
FOSL1	FOS-like antigen 1	NM_005438	75	aaccggaggaaggaactgac	ctgcagcccagatttctcat
HSPA1A	Heat shock 70kDa protein 1A	NM_005345	89	ggagtcctacgccttcaaca	ccagcaccttcttcttgtcg
BMP2	Bone morphogentic protein 2	NM_001206	189	ggtggaatgactggattg	gcatcgagatagcactg
CFL1	Cofilin 1	NM_005507	285	tcttctgcctgagtgaggac	tgatccctgtcagcttcttc
IL8	Interleukin 8	NM_000584	139	tctggcaaccctagtctgcta	agtgcttccacatgtcctcac
HSP27	Heat shock protein 27	AB020027	153	ctgcaaaatccgatgagactg	caggtggttgctttgaacttt
SOD1	Superoxide dismutase 1	NM_000454	166	tcaatttcgagcagaaggaaa	ccaccgtgttttctggataga
ACTB	Actin, beta	NM_001101	283	tgacccagatcatgtttgag	ttaatgtcacgcacgatttcc

A beta actin primer was also included as an internal loading control. Each reaction mixture was prepared using 10 µl QuantiFast SYBR Green PCR master mix, 4 µl of cDNA template with 1 µM of each primer in a total reaction volume of 20 µl. The PCR was run for 40 cycles and the thermal cycling conditions were as follows: initial heat activation at 95 °C for 10 minutes; denaturation for 10 seconds at 95 °C; combined primer annealing and extension for 60 seconds at 60 °C. The fluorescence signal was measured at the end of each extension step. After the amplification, a melting peak analysis with a temperature gradient from 72 °C to 95 °C was performed. Fluorescence emission readings were analyzed using Rotor-Gene Q software (Qiagen, Germany). The data were presented as the fold increase

of the target gene expression, normalized to the housekeeping gene beta-actin, compared to unstimulated conditions.

3.2.6. ELISA

Following treatment, conditioned medium was recovered and used to determine concentration of IL-1α, IL8, HSPA1A and FOSL1. The concentration of IL-1α and IL-8 were measured quantitatively using ELISA kits in accordance with the manufacturer's instructions. Absorbance was recorded at 450 nm using a microplate reader (Tecan, Switzerland). The unknown analyte concentrations in the samples were determined using a standard curve. The concentration range of standard curve for IL-1α was 3.9 – 250 pg/ml, for IL-8 15.6 – 1000 pg/ml, for FOSL1 31.2 to 1000 pg/ml and for HSPA1A 1.56 – 100 ng/ml. Results were presented as pictogram or nanogram of mediator released per milliliter of conditioned medium.

3.2.7. Statistical analysis

Results were expressed as means ± standard deviation of at least three independent experiments. Statistical analysis was performed by one-way ANOVA followed by Tukey's post hoc test using Minitab 16. The difference was considered to be statistically significant at p-value < 0.05.

3.3. Results

3.3.1. pH determination in water and culture medium

GHK, GHK-Cu, $Cu(OAc)_2$ and $CuCl_2$ samples were prepared and diluted in sterile water and culture medium (DMEM supplemented with 10% FBS and 1% penicillin/streptomycin) respectively to a final concentration of 580 µM and 5800 µM. The pH value was then

recorded using the S220 SevenCompact™ pH/Ion meter (Mettler Toledo, Switzerland). The result was shown in **Table 3.2**.

Table 3.2 pH of tested compounds dissolved in water and culture medium respectively.

Concentration / Solvent	5800 μM Water	5800 μM Culture medium	580 μM Water	580 μM Culture medium
GHK	7.95	7.60	7.92	7.49
GHK-Cu	6.74	7.23	6.41	7.35
CuCl2	4.69	6.91	5.09	7.21
Cu(OAc)2	5.87	6.92	5.56	7.37

3.3.2. Cytotoxicity assay in HaCaT cells

Cell viability tests were performed using HaCaT keratinocytes cells with treatment of GHK, GHK-Cu, $CuCl_2$ and $Cu(OAc)_2$ for 24, 48 and 72 h. After treatment with concentrations ranging from 0.0058 μM to 5800 μM, cell toxicity was not observed for both GHK (**Figure 3.1A**) and GHK-Cu (**Figure 3.1B**). On the other hand, the toxic effect of $CuCl_2$ and $Cu(OAc)_2$ on HaCaT cells were concentration- and time- dependent. After 24 h treatment with 580 μM $CuCl_2$ (**Figure 3.1C**) and $Cu(OAc)_2$ (**Figure 3.1D**), there were statistical difference in cell viability as compared with control but high cell viability was still observed with more than 75 % viable cells. However, it was observed that cell viability decreased subsequently after 48 h and 72 h with treatment of $CuCl_2$ and $Cu(OAc)_2$. The cell viability was 13.7% and 38.2% for $CuCl_2$ and $Cu(OAc)_2$ groups at 48 h respectively and almost all the cells were dead for the two groups by 72 h. While at the highest concentration of 5800 μM, both $CuCl_2$, and $Cu(OAc)_2$ were found to be very cytotoxic to the cells and almost all the cells died at the three time points.

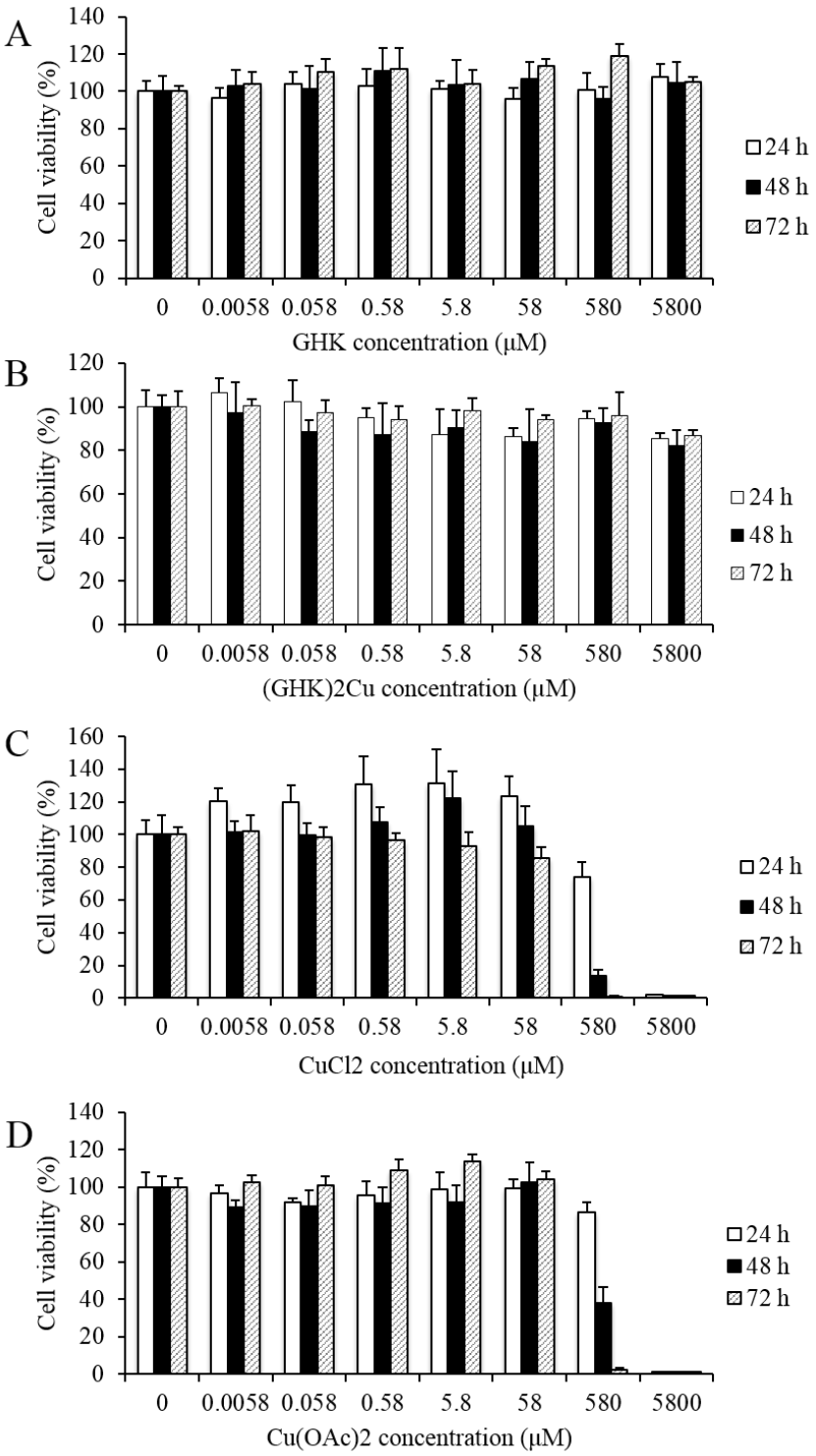

Figure 3.1 Cytotoxicity assay. Relative cell viability of HaCaT keratinocytes after incubation with GHK (A), GHK-Cu (B), $CuCl_2$ (C) and $Cu(OAc)_2$ (D) for 24, 48 and 72 hours.

3.3.3. Quantitative real-time PCR analysis

Real-time PCR was then performed to determine the expression of 8 genes, which were involved in skin irritation and inflammation. These genes were previously found to be upregulated in the presence of irritants (153, 156). The fold changes in relative gene expression of treatment cells compared to sterile water treated control cultures were determined following 24 h of treatment. The changes in relative gene expression were calculated as the normalized ratio in treatment cells compared to that in control (sterile water). Fold change in treated cells are presented as mean ± standard deviation. ANOVA was performed between the control and treatment groups for each gene followed by Tukey's post hoc test. * $p < 0.05$, is considered to be statistically significant. The result is shown in **Table 3.3**.

From **Table 3.3**., it was shown that HSP27, SOD1, CFL1 and BMP2, did not show any significant change in expression levels among all the treatment groups with $p > 0.05$. While the change in gene expression of the other four genes, IL1A, IL8, FOSL1 and HSPA1A were significantly different among the control and treatment groups ($p < 0.05$), which were further plotted in **Figure 3.2**.

From **Figure 3.2**, GHK and GHK-Cu at 58 µM and 580 µM did not induce any significant change in the expression of all the tested genes compared to control ($p < 0.05$).

For $CuCl_2$ and $Cu(OAc)_2$, the gene expression levels were concentration dependent, where treatment concentration of 580 µM induced a higher expression of genes than that of 58 µM. At 58 µM, $CuCl_2$ and $Cu(OAc)_2$ did not induce any significant upregulation of the four genes. After treating HaCaT cells with 580 µM $CuCl_2$ or $Cu(OAc)_2$, the expression of IL1A, IL8, HSPA1A and FOSL1 were significantly higher than that in the control group, ranging from 8 – 44 folds of change. Specifically, 580 µM $CuCl_2$ induced the upregulation

of IL8 up to 44 times. At the same concentration of 580 μM, $Cu(OAc)_2$ induced a higher regulation of IL1A than $CuCl_2$, while $CuCl_2$ induced a higher regulation of IL8, HSPA1A and FOSL1 than $Cu(OAc)_2$.

Table 3.3 The fold change in gene levels after treatment. * $p < 0.05$, is considered to be statistically significant among groups.

Gene symbol	GHK 58uM	GHKCu 58μM	CuCl2 58μM	$Cu(OAc)_2$ 58uM	GHK 580uM	GHKCu 580μM	$CuCl_2$ 580μM	$Cu(OAc)_2$ 580uM
IL1A*	1.21 ± 0.39	0.71 ± 0.14	1.07 ± 1.01	1.37 ± 0.37	1.24 ± 0.28	3.05 ± 1.33	8.57 ± 4.23	11.30 ± 2.16
IL8*	1.83 ± 0.89	1.73 ± 0.90	2.35 ± 1.19	1.26 ± 0.15	2.47 ± 0.98	2.97 ± 0.88	44.07 ± 8.74	11.22 ± 2.82
FOSL1*	1.12 ± 0.22	2.53 ± 1.85	3.53 ± 2.27	1.37 ± 0.14	0.95 ± 0.15	3.04 ± 1.56	17.40 ± 3.89	9.35 ± 1.58
HSPA1*	3.12 ± 1.56	0.46 ± 0.03	2.64 ± 2.09	1.26 ± 0.32	2.02 ± 1.29	0.64 ± 0.11	18.23 ± 2.60	8.27 ± 3.57
SOD1	0.37 ± 0.07	0.50 ± 0.07	1.00 ± 1.14	0.46 ± 0.24	0.37 ± 0.08	0.56 ± 0.09	0.85 ± 0.16	0.36 ± 0.14
HSP27	0.23 ± 0.02	0.41 ± 0.18	0.42 ± 0.21	0.81 ± 0.43	0.21 ± 0.06	0.55 ± 0.16	0.11 ± 0.04	0.53 ± 0.36
BMP2	0.34 ± 0.06	1.81 ± 1.29	1.52 ± 1.12	0.17 ± 0.03	0.25 ± 0.13	2.94 ± 2.97	1.03 ± 0.82	0.22 ± 0.05
CFL1	0.13 ± 0.06	2.57 ± 2.13	1.56 ± 1.45	0.11 ± 0.05	0.16 ± 0.06	4.50 ± 3.89	0.51 ± 0.37	0.06 ± 0.02

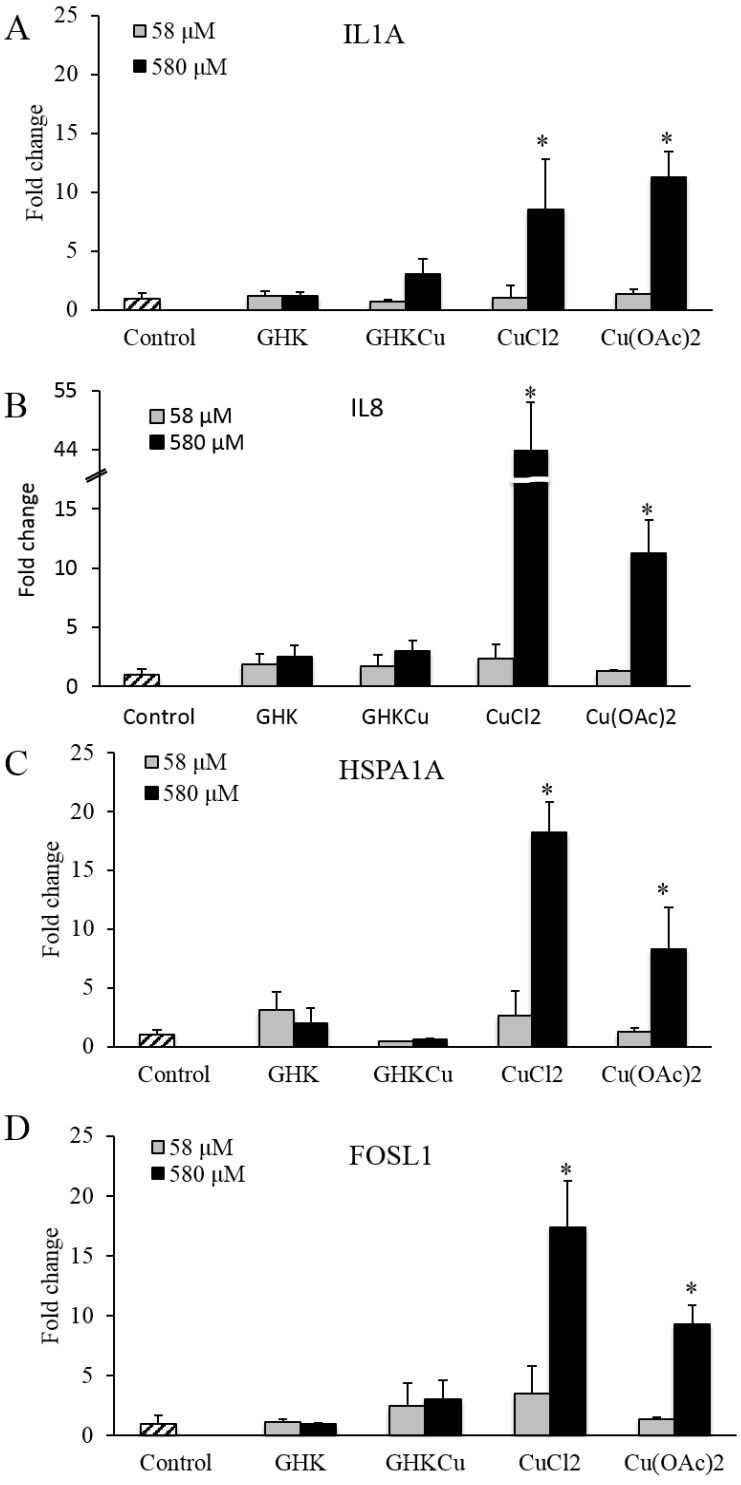

Figure 3.2 Real-time PCR analysis on expression of IL1A (A), IL8 (B), HSPA1A (C), FOSL1 (D) following treatment for 24 h in HaCaT keratinocytes. The fold change was calculated as the normalized ratio in treatment cells compared to that in control. ANOVA was performed between the control and treatment groups for each gene followed by Tukey's post hoc test. * $p < 0.05$, is considered to be statistically significant compared with control.

3.3.4. Measurement of protein expression by ELISA

The extracellular content and release of IL-1α, IL-8, HSPA1A and FOSL1 were determined using ELISA. The expression of FOSL1 in the culture medium of all samples were not detectable. The concentrations of IL-1α, IL-8 and HSPA1A released after treatment with various compounds were presented in **Figure 3.3.**

At the two tested concentrations, treatment with both GHK and GHK-Cu did not significantly increase the IL-1α, IL-8 and HSPA1A protein level. For the treatment groups with $CuCl_2$ and $Cu(OAc)_2$, copper compounds had a positive correlation with the protein level regulated.

$CuCl_2$ didn't cause any change in the IL-1α, IL-8 and HSPA1A protein levels at the concentration of 58 μM, while the protein levels upregulated significantly with 580 μM $CuCl_2$ treatment. On the other hand, the IL-1α, IL-8 and HSPA1A protein levels were increased significantly with 580 μM $Cu(OAc)_2$ treatment as well. At the same concentration of 580 μM, $Cu(OAc)_2$ induced a higher regulation of IL-1α than $CuCl_2$, while $CuCl_2$ induced a higher regulation of IL-8, HSPA1A and FOSL1 than $Cu(OAc)_2$. Furthermore, 58 μM $Cu(OAc)_2$ also upregulated the IL-1α expression significantly.

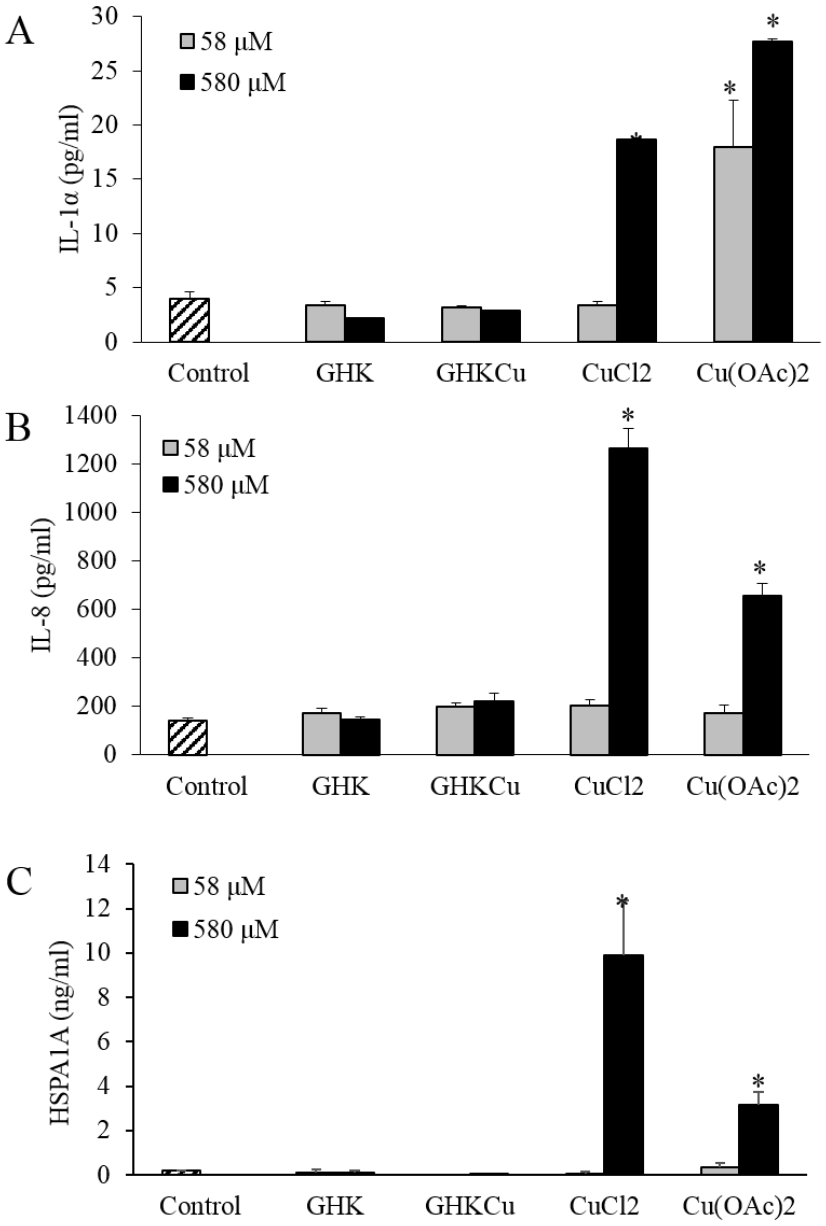

Figure 3.3 Concentration of IL-1α (A), IL-8 (B) and HSPA1A (C) in cell culture medium quantified by ELISA. Results were presented as pictogram or nanogram of mediator released per milliliter of conditioned medium. ANOVA was performed between the control and treatment groups followed by Tukey's post hoc test. * $p < 0.05$, is considered to be statistically significant compared with control.

3.4. Discussion

Keratinocytes make up 95 % of the cells in the epidermis and play an integral role in initiating, modulating and regulating skin irritation. It was found that human keratinocyte

cell line closely resembles normal keratinocytes in their growth and differentiation characteristics and hence allows the accurate prediction of response after treatment (157, 158). After exposure to an irritant, the irritant will exert toxic effects on keratinocytes. This will activate the body's innate immunity with the release of cytokines such as IL-1α in the keratinocytes. In turn, these cytokines will activate Langerhans cells, dermal dendritic cells and endothelial cells, which contribute to cellular recruitment to the site of damage. Neutrophils, lymphocytes and macrophages will then release and further promote an inflammatory cascade (159). These will lead to various signs and symptoms of irritation such as itch, erythema, edema and pain. By monitoring the inflammatory response pathways such as cytokine secretion and receptor activation, various biomarkers can give us an indication of the possibility of a safe and efficient transportation of copper through the skin to exert its beneficial effects.

Currently, endpoint measurements are related to severe cell damage such as tetrazolium reduction assays to detect viable cells and IL-1α release as inflammatory marker (157). Important early changes occur before severe cell damage but no universal markers have been identified (157). The search for new parameters or endpoints is necessary given the complexity of skin irritation mechanism. Various potential biomarkers have been studied and identified using proteomics and toxicogenomics technologies (153, 154, 160). These parameters will allow the setup of an *in vitro* test system, which resembles the *in vivo* situation as much as possible (161).

Copper is an essential mineral and has many potential benefits in skin growth and activity (110). Copper delivery through skin has many potential applications and thus is widely studied, including the evaluation of the penetration ability of copper peptides(122), biocompatibility of copper containing IUD (136), the enhancement of skin absorption through copper nanoparticles (144) and microneedle-mediated delivery(139). Hence, the

safety associated with copper delivery through skin needs to be established. In this study, we investigated the skin toxicity of copper compounds using a cell-based *in vitro* test and evaluated the expression of various cytokines at genomic and proteomic levels to discover irritancy biomarkers suitable for the evaluation of copper compounds.

Before the cell testing, we analyzed the pH of the samples tested and it excluded the pH of copper compounds as the influencing factor of their potential toxicity (**Table 3.2**). Subsequently, the viability of HaCaT keratinocytes were assessed using MTT assay after treatment with test compounds, GHK, GHK-Cu, $CuCl_2$ and $Cu(OAc)_2$. Cultured human keratinocytes have been suggested as good models to predict dermal irritancy of substances in human subjects (162). The material required for primary keratinocyte culture is limited and variable; and the susceptibility to irritants varies with the number of passages. On the other hand, the non-tumorigenic, spontaneously immortalized keratinocyte cell line - HaCaT cells can provide almost unlimited supply of identical cells, ensuring high intra- and inter-laboratory reproducibility. Besides, *in vitro* cytotoxicity with HaCaT keratinocytes and human *in vivo* data was well correlated (158, 163, 164). HaCaT keratinocytes also have been proven to be good candidates for assessing skin irritancy and toxicity in conventional monolayer assays measuring using MTT reduction as the viability endpoint (157).

MTT assay mainly reflects the damage to mitochondria; and it is commonly used for *in vitro* cytotoxicity (including skin irritation) measurement. Our result indicated that neither GHK nor GHK-Cu showed cytotoxic activity after 72 hours exposure to HaCaT cells. $CuCl_2$ and $Cu(OAc)_2$ were only found to be cytotoxic at 5800 µM and cell viability decreased significantly after 48 h treatment at 580 µM. At 58 µM and 580 µM, cytotoxicity was not observed following 24 h treatment with all the samples. Another study with $CuCl_2$ treated Hep G2 cell line demonstrated that mitochondrial toxicity is an intermediate-level

event associated with copper toxicity to Hep G2 cells while lysosomal damage is the early event and plasma damage a late feature associated with copper toxicity (165). Considering the copper associated mitochondrial toxicity may have delay in the toxicity process, we further explored the skin irritation related biomarker change at the genomic level. In response to chemical stress, keratinocytes produce and release inflammatory cytokines, chemokines and other signaling markers that rapidly generate cutaneous inflammation (166). Among the genes tested, expression levels of genes were not significantly different in GHK and GHK-Cu group as compared to control. However, we found that four genes, IL1A, IL8, HSPA1A and FOSL1, were significantly induced by $CuCl_2$ and $Cu(OAc)_2$ without inhibiting the cell viability. The protein expression of the four genes in culture medium were further tested with ELISA kits. While FOSL1 was not detectable for all samples in the ELISA test, the protein level regulation of IL-1α, IL-8 and HSPA1A by the copper compounds was similar with the gene level regulation. GHK and GHK-Cu didn't cause any significant change in the extracellular protein concentration of IL-1α, IL8 and HSPA1A. However, $CuCl_2$ and $Cu(OAc)_2$ significantly upregulated the extracellular protein expression of the three genes at concentration of 58 μM/580 μM without inhibiting the cell viability after 24 h.

Cytokine production and response are important as it participates in immune and inflammatory response. Specifically, IL-1α is constitutively produced and retained in keratinocytes, but in response to several stimuli, IL-1α is released, which is an essentially primary event inflammation. Triggers of IL-1α production have been observed including different stimulus, such as sulfur mustard, nickel, contact allergens or superantigens (167). IL-1α stimulates further release of secondary mediators, including IL-8. IL-8 is a powerful neutrophil attractant, and is one of the major mediators of the inflammatory response. It promotes neutrophil chemotaxis and degranulation leading to local inflammation in

damaged tissues (168). Enhanced IL-8 expression of both normal human keratinocytes and HaCaT cells were observed after stimulation *in vitro* by irritant, sensitizer and tolerogen. It indicated that IL-8 may play a critical role in the early response to immunogenic and inflammatory signals with its response to nonspecific stimuli (169). It was suggested that the differentiated production of IL-1α and IL-8 may be linked to the type of product applied either irritant or sensitizer (170, 171). Our study showed that $CuCl_2$ and $Cu(OAc)_2$ can significantly upregulate HaCaT cell expression of IL-1α and IL-8 in both gene level and protein level. The highest fold change in gene level, approximately 44 times higher in IL-8 expression was observed in 580 μM $CuCl_2$ treated cells when compared to that in control. The upregulation of these cytokines will activate and promote an inflammatory cascade, leading to various signs and symptoms.

Besides the interleukin family, other genes related to the skin inflammatory mechanism were also observed to be upregulated. FOSL1 is an early gene that belongs to the activator protein 1 family of dimeric transcription factor genes (172). It plays a role in the angiogenesis and vasculogenesis processes, where it regulates the expression of key molecules on the cell surface to modulate cell adhesion and motility (173). While HSPA1A belongs to the HSP70 family of heat shock proteins, it can be highly activated by various stressful stimulus, where it is required for refolding of damaged and unfolded proteins generated by stressful conditions (174). Both FOSL1 and HSPA1A are stress-inducible and our results showed that they were significantly upregulated in the presence of $CuCl_2$ and $Cu(OAc)_2$. Hence, FOSL1 and HSPA1A can potentially serve as useful inflammatory markers for copper compounds.

We have also studied other genes, SOD1, CFL1, BMP2 and HSP27 that were previously shown to be upregulated in the presence of sodium lauryl sulfate by DNA array or proteomic analysis (153, 154, 156). However, our results showed that no significant

upregulation were observed after treatment with various copper compounds (**Table 3.3)**. In previous studies, human keratinocytes, human epidermis model and human reconstructed skin model were used for testing the response of sodium lauryl sulfate. These new endpoints have not been widely validated for skin irritation responses. Our study may prove that these endpoints are not sufficient for irritancy testing of copper compounds in a monolayer HaCaT assay.

Copper delivery through skin can potentially be useful. However, the choice of copper compound is important. At the same concentration, different copper compounds can exhibit different irritancy potential. From our results, we observed that GHK-Cu exhibits low potential of inducing skin irritation response in comparison with $CuCl_2$ and $Cu(OAc)_2$. GHK-Cu can potentially be useful in providing a safe delivery of copper through the skin to exert its beneficial effects. Copper salts are discouraged from the direct administration on skin due to its irritancy potential and toxicity. There are several mechanisms proposed in attempt to explain copper irritancy. Copper may become potential irritants when they are oxidized and causes the formation of free acids. It is the oxidizing action of such acids that potentially result in skin irritation reactions once they reach the viable skin layers (137). It can also interact with reduced oxygen species to form hydroxyl radical that inactivates enzymes and disrupts the membranes and organelles (175).

Interestingly, GHK-Cu did not show any signs of irritation. This may be due to the complexation of copper with peptide GHK (176). When GHK is coupled with copper, the peptide may silence the redox activity of copper, facilitating the non-toxic delivery of copper into the cells (114). Complexation using other ligands can be explored but GHK is commonly used as it has additional cosmetically intriguing activities such as stimulation of collagen synthesis, chemotaxis, anti-stinging effects and others (177). Our results also showed that GHK itself is not toxic and does not induce the change of irritancy/sensitizing

related biomarkers, which provides an additional benefit when used for complexation with copper.

Accurate evaluation of cosmetological, dermatological and pharmaceutical products after application on human skin are both essential and crucial in product development. *In vitro* skin irritation test provides an alternative to animal testing and allows the screening of compounds before they undergo clinical testing. The current standard operating procedure by ECVAM recommends the use of MTT reduction as parameter to make prediction on the skin irritancy of substances using EpiSkin^{TM} test method, while IL-1α endpoint is regarded as an useful adjunct to MTT assay (178). However, measuring cytotoxicity alone is not sufficient. We have shown that $CuCl_2$ and $Cu(OAc)_2$ irritation induces the upregulation of various genes without the concomitant inhibition of cell viability. To provide a more accurate prediction of skin irritancy potential of the test compound, *in vitro* skin irritation test can include other potential biomarkers.

In this study, we evaluated various copper compounds at cellular, genomic and proteomic levels using HaCaT keratinocytes. For the first time, we have shown that different types of copper compounds have different irritancy potential at three different levels. Specifically, GHK-Cu was found to be least possible to cause skin irritation, while $CuCl_2$ and $Cu(OAc)_2$ were found to induce the expression of various skin irritation biomarkers. These biomarkers can be used in adjunct to MTT assay for a more accurate prediction of the *in vivo* response. This irritancy test approach may be extended to other similar compounds or minerals and can potentially predict the *in vivo* skin irritation response.

Further investigations can include a validation study of the genes involved in the skin irritation mechanism following direct treatment to cells. It is also necessary to confirm the

safety of GHK-Cu on human subjects. This will allow us to determine the correlation of the *in vitro* results with the actual *in vivo* response.

3.5. Conclusion

In this study, we have demonstrated that copper peptide has a low potential of inducing skin irritation response when compared to copper chloride and copper acetate. *In vitro* skin irritation test with sensitive endpoints is a possible alternative to animal testing. IL-1α, IL-8, FOSL1, and HSPA1A are potential *in vitro* biomarkers that can be used in adjunct to MTT assay in identifying irritants and assessing the low skin irritation potential of copper compounds. This irritancy test approach may also be useful to assess the skin irritancy potential of other similar inorganic compounds or minerals and can potentially provide an initial prediction of the *in vivo* response before conducting clinical testing on human subjects.

Chapter 4 High durability and low toxicity antimicrobial coatings fabricated by quaternary ammonium silane copolymers

(Adapted from *B*iomaterials Science. 2016, 4(2), 299-309)

4.1. Introduction

Adhesion and subsequent growth of microorganisms form biofilms, which presents as a great concern in various areas, such as biomedical devices, health care applications, water purification systems, dental surgery equipment, food packaging, textiles, household sanitation, *etc* (179, 180). They can cause contamination of products and corrosion. Microbial colonization of biomaterials can also lead to the systemic and implant-associated infections, the incidence of which is expected to increase with the expansion of new biomedical devices (181). It was reported that microorganisms in biofilm are more resistant to disinfection at an extent of up to 1000 times compared to free-floating microorganisms (182). Therefore, it is imperative that microbial growth can be more efficiently inhibited in the early stage of microbial adhesion and proliferation (183).

In recent years, antimicrobial polymers have attracted considerable interests from both academia and industry, owing to their advantages over small molecular biocides, being non-volatile, increased stability, low toxicity, minimal permeability though skin and the potential to maintain long-term activity (184). Researchers have tried to immobilize surfaces with polymers to prevent the formation of biofilms, thus avoiding the spread of diseases and material deterioration. The reported techniques to attach polymers to surfaces include chemical grafting techniques, layer-by-layer and surface-initiated polymerization (185-187). Different from biocide impregnated surface, the grafting of antimicrobial

polymers can produce non-leachable antimicrobial surface which can remain permanently antimicrobial (184).

Highly hydrophilic polymers have been grafted to biomaterials to prevent biofilm formation by repelling microbes and preventing their attachment. Such polymers include poly(ethylene glycol) derivatives and poly(ethylene oxide), both of which display an exclusion volume effect which renders them capable of resisting non-specific protein adsorption and cell adhesion (188). However, these polymer coatings are anti-adhesion based and don't have any biocidal activity. Microorganisms may be introduced into the patient during implantation procedures and the failure of these polymers to eliminate them can result in implant failure (189).

The antimicrobial surfaces can be further modified to kill microbes in the vicinity by conjugating polymer with agents such as antibiotics or antimicrobial peptides or complexed with silver (190-194). Wach *et al.* synthesized a hybrid molecule comprising a poly(ethylene glycol) chain with an anachelin chromophore at one end for the functionalization of surfaces and an antibiotic, vancomycin at the other responsible for antimicrobial activity (195). Penicillin has also been tethered to different surfaces by attaching to poly(2-hydroxyethyl methacrylate) chains and poly(ethylene glycol) chains. But the antibiotics may partially lose due to hydrolysis (196-198). Ramstedt *et al*. reported the synthesis of poly(3-sulfopropylmethacrylate) brushes onto gold and Si/SiO_2 surfaces by transfer radical polymerization, and the polymer brushes can easily load with silver ions to exert the antibacterial activity (191). Silver nanoparticles were loaded on decorated cellulose filter papers grafted with poly(tert-butyl acrylate) polymers, showing excellent antibacterial properties against *E. coli* (199). However, the bactericidal action of silver relies to a certain extent on the leaching of the ions, which may cause certain environment issues. An alternative way to create contact-active surfaces is to immobilize polymers

conjugated with antimicrobial proteins (AMPs) (194). AMPs are of great interest to study in recent years because they have a low propensity for developing microbial resistance (192). Covalent immobilization of AMPs onto surface can increase their long-term stability while decreasing their cytotoxicity associated with higher concentrations of soluble peptides when compared to leach- or release-methodologies (200, 201). A common approach to covalently immobilize AMPs involves the use of functionalized resins such as poly(ethylene glycol) spacers or other polymeric 'brushes' with reactive groups suitable for peptide covalent conjugation. However, the antimicrobial activity of AMPs decreased after immobilization in many reported studies (202-204). The immobilization parameters, such as peptide surface concentration, influence of the spacer (length and flexibility) or peptide orientation after immobilization, must be optimized to obtain efficient, safe, and long-lasting antibacterial coatings (205). Furthermore, the cost and complexity of their synthesis and immobilization add up to the disadvantages of AMPs as well.

A third class of antimicrobial polymeric surfaces was created by immobilizing bactericidal polymer chain to kill the bacteria upon contact (184). These polymers usually contain cationic groups, such as quaternary ammonium or phosphonium groups. Tiller *et al.* reported poly(vinyl-N-pyridinium bromide) modified surfaces exhibiting good antibacterial properties, but the complicated method may limit it from routine practices (206). Lee *et al.* grafted an antibacterial quaternary ammonium polymer directly on the surface of the glass using atom transfer radical polymerization, but this approach lacks the ease of implementation as well (207). On the other hand, quaternary ammonium siliane (QAS) monomeric agents, such as trimethoxysilyl and trihydroxysilyl quaternary ammonium compounds, have been used to prepare antibacterial surfaces easily by covalent attachment to a surface through reaction of the trimethoxysilyl groups with surface silanol groups (208). These compounds are widely used as bacteriostatic and fungistatic

treatments in human clothing and bedding, household areas, carpets and upholstery. QAS agents have the largest consumption volume as textile antimicrobials compared with triclosan and silver (209). They are also used as material preservatives in the manufacturing of paints, coatings, and concretes. However, despite the widespread use of QAS agents, severe toxicity has been observed with regard to skin and eye irritations (210) and contact dermatitis was also reported with the QAS coating (211, 212). Besides, the *in-situ* condensation coating on the surface was supposed to form a monomolecular layer and it may not be resistant to abrasion. The antimicrobial activity is lost after the surface layer is worn off.

To address these problems, we have synthesized novel QAS antimicrobial copolymers via a simple free radical addition reaction and an abrasion-resistant antimicrobial surface can be further prepared by a simple and easy thermal-curing process. The synthesized copolymers were found to be less toxic to human cell lines than a commercial antimicrobial QAS monomeric agent, namely, dimethyloctadecyl [3-(trimethoxysilyl)propyl] ammonium chloride (DTPAC). The QAS antimicrobial copolymer coatings demonstrated a broader antimicrobial activity and a better durability than those formed by DTPAC. We envision that, with a low toxicity and enhanced durability, the new QAS copolymers are appealing and represent a better substitute for the current monomeric QAS coatings.

4.2. Materials and methods

4.2.1. Materials

The monomers used for PMT copolymer synthesis are [3-(methacryloylamino)propyl]trimethyl ammonium chloride (MAPTAC, 50wt% in H_2O, Sigma-Aldrich) and 3-trimethylsilylpropyl methacrylate (TMSPMA, Sigma-Aldrich). 5-(N, N-dimethyl)-amiloride (DMA) and 1-bromohexadecane (Sigma-Aldrich, Singapore)

were used for synthesis of another antimicrobial monomer DMA-C_{16}Br. Potassium persulfate ($K_2S_2O_8$, Sigma-Aldrich) and 2,2'-Azobis(2-methylpropionitrile) (AIBN, DuPont, USA) were employed as free radical initiator for polymerization and acetone (Merck) was used to precipitate the synthesized polymers. A commercialized antimicrobial agent, DTPAC (42 wt% in methanol, Sigma-Aldrich) was used as a positive control in the antimicrobial test of coatings. Acetic acid (Merck) was used to prepare the acidic solution for QAS polymers' hydrolysis. The bacteria were grown in nutrient broth (Neogen, USA) and on nutrient agar prepared from bacteriological agar (Neogen, USA). The fungus was grown in tryptone soya broth (Neogen, USA) and on tryptone soya agar (Neogen, USA). The source of materials for cell culture were same with that used in Chapter 2.

4.2.2. Synthesis of MAPTAC based QAS copolymers

QAS copolymers PMT-5% and PMT-10% were synthesized from the monomers MAPTAC and TMSPMA in the presence of 1wt% $K_2S_2O_8$. PMT-5% was synthesized from the monomer weight ratio of 95% MAPTAC (19.0 g) to 5% TMSPMA (0.5 g) while PMT-10% was synthesized from 90% MAPTAC (18.0 g) to 10% TMSPMA (1.0 g). Homopolymer PMAPTAC was synthesized from MAPTAC (20.0 g) in the presence of 1 wt% $K_2S_2O_8$. The reaction proceeded at 70 °C with 400 rpm stirring speed for 1 hour. Thereafter, 15 ml of water was added to terminate the reaction and decrease the viscosity of the mixture. The resulted copolymers and homopolymer were precipitated against acetone (3 times) and vacuum dried at 50 °C for 48 hours.

4.2.3. Synthesis of [2-(methacryloyloxy)ethyl]dimethylhexadecylammonium bromide (DMA-C_{16}Br) and its corresponding QAS copolymer

In-house synthesis of DMA-C_{16}Br monomer was performed in accordance to literature (213). Briefly 124 mmol (19.5g) DMA and 62 mmol (18.9g) 1-bromohexadecane (Sigma-

Aldrich, Singapore) were mixed in a 100 ml flask using magnetic stirrer purged with nitrogen gas for 5 minutes. Hydroquinone (100 mg) was added to prevent spontaneous radical polymerization of DMA. The reaction flask was then placed in a 50˚C water bath and stirred continuously for 12 hours. The white-grey precipitate was filtered from the reaction mixture and washed with 100 ml of cold diethyl ether three times to remove unreacted reactants. The final product was recrystallized using acetone and dried under vacuum at room temperature with 85% yield. The newly synthesized DMA-C_{16}Br was characterized by ^{1}H-NMR ($CDCl_3$, δ ppm) of 5.6 (H^a, 1 H), 6.1 (H^b, 1 H), 1.9 (H^c, 3 H), 4.6 (H^d, 2 H), 4.1 (H^e, 2 H), 3.5 (H^f, 6 H), 3.6 (H^g, 2 H), 1.3 (H^h, 28 H), 0.8 (H^i, 3 H) (**Figure 4.1**). Infrared spectroscopy analysis was also consistent with structure of DMA-C_{16}Br (**Figure 4.2**).

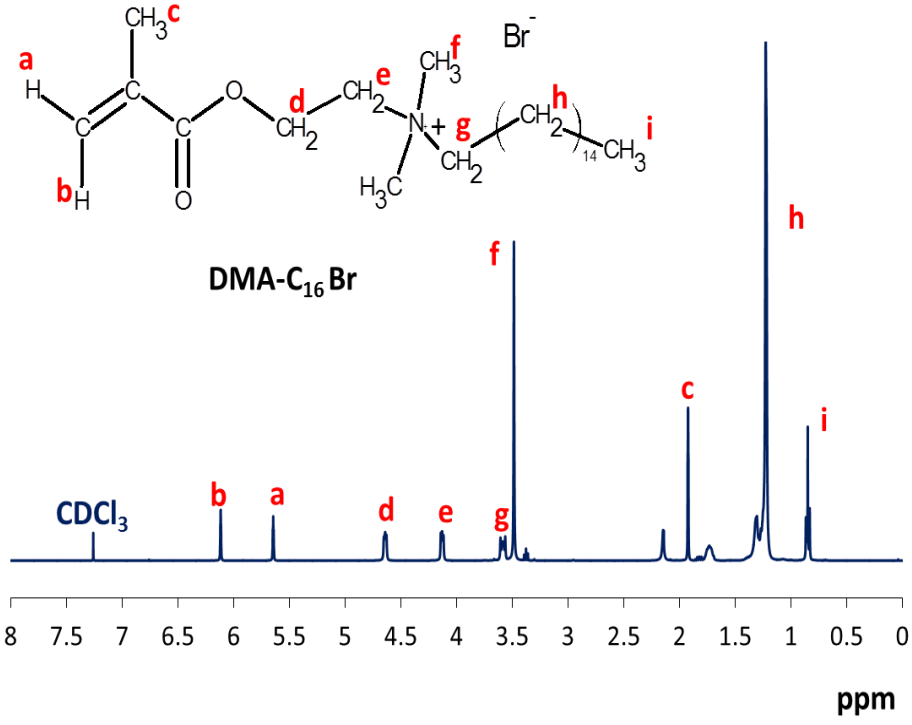

Figure 4.1 ^{1}H-NMR ($CDCl_3$, δ ppm) characterization of DMA-C_{16}Br : 5.6 (H^a, 1 H), 6.1 (H^b, 1 H), 1.9 (H^c, 3 H), 4.6 (H^d, 2 H), 4.1 (H^e, 2 H), 3.5 (H^f, 6 H), 3.6 (H^g, 2 H), 1.3 (H^h, 28 H), 0.8 (H^i, 3 H).

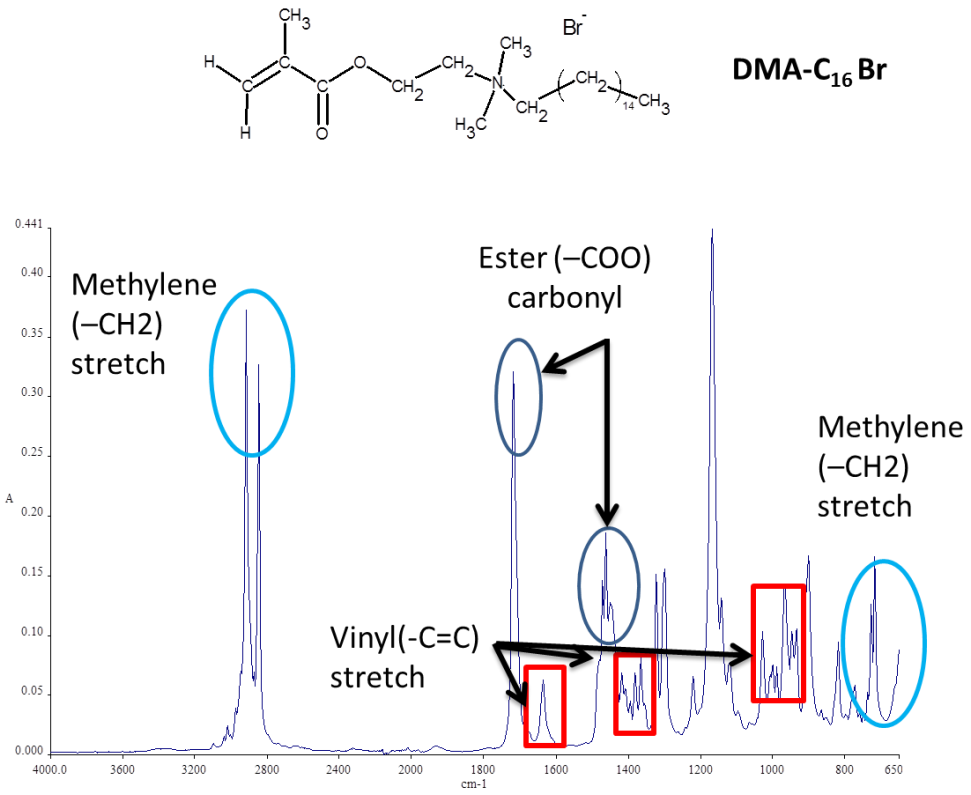

Figure 4.2 ATR-FTIR spectrum of DMA-C_{16}Br.

QAS copolymer PDT-10% was synthesized from DMA-C_{16}Br and TMSPMA in the presence of AIBN. A 50 ml Schlenk flask equipped with a magnetic stirrer was connected to a vacuum line, and the moisture was removed by heating under vacuum. When the flask was cooled down, dry nitrogen was filled in. Under a nitrogen atmosphere, DMA-C_{16}Br (2 g), isopropanol (10 g), and AIBN (0.05 g) were added into the flask that was tightly sealed with a rubber septum. The mixture was then heated to 90 °C and stirred constantly at 400 rpm. During the heating process, 150 ml TMSPMA (0.15 g) was injected into the flask dropwise, and the reaction was allowed to proceed for 1 hour before adding another 150 ml TMSPMA. After 2 hours, a combination including DMA-C_{16}Br (1.25 g), isopropanol (5 g), and AIBN (0.05 g) was purged and injected into the flask, followed by adding 100 ml TMSPMA dropwise. The same composition of DMA-C_{16}Br, isopropanol, AIBN, and TMSPMA was refilled again after 3 hours and the whole reaction mixture was further

heated for 12 hours at 90 °C with stirring. Thereafter, another 0.05 g AIBN was added to achieve a high monomer conversion and the polymerization was terminated 2 hours later. Final solution was dropped into excess amount of cold diethyl ether to precipitate PDT-10%. The dissolution-precipitation cycle was repeated for two times to remove the residual monomers. The obtained viscous product was isolated and dried under vacuum.

4.2.4. Preparation of QAS copolymer coatings

Glass slides (25.4 × 76.2 mm, Continental Laboratory Products, USA) were used as the substrates to study the coating process of PMT-5%, PMT-10% and PDT-10%. Prior to coating, the glass slides were immersed in 10% sodium hydroxide for 1 hour, thoroughly rinsed with water and cleaned with 96% ethanol before air drying. 10 mg/ml of PMT-5% and PMT-10% solution was prepared by dissolving in a pH 2.5 acetic acid solution, respectively. 5 mg/ml PDT-10% was solubilized in a mixture containing 90% of isopropanol and 10% of acetic acid solution (pH 2.5) following by heating at 50 ˚C for 30 min. 5 mg/ml and 10 mg/ml DTPAC was prepared in acetic acid solution (pH 2.5). An acidic condition can help hydrolyze the silyl ether to corresponding reactive silanol groups in copolymers. PMT-5%, PMT-10% and DTPAC solution was transferred to the pre-treated glass slide by 29 µl/cm^2 and spread evenly using a pipette. PDT-10% solution has a good spreadability on glass slide and thus 20 µl/cm^2 was pipetted on the glass slide for coating. Crosslinking of silanol groups to form siloxane linkage was initiated by drying the substrate at 130 °C for 30 minutes.

4.2.5. Characterization of QAS copolymers and coatings

A Spectrum 100 FTIR spectrophotometer (PerkinElmer, USA) with an ATR set-up was used to monitor the polymer synthesis, hydrolysis and crosslinking reactions. Infrared spectra were collected between 4000 and 650 cm^{-1} at a resolution of 4 cm^{-1}.

Water contact angle was measured with a static contact angle measurement device (Attension, BiolinScientific). The machine was equipped with a digital camera, automatic liquid dispensers, and sample stage allowing hands-free contact angle measurement via automated placement of a drop of water. The drop shape is captured automatically and then analyzed via OneAttension software to determine the static contact angle.

Mass loss of synthesized polymers, weighing approximately 10 mg, were measured by thermogravimetric analysis (TGA), using a TGA-Q5000 apparatus (TA Instruments Ltd, USA). The samples were heated from room temperature to 600 °C at 10 °C/min in a nitrogen gas flow of 20 cm^3/min.

After coating, glass slides were subjected to abrasion test by using a Taber Linear Abraser 5750 instrument with a vertical load of 1 kg, and 10 cycles were performed with a magnitude of 1 inch. The characteristic peak absorbance from ATR-FTIR examination of coating before and after abrasion at the same location was used to calculate the retention of coating on the glass slides. The retention of coating was expressed as the peak height of the characteristic peaks before abrasion divided by that of after abrasion.

4.2.6. Antimicrobial assays of QAS copolymers and coatings

15% glycerol cell stocks of *Staphylococcus aureus* (*S. aureus*, ATCC 6538P, Oxoid, Singapore), *Escherichia coli* (*E. coli*, ATCC 8739, Oxoid, Singapore) and *Candida albicans* (*C. albicans*, ATCC 2091, MicroBiologics, France) were prepared and divided into aliquots and frozen at -80 °C. All microbes were prepared from the stocks and were growth to their exponential phase before they were harvested for antimicrobial assays. *S. aureus* and *E. coli* were grown in nutrient broth (Acumedia, Michigan) at 37 ˚C with shaking, while. *C. albicans* were grown in tryptone soya broth (Oxoid, England) at 28 ˚C with shaking.

The minimum inhibitory concentration (MIC) assay was carried out via the broth microdilution method using sterile 96-well flat-bottomed microplates (Costar, Corning, USA*). S. aureus* (Gram-positive), *E. coli* (Gram-negative) and *C. albicans* (fungus) were grown to their exponential phase and appropriately diluted to achieve the inoculum size of approximately 10^5 colony forming units (CFU)/ml in each well. MAPTAC homopolymer (PMAPTAC), PMT-5% and PMT-10% were dissolved in sterile PBS to get a concentration of 5 mg/ml. 2.5 mg/ml PDT-10% was prepared in 50% DMSO. Then the copolymer solutions were sterilized via filtration with a 0.20 µm filter and serially diluted with PBS (water for PDT-10% dilution) to achieve a broad range of polymer concentrations. 20 µl polymer solution with different concentrations was added to 180 µl inoculum in each well. The microplate was incubated at 37 °C (for bacteria)/28 °C (for fungus) with shaking at 200 rpm for 24 hours before being assayed at 600 nm using a microplate reader (Tecan, Switzerland). The MIC is defined as the lowest polymer concentration at which there is no increase in optical density. Sterile broth, sterile polymer solutions of various concentrations dissolved in broth, and broth containing microorganism with different DMSO concentrations were used as controls. After the microplate used in the MIC assay has been incubated for 24 hours, minimum bactericidal/fungicidal concentration (MBC/MFC) determination was done for concentrations at and above MIC. Briefly, a 100 µl aliquot was removed from each well showing no growth except wells containing the sterility controls. Each aliquot was plated onto nutrient agar in duplicate and incubated at 37 °C at least for 24 hours (or plated onto tryptone soya agar plates and incubated at 28 °C for 3 days for *C. albicans*) before conducting a colony count. MBC/MFC is defined as the lowest concentration that achieves a ≥ 99.9% or a three-log reduction in the initial MIC inoculum within 24 hours. This was determined by calculating the maximum allowable number of colonies per plate. The rejection value (CFU/plate) was expressed as initial inoculum (CFU/ml) × 0.1 ml × 0.1%.

The test for antimicrobial activity of the polymers' coating was further conducted on glass cover slip (Menzel-Gläser, Germany) (214, 215). Before coating, glass cover slips were treated in the same way as glass slides previously described in the method part. The treated surfaces of cover slips (22 × 22 mm) were covered with acidified PMT-5% (10 mg/ml), PMT-10% (10 mg/ml) and DTPAC solutions (5 and 10 mg/ml) at 29 µl/cm^2, while covered with acidified PDT-10% at 20 µl/cm^2 due to its good wettability, respectively. Then the cover slips were dried at 130 °C for 30 minutes. For antimicrobial assessment of coatings, the microorganisms were grown to their exponential phase and appropriately diluted to achieve the standard inoculum size between 9×10^5 to 10^6 CFU/ml. Then coated substrate was placed in sterile Petri dish and appropriate amount of bacteria inoculum was dropped on the surface, then it was covered with a plastic film (18 × 18 mm) to achieve the inoculum amount at least 10^4 cells per 1 cm^2 cover film. Uncoated substrates were used as controls. Inoculated bacteria were recovered by removing the film-covered substrates and placing them into 50 ml Falcon tubes containing 10 ml of PBS. The tubes were vortexed for 1 minute before serially diluting the samples in PBS. A viable count was conducted using the spread plate method after appropriate dilution. Bacteria recovery was carried out after incubation at 37 °C in humidified condition for 24 hours while incubation temperature of 28 °C was used for *C. albicans*. The unit number of viable microbes was obtained from the counts the colonies calculated according to following equation:

$$N = C\times D\times V/A$$

Where, N: Number of viable microbe per 1 cm^2. C: Count of colonies. If C <1, C is taken as 1. D: Dilution factor. V: Volume of recovery solution. A: Area of cover film (cm^2). The antimicrobial activity was expressed as log reduction number of the microorganisms after 24 hours compared with control.

4.2.7. Cytotoxicity assay

The cytotoxicity of the polymers was evaluated via the determination of mitochondrial succinate dehydrogenase activity using MTT assay with HDF, HaCaT keratinocytes and human embryonic kidney 293 (HEK293) cells. PMAPTAC, PMT-5%, PMT-10% and DTPAC were dissolved in PBS with a concentration of 2.5 mg/ml, sterilized via filtration and further diluted with PBS to the desired concentrations. On the other hand, 2.5 mg/ml PDT-10% in 50% DMSO solution were sterilized via filtration and serially diluted two-fold with sterile water. Cells were seeded at a density of 10^4 cells per well in 96-well flat-bottomed microplates (Costar, Corning) and incubated with DMEM culture medium (supplemented with 10% FBS and 1% penicillin-streptomycin solution) for 24 hours. Thereafter, the culture medium was replaced with 180 µl of fresh medium and 20 µl of polymer solution in each well. The cells were incubated with the different concentrations of polymers and DTPAC for 24 hours at 37 °C, 5% CO_2 and 95% relative humidity before removal of the medium. 200 µl of fresh medium and 20 µl of filtered MTT solution (5 mg/ml in PBS) were further added and incubated with the cells for another 4 hours at 37 °C. Then, the supernatant was removed by aspiration, and resultant formazan crystals were dissolved in DMSO with shaking. The absorbance at 595 nm (A_{595}) was measured using a microplate reader (Tecan, Switzerland). Wells containing DMSO alone were used as a blank, and cells treated with PBS alone were used as control for the assay. Relative cell viability was expressed as (A_{595} sample − A_{595} DMSO)/ (A_{595} control − A_{595} DMSO) × 100%. For each sample, the final absorbance was the average of those measured from six wells in parallel. Since DTPAC was provided in 42 wt% in methanol and DMSO was used as solvent system for PDT-10% solution preparation, the toxicity of methanol and DMSO was also tested against the three kinds of cells after proper dilution. Methanol with the

same concentrations in tested DTPAC solutions and DMSO with the same concentrations in tested PDT-10% solutions showed no significant difference with control.

4.2.8. Statistical analysis

Statistical analysis was performed by ANOVA followed by Tukey's post-hoc test. The difference was considered to be significant at p-value < 0.05.

4.3. Results

4.3.1. Fabrication and characterization of QAS copolymers and coatings

Figure 4.3A illustrates the reaction scheme for the synthesis of QAS copolymers from two monomers, namely, [3-(methacryloylamino)propyl]trimethyl ammonium chloride (MAPTAC) and 3-trimethylsilylpropyl methacrylate (TMSPMA), with two different weight ratios. The synthesized copolymers, named PMT-5% and PMT-10%, derive their antimicrobial properties from the cationic quaternary ammonium group in MAPTAC while utilizing the silane functionality in TMSPMA as an anchor. $K_2S_2O_8$ functions as a free radical initiator for polymerization which proceeds via a free radical addition reaction involving the saturation of the α,β-unsaturated amide in MAPTAC and the α,β-unsaturated ester in TMSPMA. The unreactive silyl ether acts as a protective group for the silane functionality during this reaction. Subsequently, it is activated via hydrolysis in acidic medium which was achieved by dissolving the polymers in pH 2.5 acetic acid solutions. This yielded highly reactive silanol groups which readily undergo dehydration reactions involving the loss of water. Drying the acidified polymer solution under high temperatures of 130 °C gave rise to the formation of siloxane crosslinking amongst polymers as well as between polymers and the substrate surfaces where reactive groups present. Similarly, **Figure 4.3B** showed that PDT-10% was also synthesized via a free-radical polymerization

process from DMA-C_{16}Br and TMSPMA with AIBN as a free radical initiator. The quaternary ammonium moiety, DMA-C_{16}Br contains a 16-carbons long alkyl chain. The water solubility of PDT-10% is not very good, so acidified isopropanol was used to dissolve the polymer and facilitate the hydrolysis of silyl ether group. The synthesized copolymers appear yellow which is typical of the physical appearance of most QACs (216).

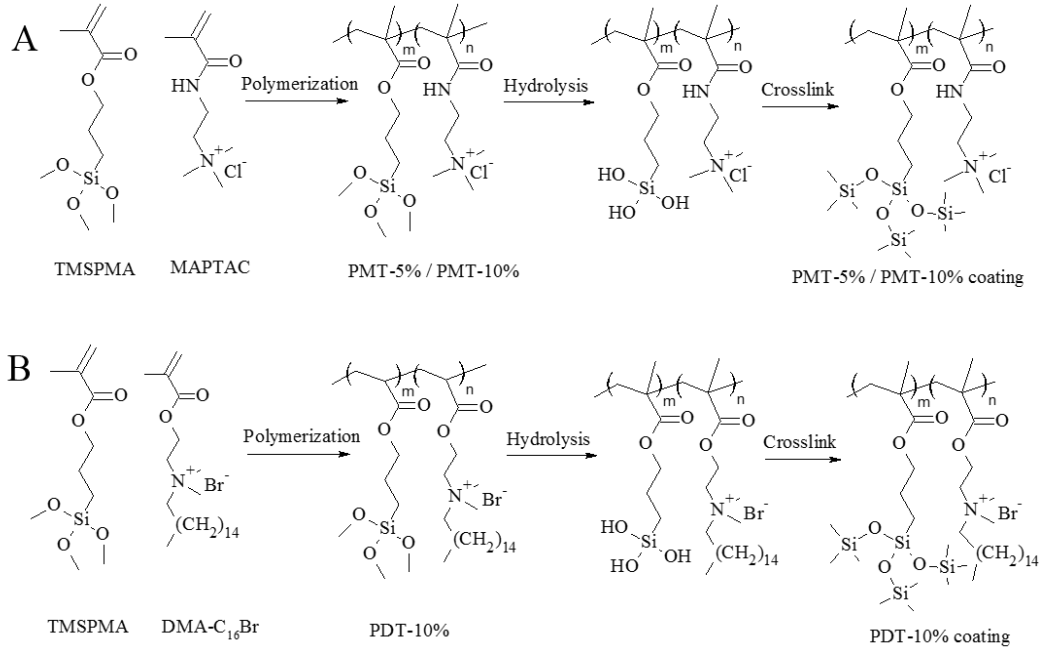

Figure 4.3 Synthesis scheme of QAS copolymers and coatings. (A) PMT-5% and PMT-10% and their coatings. (B) PDT-10% and its coating.

The ATR-FTIR spectra were used to monitor the PMT copolymer synthesis, extent of hydrolysis and condensation reactions undergone by the copolymers during the coating process (**Figure 4.4**). Characteristic stretches of the Si─O bond in alkoxysilane compounds appear as strong bands at 1090 cm^{-1} and sharp bands around 2840 cm^{-1} and in the copolymers' spectra, that is 2850 cm^{-1} in PMT-5%'s spectrum and 2842 cm^{-1} PMT-10%'s spectrum. The Si─O bond of silanol groups showed absorption as a single band at 915 cm^{-1}. These peaks confirmed the successful polymerization of the copolymers. Changes to the bands characteristic of the Si─O stretching vibration of the silyl ether supported the

inference that copolymer hydrolysis had occurred. Specifically, the disappearance of the sharp band at 2850 cm^{-1} in PMT-5%'s spectra and 2842 cm^{-1} in PMT-10%'s spectra can be observed. There was also a discernible reduction in the intensity of the strong band located at 1090 cm^{-1} in the copolymers' spectra after coating. As both bands were associated with the Si─O stretching vibration of the silyl ether group, these observations were consistent with the occurrence of hydrolysis. During the drying process, the formation of siloxane crosslink in the copolymer coatings restrained the stretching vibration of the carbonyl group in the ester functionality, causing the carbonyl stretch in the 1700 cm^{-1} region to disappear. Evidence for the successful crosslinking in the current study was thus shown by the disappearance of the carbonyl bands at 1718 cm^{-1} in PMT-10%'s spectra (**Figure 4.4B**). The reduction of the Si─O bond of silanol groups at 915 cm^{-1} indicated the existence of conversion of silanol groups to siloxane crosslink during drying process.

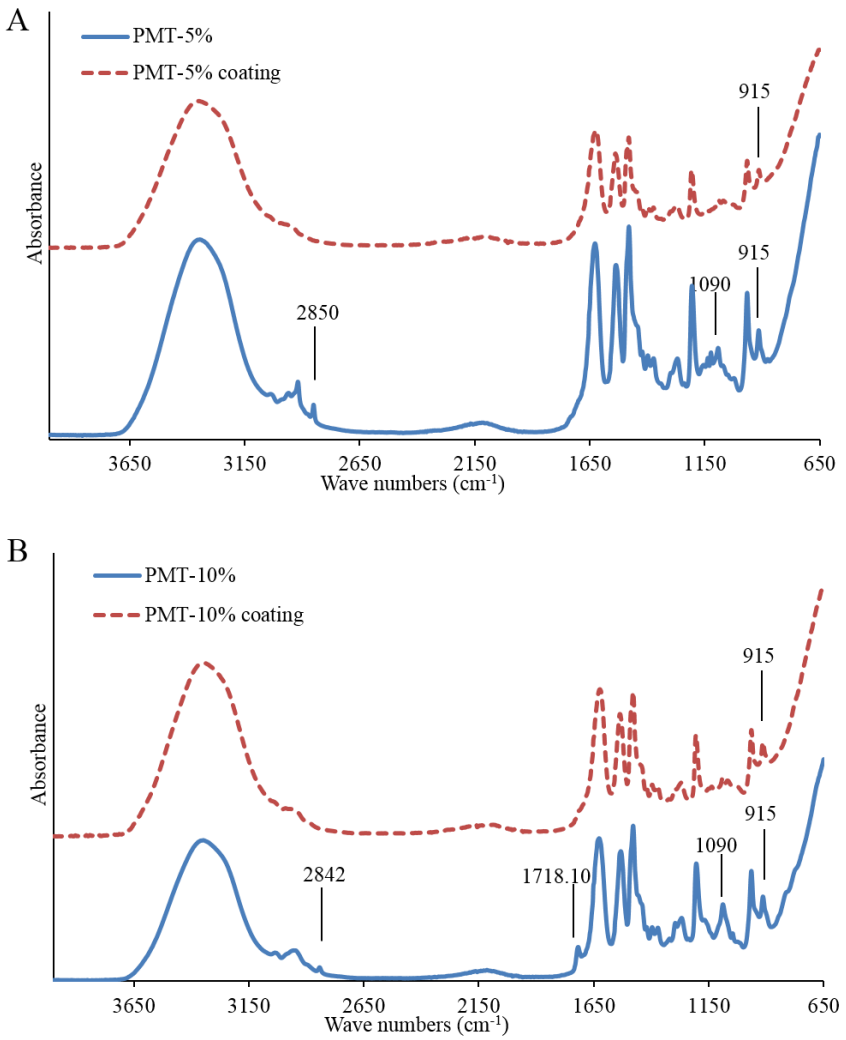

Figure 4.4 ATR-FTIR spectra of: (A) PMT-5% copolymer and coating; (B) PMT-10% copolymer and coating.

On the other hand, the synthesis of PDT-10% was characterized by the disappearance of 5.6 ppm and 6.1 ppm peaks in ^{1}H-NMR spectrum of PDT-10% when compared to DMA-C_{16}Br which corresponds to the terminal vinyl hydrogen (H^{a}, and H^{b}) of DMA-C_{16}Br, since vinyl carbons of DMA-C_{16}Br and TMAPMA would be saturated as a result of monomers joining together during polymerization (**Figure 4.5A**). ATR-FTIR spectroscopy was also used to monitor the synthesis and coating process of PDT-10%. Characteristic stretches of the Si─O bond of methoxysilane (–Si-O-CH_3) showed as a strong band at 1089 cm^{-1} in the spectra of PDT-10%. The peak disappeared after the coating as methoxysilane group was

subjected to hydrolysis and formation of siloxane crosslink during the coating process (**Figure 4.5B**).

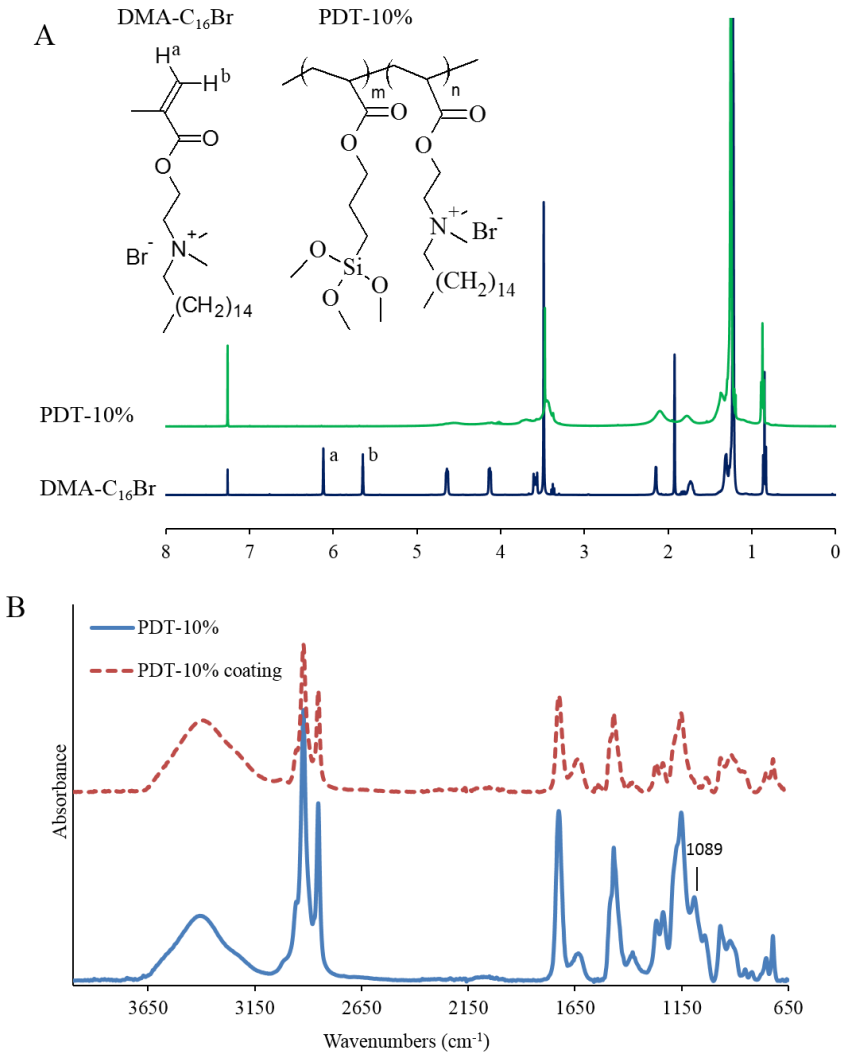

Figure 4.5 Characterization of PDT-10% and PDT-10% coating. (A) ^{1}H-NMR spectra overlay of DMA-C_{16}Br and PDT-10%. Disappearance of 5.6 and 6.1 ppm peaks on PDT-10% spectrum, which correspond to the terminal vinyl hydrogen (H^a, and H^b) on DMA-C_{16}Br, indicated free radical polymerization reaction had taken place. (B) ATR-FTIR spectra of PDT-10% copolymer and coating.

The thermal degradation of QAS polymers was investigated by using thermogravimetric analysis (**Figure 4.6**). The initial degradation temperature of PMAPTMC, PMT-5% and PMT-10% were found to range from 292 °C to 299 °C, while initial degradation

temperature of PDT-10% was 214.4 °C. The high degradation temperature indicated high thermal stability of the synthesized polymers.

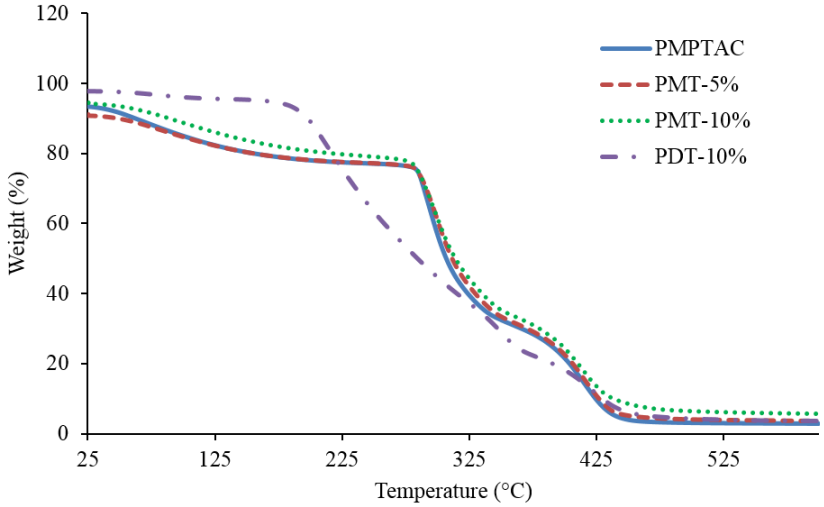

Figure 4.6 TGA of PMPTAC, PMT-5% and PMT-10% and PDT-10%.

The surface energy and hydrophobicity of QAS coatings were evaluated by static contact angle. **Figure 4.7** showed the contact angles of PMT-5%, PMT-10%, PDT-10% and the commercial antimicrobial agent DTPAC coatings against glass control, which can be considered as hydrophilic surface due to the low value (26.1°). The QAS coatings are more hydrophobic and have higher contact angle values than the glass control. Furthermore, the QAS copolymer PMT-5% and PMT-10% coated glass substrates have even higher contact angles (107.4° and 104.7°) than PDT-10% coating (83.6°) and DTPAC coating (80.9°).

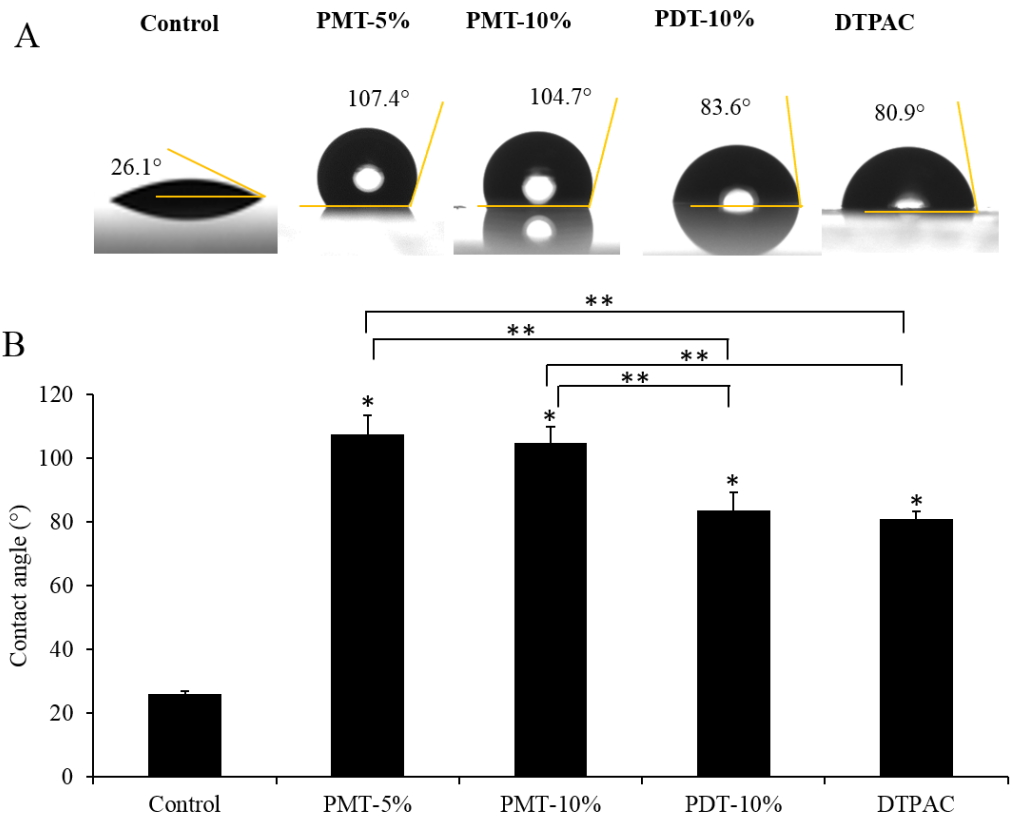

Figure 4.7 (A) Water droplets on the surfaces of uncoated and coated glass. (B) Contact angles of the surfaces of uncoated and coated glass. Data represents the standard deviation of at least three tested samples. *p*-value < 0.05 indicates statistically significant, and * shows significance between coated samples and control, while ** shows significance between different coated samples.

The durability of the QAS copolymer coatings were evaluated by abrasion test combined with ATR-FTIR analysis. As a control, coatings formed by MAPTAC homopolymer (PMAPTAC) and the commercial QAS monomeric antimicrobial agent, DTPAC were tested. As shown in **Figure 4.8**, the PMAPTAC coating shows a low retention of less than 20%. On the other hand, the corresponding copolymer (PMT-5% and PMT-10%) coatings with a silane anchor showed high retention of 81.3% and 92.5%, respectively. The other QAS copolymer with a silane anchor, PDT-10%, had a retention of 70.3% after abrasion test. It is noted that the coating retention of the monomeric QAS agent DTPAC was 42.5%, almost half of PMT copolymer coatings.

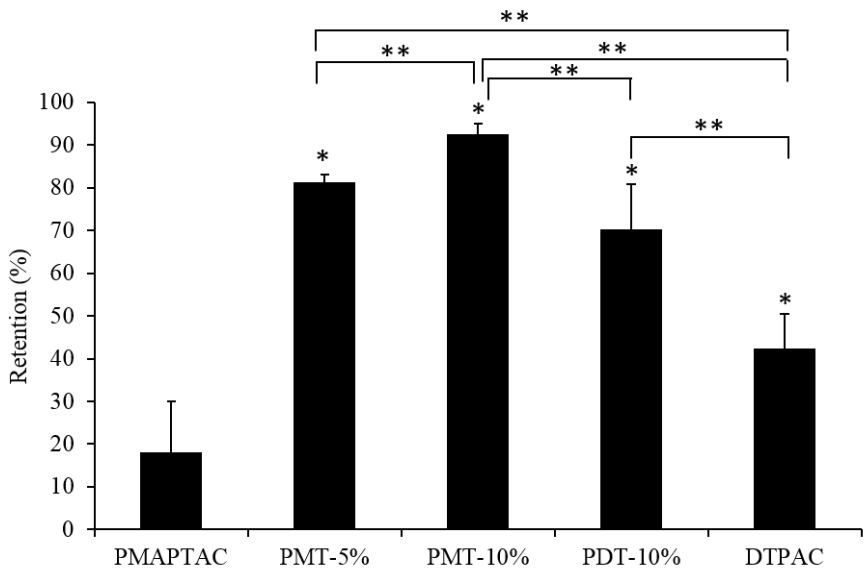

Figure 4.8 Retention of characteristic peaks of antimicrobial coatings after abrasion test. Data represents the standard deviation of three tested samples. *p*-value < 0.05 indicates statistically significant, and * shows significance between the QAS coated samples and PMAPTAC coated samples, while ** shows significance between different QAS coated samples.

4.3.2. Antimicrobial efficacy of QAS in solutions

The antimicrobial activities of the synthesized polymers together with DTPAC were tested against Gram-positive bacteria *S. aureus*, Gram-negative bacteria *E. coli* and fungus *C. albicans*. As shown in **Table 4.1**, the synthesized PMT polymers had MICs in the range of 62.5 to 125 µg/ml against *E. coli* and *S. aureus* and > 500 µg/ml against *C. albicans*. A comparison of the antibacterial activity of PMT-5% and PMT-10% to that of PMAPTAC revealed a similar minimum inhibitory concentration (MIC) and minimum bactericidal concentration (MBC) values of 62.5 µg/ml with the sole exception of PMT-5% displaying slightly lower activity against *E. coli* at 125 µg/ml. The similar MIC of PMAPTAC with that of PMT-5% and PMT-10% provided evidence that the copolymerization of quaternary ammonium monomer (MAPTAC) with TMSPMA did not affect its antimicrobial activity. Another notable aspect of the QAS copolymers' antimicrobial activity is their comparable efficacy against both *S. aureus* and *E. coli*, as evidenced by their similar MIC values. PMT-

5% required only a concentration twice its MIC against *S. aureus* to inhibit the growth of *E. coli* while PMT-10% inhibited the growth of both bacteria at the same concentration. On the other hand, although the monomeric QAS agent DTPAC and PDT-10% has a lower MIC value against *S. aureus* than that of the synthesized QAS polymers, their MIC values against *E. coli* are comparable. PDT-10% and DTPACT shared the similar MIC values against *S. aureus* and *E. coli*. In addition, the MBC:MIC ratios for all the QAS compounds and bacteria are ≤ 4, indicating the antimicrobial mechanism of action is bactericidal rather than bacteriostatic (217). However, the copolymers were less effective against the fungus *C. albicans*. PMT polymers failed to inhibit fungus growth even at higher concentrations of > 500 µg/ml, while PDT-10% and DTPAC showed effective against *C. albicans* with a MIC value of 125 and 15.6 µg/ml, respectively.

Table 4.1 MIC and MBC/MFC against *E. coli*, *S. aureus* and *C. albicans* at an inoculum size of approximately 10^5 CFU/ml. The unit of the MIC and MBC/MFC values is µg/ml.

Microorganisms		PMAPTAC	PMT-5%	PMT-10%	PDT-10%	DTPAC
S. aureus	MIC	62.5	62.5	62.5	7.8	3.9
	MBC	250	125	125	7.8	3.9
E. coli	MIC	62.5	125	62.5	62.5	62.5
	MBC	62.5	125	62.5	62.5	62.5
C. albicans	MIC	> 500	> 500	> 500	125	15.6
	MFC	> 500	> 500	> 500	>125	62.5

4.3.3. Cytotoxicity assay of QAS in solutions

The cytotoxicity of QAS polymers were tested against HDF, HaCaT keratinocytes and HEK293 cell lines. Human cells' viability predictably decreased with increasing concentration of PMAPTAC, PMT-5%, PMT-10%, PDT-10% and DTPAC (**Figure 4.9**) as quaternary ammonium polymers possess membrane-disruption ability (218). Here, LC50 (the concentration that is lethal to 50% of the cells) was further used to evaluate the

different QAS compounds. The LC50 values of PMAPTAC, PMT-5% and PMT-10% PMT-5% against HDF and HEK 293 cells were all ≥ 62.5 µg/ml, while the value for PDT-10% and DTPAC were > 31.3 µg/ml and > 15.6 µg/ml, respectively. For the test with HaCaT keratinocytes, PMT-5% showed a LC50 value of 31.3 µg/ml, PMAPTAC and PMT-10% > 62.5 µg/ml, PDT-10% > 15.6 µg/ml, while DTPACT > 7.81 µg/ml.

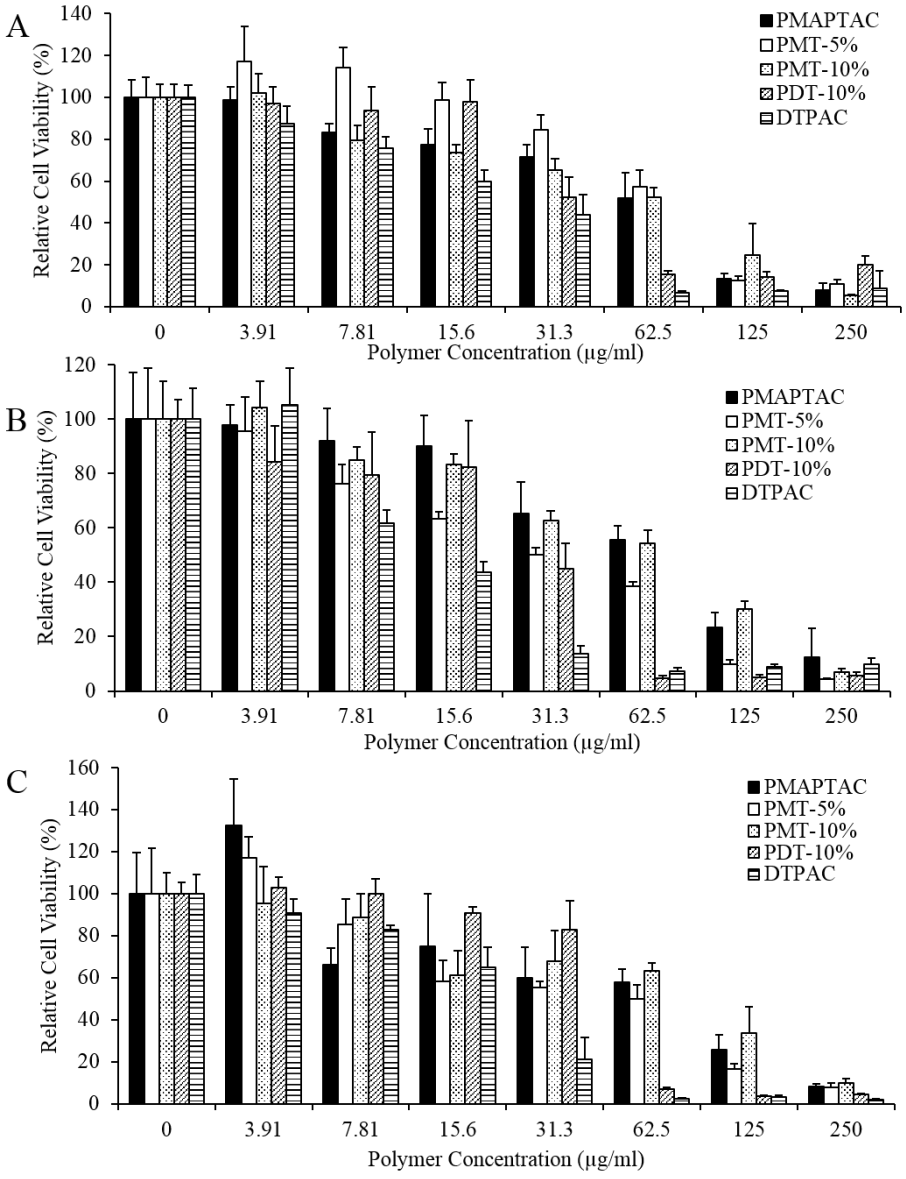

Figure 4.9 Relative human cell viability after 24 hours' exposure to different PMAPTAC, PMT-5%, PMT-10%, PDT-10% and DTPAC concentrations: (A) HDF, (B) HaCaT keratinocytes, and (C) HEK 293 cells.

4.3.4. Antimicrobial efficacy of QAS coatings

We further tested the antimicrobial activity of the QAS copolymers when they were coated on glass substrates. In comparison, blank glass substrates and coatings formed by the monomeric QAS antimicrobial agent, DTPAC were used as controls.

As shown in **Figure 4.10**, the QAS coatings of PMT-5% (10 mg/ml), PMT-10% (10 mg/ml), PDT-10% (5 mg/ml) and DTPAC (10 mg/ml) were all very effective against *S. aureus* and *E. coli* with log reduction values higher than 4. In fact, there were no viable bacterial recovered from all the QAS coated samples after 24 hours. However, when a lower concentration of DTPAC (5 mg/ml) was used for the coating, the resulting coating was still very effective (with log reduction value higher than 4) against *S. aureus* but less effective against *E. coli* (with log reduction value of 1.5). On the other hand, the antimicrobial activities (i.e., log reduction value) of PMT-5% (10 mg/ml), PMT-10% (10 mg/ml) and PDT-10% (5 mg/ml) coatings against *C. albicans* were all no less than 2, while the values of DTPAC coatings were only 0.2 no matter the concentration of coating solution is 10 mg/ml or 5 mg/ml. According to the test for measuring the antimicrobial activity of surfaces, significant antimicrobial effectiveness is defined as antimicrobial activity ≥ 2.0 after 24 hours. Therefore, QAS copolymeric coatings showed significant antimicrobial effectiveness against all the three microorganisms, while DTPAC were only effective against *S. aureus* and *E. coli*, but not effective against *C. albicans*.

A

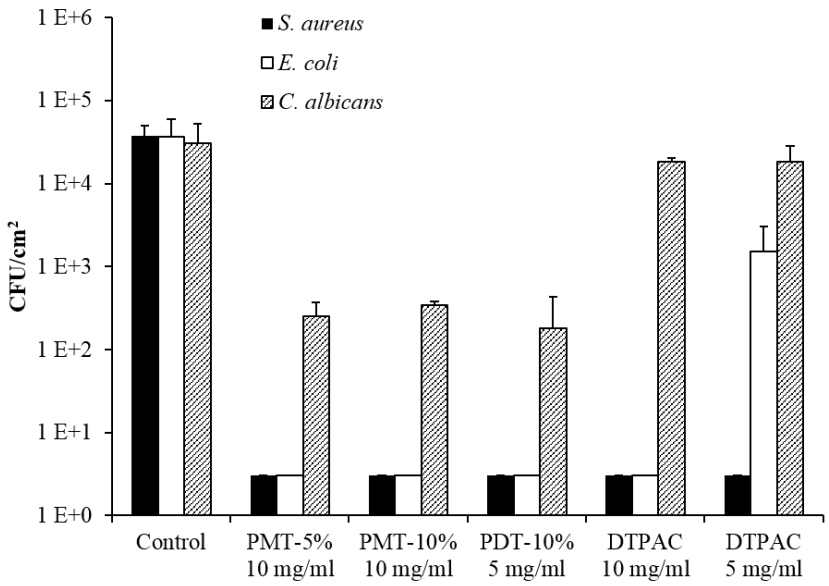

B

	S. aureus	*E.coli*	*C. albicans*
PMT-5% 10 mg/ml	4.1	4.1	2.1
PMT-10% 10 mg/ml	4.1	4.1	2.0
PDT-10% 5 mg/ml	4.1	4.1	2.2
DTPAC 10 mg/ml	4.1	4.1	0.2
DTPAC 5 mg/ml	4.1	1.4	0.2

Figure 4.10 Viable microbial counts of QAS coatings against *S. aureus*, *E. coli* and *C. albicans* after 24 hours of exposure to coated glass cover slips (A) and the corresponding numeric values of log reduction (B).

4.4. Discussion

Microbial contamination and subsequent biofilm formation is a major cause of infection, contamination, and product deterioration. Considering it is very difficult to remove the biofilm after its formation, a useful strategy is to prevent biofilm formation before it starts. QAS agents can be used to coat various substrates to impart the products with antimicrobial property to prevent the microbial contamination (208). To reduce the toxicity of the QAS monomeric agent while keeping its antimicrobial efficacy and coating simplicity, we designed the novel QAS copolymers from a quaternary ammonium containing monomer and a silane

containing monomer. The polymerization process is simple, potentially easy to scale up. At the same time, the coating process of the copolymers to a surface can remain the same to that of QAS monomeric agents, which doesn't need elaborate techniques. The monomer used for PMT-5% and PMT-10% synthesis, MAPTAC is a commercial agent and was used as proof of concept for copolymer synthesis. On the other hand, DMA-C_{16}Br is a customized monomer with a long 16-carbons long alkyl chain with an expectation to possess a better antimicrobial activity, since quaternary ammonium compounds were regarded to have the best antimicrobial activity with suitable long alkyl chains (C12-16) (219).

The QAS polymer coatings were characterized by using ATR-FTIR and further confirmed by contact angle measurement. It was shown that the QAS copolymer coatings increased the hydrophobicity of the glass surfaces. PDT-10% and DTPAC coatings resulted in similar hydrophobicity of the glass surfaces, while PMT-5% and PMT-10% coatings showed an even higher hydrophobicity. The hydrophobicity of the PDT-10% coating may mainly result from reorientation of the long alkyl groups (tail) of the silane compounds, just like what was suggested for DTPAC coatings (220, 221). On the other hand, PMT-5% and PMT-10% copolymers increased the hydrophobicity of the coated surface even more, which may be due to the formation of the long alkyl chains of the synthesized polymers.

Durability and non-leaching property are critical factors for antimicrobial coatings to provide long-lasting antimicrobial performance without toxicity concerns. Abrasion test showed that the QAS copolymer coatings became much more resistant to abrasion with TMSPMA containing siloxane linkages, which can anchor the substrate by covalent bonding other than physical attachment. The improved resistance of PMT-10% against abrasion over PMT-5% should be attributed to the

higher TMSPMA content which provided more "anchors" with the coated substrates. Considering this, PDT-10% was designed from DMA-C_{16}Br together with 10% TMSPMA. Furthermore, the QAS copolymers also showed more resistant to abrasion than the QAS monomeric agent DTPAC. The retention of PDT-10% and DTPAC coating were further evaluated after 100 cycles of abrasion test, and it was shown that PDT-10% still had a retention of 62.0 ± 9.9%, while the peaks for DTPAC was not detectable. Actually, at the same concentration, DTPAC has a much greater amount of methoxysilane groups but non-specific siloxane bond formation may happen between DTPAC molecules instead of with the glass substrate. Thus, this *in situ* polymerization could cause most of the non-specific DTPAC polymers to be removed after abrasion test. On the other hand, the synthesized QAS copolymers possess long "fiber-like" structure that could possibly further cross-link with each other and formed a mesh network during the coating process. Then, the complex mesh network was subsequently grafted onto the substrate. Therefore, the formation of this complex mesh network could explain the enhanced resistance of the QAS copolymer coatings during abrasion test (**Figure 4.11**).

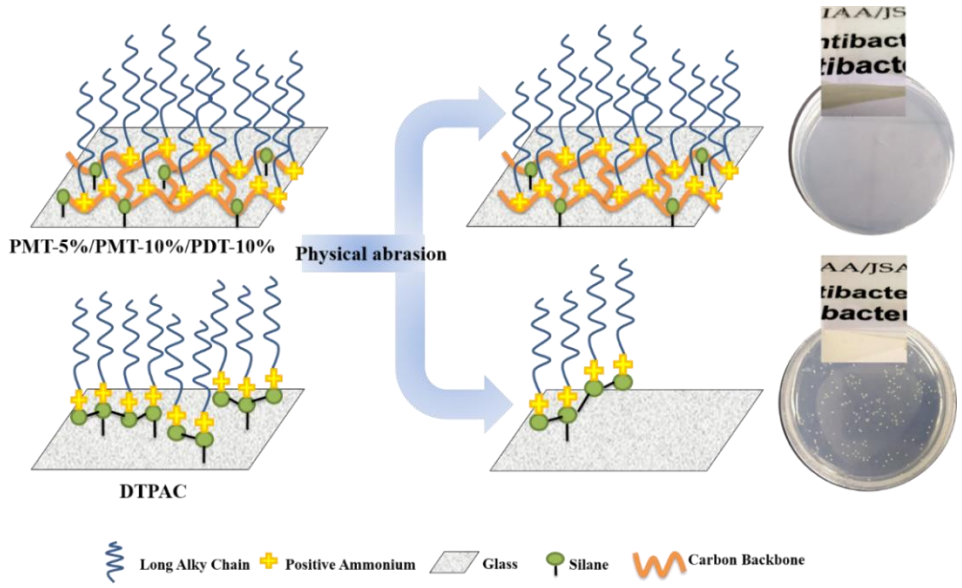

Figure 4.11 Graphic illustration that the novel QAS antimicrobial copolymers (PMT-5%, PMT-10% and PDT-10%) exhibited improved biocompatibility as compared to the commercial antimicrobial QAS monomer (DTPAC). The copolymers can form transparent and durable coatings via a facile thermal-curing process.

Crucial characteristics of polymers intended for the use as antimicrobial materials in household, industrial and clinical applications include not only the presence of antimicrobial activity but also the absence of toxicity to human cells. Differential cytotoxicity to microbial cells and human cells should invariably be addressed when evaluating of the QAS copolymers for future *in vivo* applications. LC50 values clearly showed that PMT-5% and PMT-10% were less toxic than PDT-10%, while PDT-10% was less toxic than the commercial QAS agent, DTPAC. The human cell toxicity of the QAS compounds were thus negatively correlated with their antimicrobial activity against *S. aureus* and *C. albicans* in solution, although the MIC values of these QAS compounds against *E. coli* were similar at 62.5 μg/ml. These findings suggest that our synthesized QAS copolymers are less toxic to human cells than the commercial QAS monomeric agent, DTPAC. So the synthesized QAS copolymers are supposed to be safer than DTPAC during handling.

The MIC and MBC/MFC tests showed that the QAS copolymers are less effective than the commercial QAS monomeric agent, DTPAC, especially against fungus *C. albicans*. However, results from the MIC and MBC/MFC tests represent the QAS compounds' antimicrobial activity in solution and are not direct indicative of their properties upon coating (184, 194). Hence, antimicrobial testing with the QAS copolymer treated surfaces were carried out. The results showed that antimicrobial efficacy of both QAS copolymer (PMT-5% and PMT-10%) coatings are as effective as that of QAS monomeric agent (DTPAC at 10 mg/ml) coating against *S. aureus* and *E. coli*. For a better comparison between PDT-10% and DTPAC, DTPAC coating was also carried out at the same coating solution concentration of 5 mg/ml as that of PDT-10% coating, but it lost the effectiveness against *E. coli* (log reduction less than 2) although the effectiveness against *S. aureus* remained. Furthermore, the antimicrobial result of QAS coatings against *C. albicans* was different from that of QAS solutions. DTPAC, the monomeric QAS agent was not effective against *C. albicans* upon coating although it was effective against *C. albicans* in solutions. More interestingly, the QAS copolymers were effective against *C. albicans* upon coating on glass surfaces, although PMT-5% and PMT-10% were ineffective against *C. albicans* and PDT-10% are less effective than DTPAC in solutions.

Our results further confirmed previous observation that antimicrobial activity in solution are not direct indicative of their real property upon attachment to a surface (184, 194). High surface concentration of antimicrobial groups (cationic quaternary ammonium groups) may make surface-attached polymers bactericidal/fungicidal to microbes resistant to these polymers in solution (184). Although PMT-5% and PMT-10% do not possess the long alkyl chain as PDT-10% and DTPAC, a higher hydrophobicity was obtained with PMT-5% and PMT-10% copolymer coatings,

which may lead to higher resistance to bacteria adherence (221). Furthermore, the QAS copolymer coatings are supposed to have a higher mobility compared to monomeric QAS agent because of their long flexible alkyl backbone chain pendent with cationic quaternary ammonium groups, which may have impact on the antimicrobial activity as well.

After antimicrobial experiment, the substrates were rinsed and dried, then subjected to ATR-FTIR testing again to check the durability of QAS coatings after bacterial challenge. The characteristic peak of copolymers still remained even though the coatings have experienced vigorous solution mixing and rinsing during the previous antimicrobial assays. It not only demonstrated strong adhesion of polymer coatings, but also the high stability of the polymer coatings. Ideally, the activity of these QAS coatings shall be permanent because their quaternary ammonium groups are not consumed during the biocidal process.

The QAS copolymers are expected to be able to be coated on a large range of substrates and exhibit durable antimicrobial activities similar to other QAS monomeric compounds (222). The coating on glass serves as a proof of concept. Glass has many applications, including packing, windows, optical lenses and medical devices. Our studies have demonstrated the low toxicity of the QAS copolymer and the superior antimicrobial efficacy of QAS copolymer coatings on the glass surfaces, which are expected to provide a long-lasting effect in inhibiting microbial infection.

4.5. Conclusion

Novel antimicrobial QAS copolymers, namely, PMT-5%, PMT-10%, and PDT-10%, have been successfully synthesized. The synthesis process is not labor-intensive or

costly, rendering their production potentially feasible on the industrial scale. Cytotoxicity assays with HDF cells, HaCaT keratinocytes and HEK293 cell lines indicated that the QAS copolymers are less toxic to human than a commercial QAS monomeric antimicrobial agent. Moreover, QAS copolymers were capable of forming effective antimicrobial coatings against both bacteria (*S. aureus* and *E. coli*) and fungus (*C. albicans*) via a facile thermal-curing process. Abrasion resistant results showed that QAS copolymer coatings were more durable than a coating formed by DTPAC. The new QAS copolymers have a great potential to be used as a safer substitute for the current monomeric QAS coating agents.

Chapter 5 Fabrication of antimicrobial microneedles with a QAS copolymer coating

5.1. Introduction

Microneedle-based drug delivery systems are not equivalent to conventional transdermal patches, in that they are not simply applied to the surface of skin. Microneedles function principally by breaching the protective barrier of skin, the *stratum corneum*, and often penetrate into the viable epidermis and dermis (223). The *stratum corneum* can prevent the foreign materials, including microorganisms, from entering the body. As such, one of the most important factors limiting the clinical usage of microneedles is the risk of infection because of the compromised *stratum corneum*. Microneedle treatment was found to permit the permeation of bacteria by means of various *in vitro* models, including Silescol membranes, excised porcine skin and mouse skin, although the extent of the permeation was not greater than that enabled by hypodermic injection (87, 88). In addition, microorganisms were shown to adhere to microneedles after its application (87). Therefore, inappropriate reuse of microneedles will increase the risk of infection. Furthermore, clinical trials that demonstrated lack of infection with microneedle usage recruited healthy volunteers and prior to application of microneedle arrays, skin treatment sites were typically cleansed with alcohol wipes to reduce the skin's microbial bioburden. However, the infection risk of microneedles in immunocompromised patients is unknown (89). As such, it is suggested that patient safety would be enhanced by manufacturing microneedles using sterile techniques. The risk of infection associated with microneedles use may also be reduced by imparting microneedles with antimicrobial properties.

Some polymeric microneedles can have antimicrobial effect because of the material itself (224). For other microneedles, antimicrobial properties can be achieved by coating the

microneedles with thin films of antimicrobial materials. Gittard *et al.* reported a silver coated antimicrobial ceramic microneedles by using a physical vapour deposition technique. An agar plating method demonstrated the efficacy of the silver-coated microneedle array against *S. aureus* (225). However, this antimicrobial system is leachable, which may lose the antimicrobial activity gradually and cause environmental issues. Besides, bacteria resistance may be a problem as well, because silver's broad-spectrum antimicrobial activity is attributed to the inhibition of DNA replication, expression of ribosomal and other cellular proteins, and disruption of the bacterial electron transport chain (226-229). Similarly, Gittard fabricated antimicrobial polymeric microneedles with silver and zinc oxide coatings, which were intended for the treatment of local skin infections (230). Microneedles coated or incorporated with other antimicrobial materials have also been reported but were designed for treatment purpose. For example, amphotericin B were coated on Gantrez® AN 169 microneedles by piezoelectric inkjet printing for the treatment of cutaneous fungal infections and cutaneous leishmaniosis (231). Antifungal pharmaceutical agent, voriconazole was loaded on polyglycolic acid microneedles by a similar coating method (232). Green tea extract was incorporated inside hyaluronic acid microneedles to reduce wound infection (233).

In Chapter 4, we described the development of some novel QAS copolymers and demonstrated their antimicrobial effectiveness upon coating. These compounds contain the antimicrobial quarternary ammonium component and a methoxysilane group, capable of being immobilized on surfaces to form a durable coating. In this chapter, one of these QAS copolymers, PDT-10% was used to form a permanent antimicrobial coating on 3M MSS. 3M MSS is provided in a sterile state, but it is accessible by end users for home usage. So reuse is quite possible on uncleansed skin. The antimicrobial coating is not designed for treatment purpose, but to prevent possible risk of infection during microneedle application

and in the case of inappropriate microneedle reuse. We hypothesize that PDT-10% can be successfully coated on the microneedles and the coating is effective, durable and safe.

5.2. Materials and Methods

5.2.1. Materials

PDT-10% was synthesized in house referring to Chapter 5. Isopropanol is purchased from Tedia, USA. Acetic acid is purchased from Merck, USA. Rhodamine B was purchased from Alfa Aesar, UK. The source of materials for antimicrobial test and cell culture were the same with that used in Chapter 5.

5.2.2. Preparation of PDT-10% coated microneedles

5 mg/ml of PDT-10% coating solution was solubilized in a mixture containing 90% of isopropanol and 10% of acetic acid solution (pH 2.5) following by heating at 50 ˚C for 30 min. Before coating, 3M MSS microneedle array was primed with oxygen plasma in a plasma cleaner for 3 min to render them hydrophilic. Then 90 µl of the PDT-10% coating solution was transferred to the treated microneedle array and the array was heated at 50 ℃ for 1 h to ensure the coating of PDT-10% on the needles. The coated needles were washed under tap water for 10 seconds, and the washing was repeated for 5 times with 10 seconds' interval between each washing before drying again in oven. 1 mg/ml and 0.2 mg/ml of PDT-10% coating solution was further prepared and was used to coat 3M MSS for antimicrobial and cytotoxicity test.

5.2.3. Characterization of PDT-10% coating on microneedles

SEM was applied to analyze the microneedle morphology change after coating followed by energy dispersive X-ray spectrometer (EDS) characterization. Platinum sputtering was

applied to coat the samples at 10 mA for 180 s. The analysis was performed on FE-SEM (JSM-6700F, JEOL, Japan) equipped with Oxford Instruments INCA X-ran microanalysis system (EDS).

Rhodamine B staining method was used as an indirect method to characterize the change of microneedle surface property after PDT-10% coating. The coated microneedle array was flood-stained with 90 µl of 1 mg/ml rhodamine B solution and dried at 50 °C for 1 h, then the microneedles were observed under a stereomicroscope. To exclude that coating solvent of PDT-10% will not change the microneedle properties, microneedle arrays that experienced plasma treatment and flood-coating of a mixture containing 90% of isopropanol and 10% of pH 2.5 acetic acid solution were used as negative control.

ATR-FTIR was used to monitor the crosslinking reaction between the microneedle array and PDT-10%. The back of the microneedle array has a flat surface and was used for this characterization. The back of the microneedle array was coated with PDT-10% in the same way as described above for microneedles and then subjected to ATR-FTIR examination. Infrared spectra were collected between 4000 and 650 cm^{-1} at a resolution of 4 cm^{-1}.

5.2.4. Durability of PDT-10% coating on microneedles

In order to evaluate the durability of PDT-10% coating on microneedles, the coated microneedles were applied on human dermatomed skin at a force of 22.2 N for 20 times, then the microneedles were subjected to rhodamine B staining for characterization.

5.2.5. Antimicrobial assays of QAS copolymers and coatings

S. aureus was grown to their exponential phase and appropriately diluted in 0.3% agar slurry to achieve the standard inoculum size around $4 – 7 \times 10^6$ CFU/ml. The agar slurry was prepared in 0.85% NaCl solution and autoclaved before use. Then 100 µl of the

bacterial agar slurry was added on the PDT-10% coated microneedles and spread with pipette tips to ensure the good contact. Uncoated microneedles were used as controls. Bacteria recovery was carried out after incubation at 37 °C in humidified condition for 24 hours. Inoculated bacteria were recovered by placing the tested microneedles into 50 ml Falcon tubes containing 10 ml of PBS with 0.5% Tween 80. The tubes were sonicated for 1 min in an ultrasonic water bath (Ultrasonic LC60H, Fisher Scientific) and then vortexed for 1 min before serially diluting the samples in the Tween 80 containing PBS. A viable count was conducted using the spread plate method after appropriate dilution. The CFUs were counted and the antimicrobial activity was expressed as log reduction number of the microorganisms after 24 hours compared with control. If no colony was found on the plate even at the lowest dilution time, then the count was taken as one for calculation.

5.2.6. Cytotoxicity assay

The biocompatibility of the coated microneedles was evaluated by testing their cytotoxicity against HDF and HaCaT keratinocytes using MTT assay. Microneedles coated with different concentrations of PDT-10% were extracted in 3 ml of PBS at 37 °C for 24 hours. Cells were seeded at a density of 10^4 cells per well in 96-well flat-bottomed microplates (Costar, Corning) and incubated with DMEM culture medium (supplemented with 10% FBS and 1% penicillin-streptomycin solution) for 24 hours. Thereafter, the culture medium was replaced with 180 µl of fresh medium and 20 µl of microneedle extraction solution in each well. For control group, 180 µl fresh culture medium and 20 µl of PBS were added. The culture medium was removed after 24 hours of incubation. Then 20 µl of fresh medium and 20 µl of sterile MTT solution (5 mg/ml in PBS) were further added. After another 4 hours of incubation at 37 °C, the supernatant was removed by aspiration, and resultant formazan crystals were dissolved in 150 µl of DMSO with shaking. The absorbance at 570

nm was measured using a microplate reader (Tecan, Switzerland) with 650 nm as reference wavelength. Relative cell viability was represented as the percentage of the control group.

5.3. Results

5.3.1. Preparation and characterization of microneedles coated with PDT-10%

Figure 5.1 showed that the contact angle of microneedle back surface was reduced from around 78° to 20° after plasma treatment, which means that plasma treatment rendered the surface more hydrophilic. The plasma activated microneedles were further coated with PDT-10%.

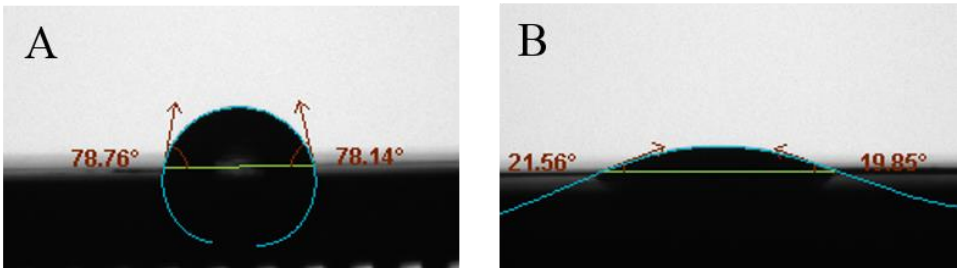

Figure 5.1 Contact angles of the back surface of microneedle array. (A) Untreated surface. (B) After plasma treated for 3 min.

We further evaluated how long this effect would last. **Figure 5.2** indicates that the contact angle only increased with time slightly after plasma treatment. This ensured enough working time for the following coating work.

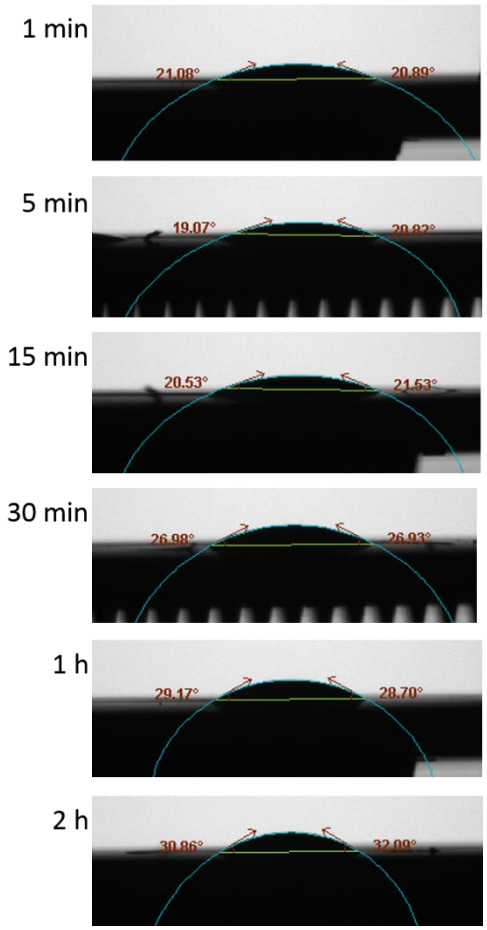

Figure 5.2 Change of contact angle with time after plasma treatment.

The appearance of the PDT-10% coated microneedles remained the same white colour as control and no difference was observed under stereomicroscopy (up to 12.25 times magnification) compared with control microneedles. By using SEM, a high magnification of microneedles was shown. It was shown in **Figure 5.3** that the surface of PDT-10% coated microneedles was rougher than the control microneedle. The change of surface property may be mainly due to the PDT-10% coating. The EDS analysis demonstrated the existence of bromine atom on the coated microneedles, which further confirmed the successful coating of PDT-10% on microneedles.

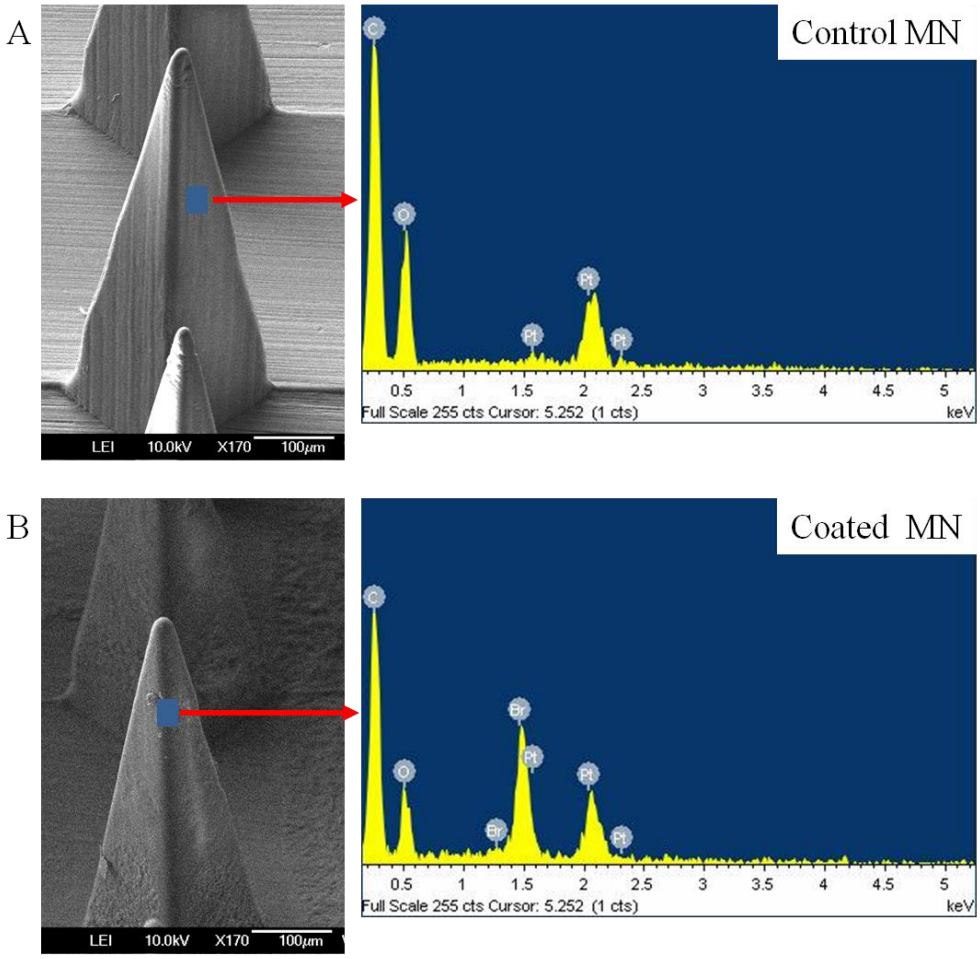

Figure 5.3 SEM/EDS analysis. (A) Control microneedles. (B) Microneedles coated with PDT-10%.

Rhodamine B staining method was used as an alternative method to characterize the change of surface property of microneedles after PDT-10% coating. **Figure 5.4A** showed that rhodamine B only accumulated at the base of the needles and did not stain on the tips of control needles. On the other hand, the whole needle body was stained with rhodamine B on PDT-10% coated microneedles (**Figure 5.4B**), which indicated that the tips of microneedles were successfully coated with PDT-10% by the flood coating method. After 20 times of penetration test on skin, the PDT-10% coated microneedles were well stained by rhodamine B as well (**Figure 5.4C**). This indicated that the PDT-10% coating was not removed during the multiple penetration of microneedles into skin.

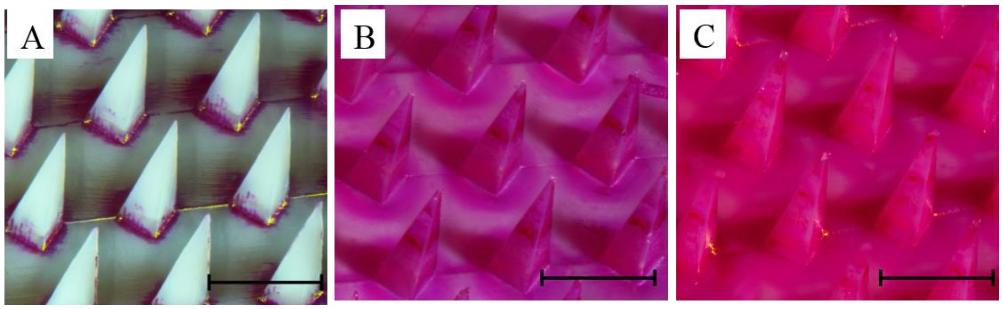

Figure 5.4 Characterization of microneedle surface by rhodamine B coating method. (A) Negative control microneedles. (B) PDT-10% coated microneedles. (C) PDT-10% coated microneedles after 20 times of penetration test on skin. Scale bars represent 500 μm.

ATR-FTIR demonstrated that the coating of PDT-10% on microneedles was not physical deposition, but by forming chemical bonds (**Figure 5.5**). PDT-10% has a strong peak at 1089 cm^{-1} which is the characteristic stretch of the Si─O bond of methoxysilane (–Si-O-CH_3). The formation of siloxane crosslink during the coating process was confirmed by the disappearance of the 1089 cm^{-1} peak after coating, because methoxysilane group was subjected to hydrolysis and formation of siloxane crosslink during the coating process. The ATR-FTIR also showed that the PDT-10% was not washed away as indicated by the similar profiles before and after washing.

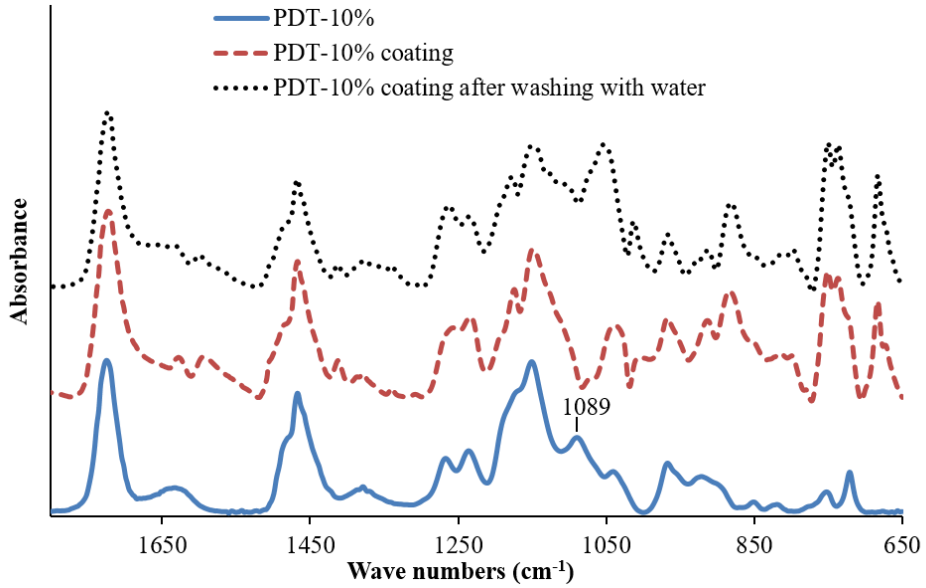

Figure 5.5 FTIR characterization of PDT-10% coating on microneedles.

5.3.2. Antimicrobial test

As shown in **Figure 5.6**, the antimicrobial efficacy of the PDT-10% coated microneedles depended on the concentration of the PDT-10% coating solution and varied against different microbial species. It was shown that microneedles coated with 5 mg/ml and 1 mg/ml of PDT-10% displayed excellent antimicrobial activity against *S. aureus* and *C. albicans* with log reduction more than 2. The antimicrobial activity against *E. coli* was less effective than that against *S. aureus* and *C. albicans*, with log reduction at 1 when microneedles were coated with 5 mg/ml of PDT-10%.

A

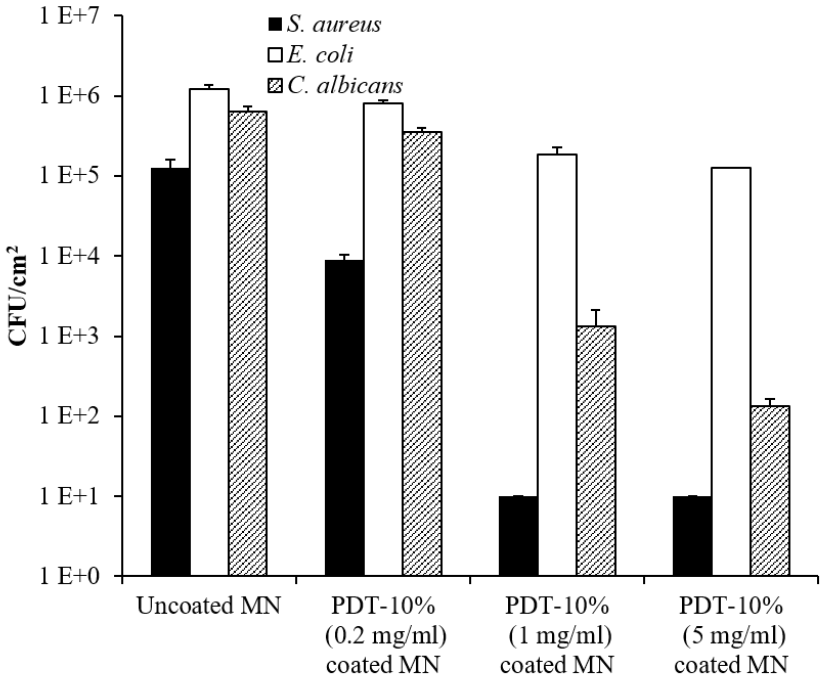

B

	S. aureus	*E. coli*	*C. albicans*
PDT-10% (0.2 mg/ml) coated MN	1.2	0.2	0.2
PDT-10% (1 mg/ml) coated MN	**4.1**	0.8	**2.7**
PDT-10% (5 mg/ml) coated MN	**4.1**	1.0	**3.7**

Figure 5.6 Viable bacterial counts of PDT-10% coated microneedles (MN) against *S. aureus*, *E. coli* and *C. albicans* after 24 hours of exposure (A) and the corresponding numeric values of log reduction (B).

5.3.3. Cytotoxicity test

After incubation with the extract of PDT-10% coated microneedles for 1 day, no significant difference in cell viability was observed as compared to controls (**Figure 5.7**). It indicated that PDT-10% coated microneedles were not toxic to either HaCaT keratinocytes or HDF cells.

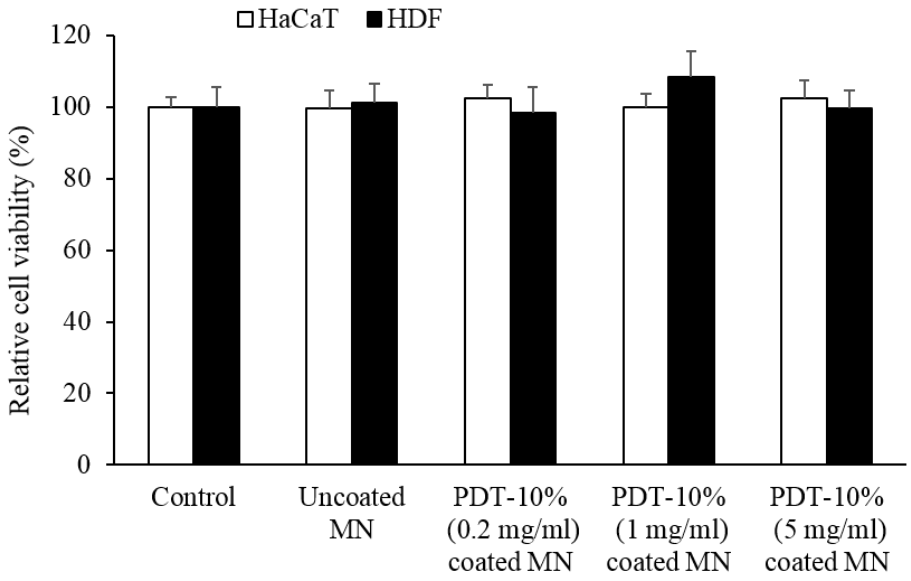

Figure 5.7 Relative human cell viability after 24 hours of exposure to the extract of PDT-10% coated microneedles (MN)

5.4. Discussion

Quaternary ammonium silane compounds have been used for a long time by offering a surface protection method without addition of chemicals to the environment (222). Our synthesized QAS copolymers demonstrated a lower toxicity as well as superior and durable antimicrobial activity upon coated on glass surface (234). PDT-10% showed a superior antimicrobial activity among these QAS copolymers and it was further proposed to confer the microneedles (3M MSS) with antimicrobial activity. 3M MSS is injection molded from liquid crystal polymers (LCP) due to their excellent properties, e.g., high mechanical properties, high temperature resistance,

chemical stability and good biocompatibility (235). However, the low surface energy of the LCP polymer and the resulting poor adhesion of additional coatings make it difficult to be coated. On the other hand, low pressure and low temperature non-equilibrium plasma activation is a suitable method for pre-treating the surface of many polymers. The excited species of the plasma can modify most polymer surfaces to a depth of several nanometers to achieve desired polarities while maintaining the bulk properties, regardless of their substrate pattern geometry and chemical reactivity (236).

It was observed that the plasma treatment lowered the contact angle of the microneedle back surface. This is because the plasma can activate the polymer surface to generate more oxygen-containing functional groups (such as –OH and –OOH) on the polymer surface thus increasing the hydrophilicity of the surface (237). The same reactive functional groups are expected to exist on the needle surface after plasma treatment, which can then form crosslink with the silane group of PDT-10%. The crosslink process was confirmed by FTIR characterization. SEM and indirect rhodamine B characterization further indicated the change of the microneedle surface properties after PDT-10% coating. Besides, the PDT-10% coating was durable as indicated by 20 times of penetration test.

As expected, antimicrobial activity of PDT-10% coated microneedles was dependent on the concentration of coating solution and varied against different microbial species. It was demonstrated that PDT-10% coated microneedles were effective against *S. aureus* and *C. albicans* with log reduction values of more than 2 at the coating concentration of 5 mg/ml and 1 mg/ml, while significant reduction of bacteria number was also observed against *E. coli* at the same coating concentration. The results further indicated that previous observation that antimicrobial activity in

solution are not direct indicative of their real property upon attachment to a surface and the antimicrobial activity varied when coating on different surfaces (184, 194). Currently, only a few papers were published on antimicrobial microneedle fabrication. Gittard *et al.* demonstrated the antimicrobial efficacy of a silver coated microneedles by agar diffusion method (225). This method is not suitable to test our non-leachable antimicrobial system. Other antimicrobial microneedles were designed to delivery antimicrobial substances for treatment purpose, which is different from our antimicrobial micorneedles (230-233).

Cytotoxic assay further demonstrated that these antimicrobial coating was not toxic to human cell lines and indicated that they may be safe to human body.

In summary, this study demonstrated a method to confer microneedles with effective antimicrobial activity against *S. aureus, E. coli, C. albicans* with a QAS copolymer coating by a simple thermal-curing process. *S. aureu*, *E. coli* and *C. albicans* are commonly existing bacteria on skin. Other skin pathogens, such as *Streptococcus pyogenes, Staphylococcus epidermidis* may also be tested (238). Furthermore, the plasma treatment method changed the surface property of the microneedles and rendered the coating possible. This plasma pretreatment method can potentially be used to coat other drug molecules on microneedles as well. A recent study also indicated that plasma treatment significantly increased the surface energy and roughness of the polycarbonate and polyether ether ketone microneedles resulting in better adsorption and release of BSA (239). The flood coating method used in our study seems suitable for characterization or the antimicrobial coating, but it may not be suitable for a quantitative drug coating. Other quantitative coating method may be employed for drug coating purpose. Furthermore, PDT-10% is expected to be coated on a large range of substrate as other QAS compounds (222). So in future study,

microneedles made from other materials can also be tested with PDT-10% coating to harvest the antimicrobial activity to reduce the risk of infection.

5.5. Conclusion

Microneedles with durable and effective antimicrobial properties were developed by coating the microneedles with a QAS copolymer, PDT-10% after plasma treatment. Biocompatibility of the coating was demonstrated by *in vitro* cytotoxicity assay. The antimicrobial coating can potentially be applied on microneedles made from other materials as well.

Chapter 6 Development of lidocaine HCl dry patch with microneedle pretreatment for fast anesthetic effect

6.1. Introduction

Pretreatment of skin by microneedles following with a drug-loaded topical formulation is one of the frequently studied microneedle-assisted drug delivery systems. However, the influence of drug formulation on drug diffusion through the microneedle pretreated skin is not thoroughly investigated. Since the stratum corneum is bypassed by microneedles, the current formulations for passive transdermal drug delivery may not be suitable for microneedle assisted transdermal drug delivery. In this chapter, we investigated the development of percutaneous lidocaine delivery with microneedle pretreatment.

Various formulations have been developed for skin application of lidocaine on intact skin, including liquid, cream, gel, patches, *etc*. Creams and gels have a higher drug loading on skin than liquid, but the doses are variable and contamination of hands happens, which are the same issues associated with liquid formulation. Considering these issues, patches are more preferable although they are more expensive. Furthermore, with an occlusion by a backing layer, higher drug absorption is expected with patches used on skin. Among different types of transdermal patches, the drug-in-adhesive system, in which the drug is incorporated in the adhesive layer contacting skin, is very commonly used (240). When developing a drug-in-adhesive system, the adhesive should be compatible with drug and excipients, including the solubility of drug and excipients in adhesive, effect of dissolved/dispersed additives on mechanical properties of adhesive, and long-term stability of dissolved/dispersed components (241). In order to increase the thermodynamic activity hence the skin permeation, saturated drug is usually used in adhesive matrix. However, high drug loading has a tendency to form crystals during storage, which may not only

decrease delivery rate but also decrease the adhesion of the patch (242). On the other hand, only a small portion of drug was effectively absorbed by skin despite the high drug loading. For example, for a commercial lidocaine patch, Lidoderm®, only less than 5% of the dose applied is expected to be absorbed. At least 95% of the drug remains in an used patch, which is a potential risk for a child or a pet to suffer serious adverse effects from chewing or ingesting the used patch (243). Furthermore, in order for a drug to be successfully absorbed, the drug has to release from the adhesive matrix system to the skin surface, then diffuse through the stratum corneum, which is considered as the main barrier for percutaneous drug delivery. The passive drug diffusion process results in a delay between the patch application and the development of a desired minimum effective concentration, which is called lag time. For example, the commercial lidocaine formulations, including EMLA® cream, EMLA® patch and Lidoderm patch take 60 min to 4 h to produce analgesia (243, 244). Therefore, there is a need for a further development of percutaneous lidocaine delivery system, including effective usage of drug and a decrease in lag time. On the other hand, it was found that microneedles can not only enhance the skin permeation but also decrease the onset time of drug effect by bypassing the *stratum corneum* (35, 53, 139). However, just as discussed above, the current lidocaine formulations may not be suitable for the drug delivery with microneedle assistance because the *stratum corneum* is breached and microchannels are created. Furthermore, the adhesive and excipients of existing patch may cause skin irritation issues along with the enhanced permeability in the breached skin. To minimize the potential risk of a microneedle assisted drug system, less excipients should be used in the patch system.

In this study, we hypothesized that microneedles would create an alternative route for drug permeation though skin and it should have a preference of drug molecules based on their lipophilicity. The percutaneous delivery of lidocaine and lidocaine hydrochloride (HCl)

was compared with microneedle pretreatment. Furthermore, the drugs were fabricated into an adhesive and solvent free patch, named “dry patch” by spraying coating with limited excipient incorporated inside. The resulted single layer patch allowed drug release without the hindrance of a matrix thus allowed the effective usage of drug. Both *in vitro* permeability study on human skin and *in vivo* study on pig skin were conducted to evaluate the efficacy of the new delivery systems with or without microneedle pretreatment. This study would provide future strategies for the reasonable design of a microneedle assisted drug delivery system.

6.2. Materials and methods

6.2.1. Materials

Lidocaine was purchased from TCI, Japan. Lidocaine hydrochloride monohydrate, polyvinylpyrrolidone, sucrose, prilocaine, proteinase K, ammonium hydroxide, Na_2HPO4, PBS, 10% Neutral Buffered Formalin were purchased from Sigma-Aldrich, Singapore. HPLC-grade isopropyl alcohol and acetonitrile were supplied by Tedia, USA. The commercial patch, Lidoderm® (lidocaine patch 5%), is a product of Endo Pharmaceuticals. Water used in the paper was purified using Millipore Direct-Q.

6.2.2. Fabrication of lidocaine and lidocaine HCl dry patch

10 mg/ml lidocaine and lidocaine HCl were dissolved in 80% ethanol water solution respectively with 6.7 mg/ml polyvinylpyrrolidone and 3.3 mg/ml sucrose added. The solution was then transferred into the container of a spray machine (Spray Master ME-5000SP, Musashi, Japan). The movement of spray valve was controlled by a desktop robot (SHOTMASTER 300, Musashi, Japan) within an area of 10 cm by 10 cm on a polyethylene terephthalate film (HK-31WF, Higashiyama Film, Japan). Then the spray coated film was

dried at 130 °C for 1 min. After cooling down, the coated film was laminated with a release liner (Scotchpak® 9744, 3M). The resulted Lidocaine and Lidocaine HCl patches were named as lidocaine dry patch and lidocaine HCl dry patch, respectively. The fabrication process of dry patches was illustrated in **Figure 6.1**.

For the content assay, the dry patch was cut into 5 cm^2 by a metal punch and the drug was recovered by shaking in 5 ml of 80% ethanol water solution for 3 h at 200 rpm, followed by HPLC analysis.

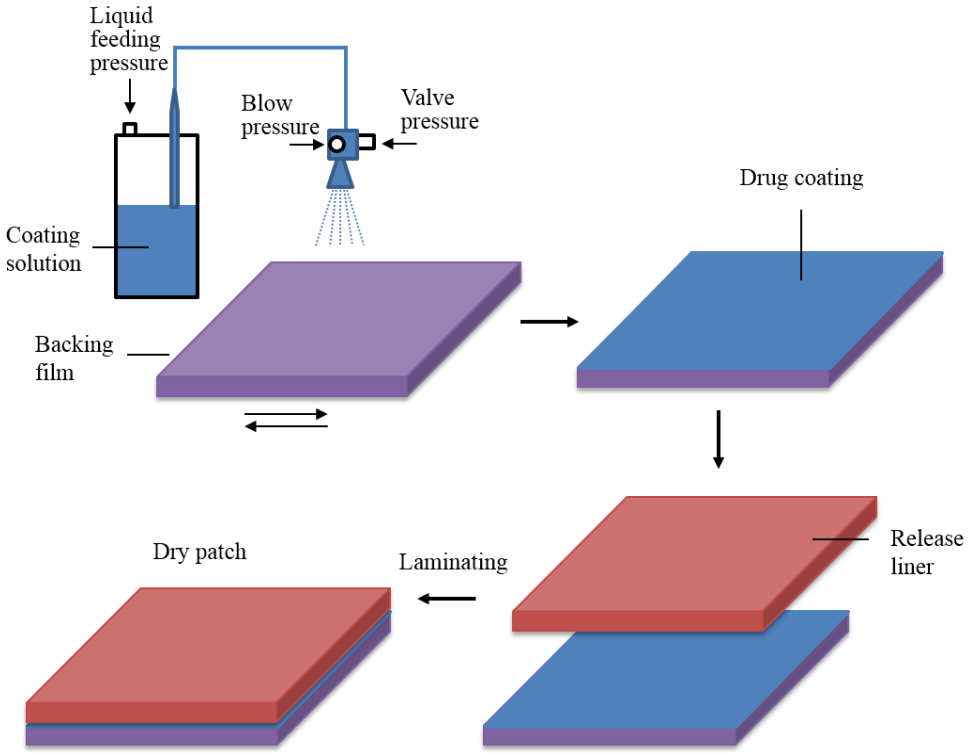

Figure 6.1 Illustration of the fabrication process of "dry patch".

6.2.3. Characterization of dry patches by microscopy methods

The thickness of the dry patches and Lidoderm patch was compared under a stereoscopic microscope by taking the cross section images (Nikon SMZ25, Japan). Furthermore, a piece of lidocaine HCl dry patch was cut in liquid nitrogen to get a smooth cross section

then attached to a stub by a carbon tape (NEM tape, Nisshin EM. Co. Ltd.), and platinum sputter-coated using a JFC-1600 autofine coater (JeOL, Japan) at a current of 10 mA for 80 s. The cross section images of the dry patch were then taken using a JSM-6700F FE-SEM (JEOL, Japan) followed by energy dispersive X-ray spectrometer (EDS) characterization.

6.2.4. Characterization of the release liner after removal from dry patches

The release liner was examined for residue drug after removal from the dry patches by using a Spectrum 100 Fourier transform infrared (FTIR) Spectrophotometer (PerkinElmer, USA) with an attenuated total reflectance (ATR) set-up. Lidocaine or lidocaine HCl was used as positive control while a blank release liner as negative control. Infrared spectra were collected between 4000 and 650 cm^{-1} at a resolution of 4 cm^{-1}.

6.2.5. *In vitro* release study

Drug release from lidocaine and lidocaine HCl dry patches was compared with that from the commercial patch, Lidoderm using Franz diffusion cells. A cellulose nitrate membrane was placed between the donor compartment and the receptor compartment. A patch with 1 cm^2 was pressed on the membrane. The receptor compartment contained 4.8 ml of PBS solution. The cells were placed inside a chamber with temperature controlled at 32 °C, and there was a magnetic stirrer in the receptor cell with a stirring speed of 100 rpm. The receptor solutions were withdrawn at pre-set time intervals and replaced with fresh ones. Three replicates were conducted for each group. Lidocaine concentration in receptor solutions were analyzed by HPLC.

6.2.6. *In vitro* skin permeation study

Franz diffusion cells were also used in *in vitro* skin permeation study to evaluate the performance of different lidocaine formulations with or without microneedle treatment. Different from release study, human dermatomed skin was used between the two compartments instead of a membrane. The back skin of a 66-year-old Caucasian female cadaver was used in the experiment and the skin was obtained from Science Care (Phoenix, AZ, USA). The skin was spread over a 6 mm thick PDMS substrate mounted on a Styrofoam board with epidermis side up. A microneedle array was then pressed on the skin sample with a force of 22.2 N for 10 seconds, which was controlled by using a force gauge (HF-10, JISC, Japan).

Either intact skin or microneedle pre-treated skin was mounted onto Franz diffusion cells with epidermis facing up. Lidocaine and lidocaine HCl solution (both equivalent to 5% lidocaine), lidocaine and lidocaine HCl dry patches, together with the commercial patch Lidoderm, were evaluated by putting 0.5 ml solution in the donor compartment or pressing a 1cm^2 patch on the skin. The receptor compartment contained 4.8 ml of PBS solution. The cells were placed inside a chamber with temperature controlled at 32 °C, and there were magnetic stirrers in the receptor cells with a stirring speed of 100 rpm. The receptor solutions were withdrawn at pre-set time intervals and replaced with fresh ones. Three replicates were conducted for each group. Lidocaine concentration in receptor solutions were analyzed by HPLC. The use of human cadaver skin was approved by the National University of Singapore Institutional Review Board.

6.2.7. *In vivo* pig study

Young adult female pig (Yorkshire X, Holland), weighing 25-40 kg were used for the study. The pigs were initially sedated with ketamine (10 mg/kg), and then anesthetized with

isoflurane gas followed by administration of Atropine to reduce salivary, tracheobronchial and pharyngeal secretions. While the animal was under anesthesia, hair and dirt on the swine skin at the intended application sites were removed. Subsequently, the hair was first clipped using an electric shaver followed by a wet disposable razor and patted dry. Four replicates were conducted for each group.

The microneedle array (3M MSS) were applied on the skin with a hand force of around 20 N (estimated by using the force gauge) for 10 s. Then a lidocaine dry patch or lidocaine HCl dry patch or Lidoderm patch (0.5 cm × 1 cm) was pressed on the microneedle treated area immediately after microneedle removal. The dry patch was fixed on the skin with a medical tape (Smith & Nephew, Germany). The commercial patch, Lidoderm was used as a bench mark. Intact skin without microneedle treatment was used as control.

At predetermined time points (10 min, 30 min, 1 h, 2 h, 4 h, 6 h and 8 h), patches were removed. Then the skin was cleaned three times with a cotton swab using PBS followed by drying with dry cotton swab. Thereafter, skin biopsies were collected by using sterile biopsy punches (Miltex USA, 4mm) from the center of the patch application site. The weight of skin biopsies were determined by weighing the tube with and without biopsies. The drug concentration in the skin biopsies were analyzed by liquid chromatography–mass spectrometry (LC-MS). All animal testing procedures were approved by the Institutional Animal Care and Use Committee, National University of Singapore.

6.2.8. HPLC to determine dry patch lidocaine loading and lidocaine concentration in *in vitro* release / skin permeation study

Lidocaine concentration was determined with a reversed phase HPLC (Agilent 1200, US) using a Zorbax Extended-C18 Rapid Resolution HT column (1.8 µm, 2.1 mm × 50mm, Agilent). The mobile phase comprised of 50% 25 mM of Na_2HPO_4 solution and 50%

acetonitrile in an isocratic mode at a flow rate of 0.4 ml/min. The ultraviolet detection wavelength is set at 230 nm. The standard concentration ranged from 0.1 µg/ml to 100 µg/ml.

6.2.9. LC/MS/MS to determination lidocaine concentration in skin biopsies

Skin biopsies were first digested by Proteinase K (75 µg/ml, 150µl) at 55 ℃ for 6 h. Then three parts of methanol (containing prilocaine as internal standard) were added into the homogenous digestion mixture to precipitate protein by votex mixing for 5 min followed by centrifugation at 14,000 ×g for 20 min at 4 ℃. Supernatant obtained was quantitatively analyzed by Agilent 1200 series LC/MS/MS system, comprised of capillary pump, autosampler, and triple quadrupole mass detector (Agilent 6400 series). Data were acquired and processed using Mass hunter workstation software version B.02.01. The samples were analyzed using electrospray ionization in positive ion mode with Turbo Ion Spray interface. Operating conditions optimized by Mass Hunter optimizer for Lidocaine and IS-prilocaine were: dry gas temperature at 350 ℃, nebulizer pressure at 35 psi, nitrogen gas flow rate at 12 ml/min; capillary voltage at 4000 V and fragmentor voltage at 90 V. Product ions (of lidocaine) resulting from transition of 235.2→86.1 (collision energy 16 V) and product ions (of prilocaine) 221.2→86 (collision energy 8 V) were monitored at retention time of 3.1 min (for lidocaine) and 2.4 min (for prilocaine as internal standard). A Zorbax extended-C18 column (3.5µm, 4.6×75mm, Agilent) was used for the separation. The mobile phase was made of 50% of 25 mM ammonium hydroxide and 50% of isopropyl alcohol with methanol (1:1) mixture. The flow rate controlled at 0.5 ml/min. Calibration curve was plotted over the concentration range of 1-10000 ng/ml by running the standard solutions prepared in methanol from lidocaine standard.

6.3. Results

6.3.1. Characterization of dry patches

The drug content of lidocaine and lidocaine HCl dry patches are 111.6 ± 44.0 μg/cm^2 and 122.0 ± 8.9 μg/cm^2, respectively. Compared to the commercial patch (with a drug content of 5000 μg/cm^2), the drug loading of dry patches is 40 times less (**Figure 6.2A**). The dry patch consists a backing film with a thin layer of drug coating and a release liner layer. Without hydrogel or adhesive as drug vehicle in between, the dry patch with a thickness around 100 μm was much thinner than the commercial patch, Lidoderm (**Figure 6.2B**). SEM images indicated the thin layer of drug coating around 1 μm between the backing film and release liner (**Figure 6.2C**). The drug coating was further confirmed by elemental analysis, since the chlorine atom in the EDS graph (indicated by the red arrow) was due to the existence of lidocaine HCl.

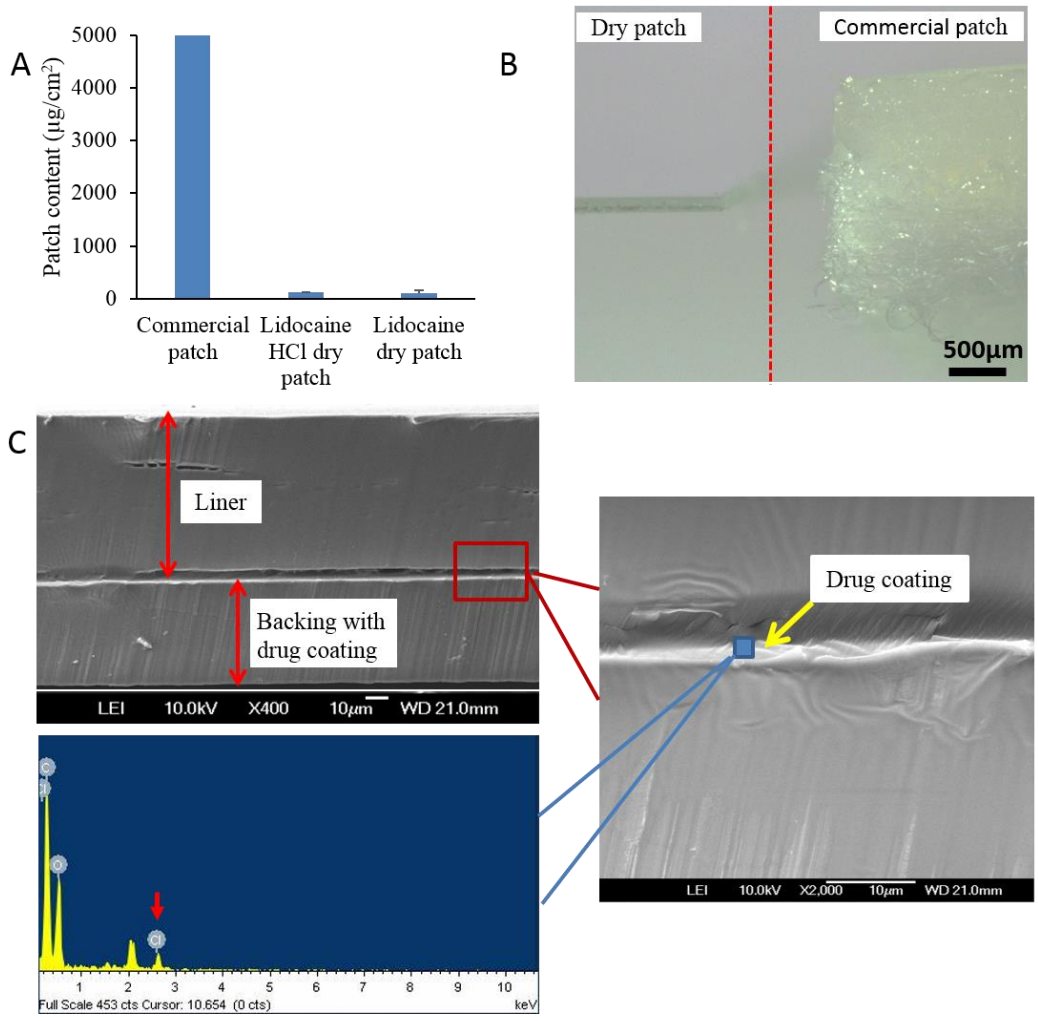

Figure 6.2 Dry patch information. (A) Patch content information. (B) Phase contrast image of the cross section of a Lidocaine HCl dry patch (left) with contrast to Lidoderm patch (right). (C) SEM image of the cross section of Lidocaine HCl dry patch with its enlarged view of the drug layer on the right and the EDS result below.

Since the drug in the dry patch is not trapped in hydrogel or adhesive, there is one concern that the drug may stick to the release liner during the liner removal. We used IR spectroscope to characterize the existence of the dry film after the liner removal. **Figure 6.3** shows that the spectrum of control liner and liner removed from the drug formulated dry patch are identical, indicating the drug formulation didn't transfer to the liner after the removal.

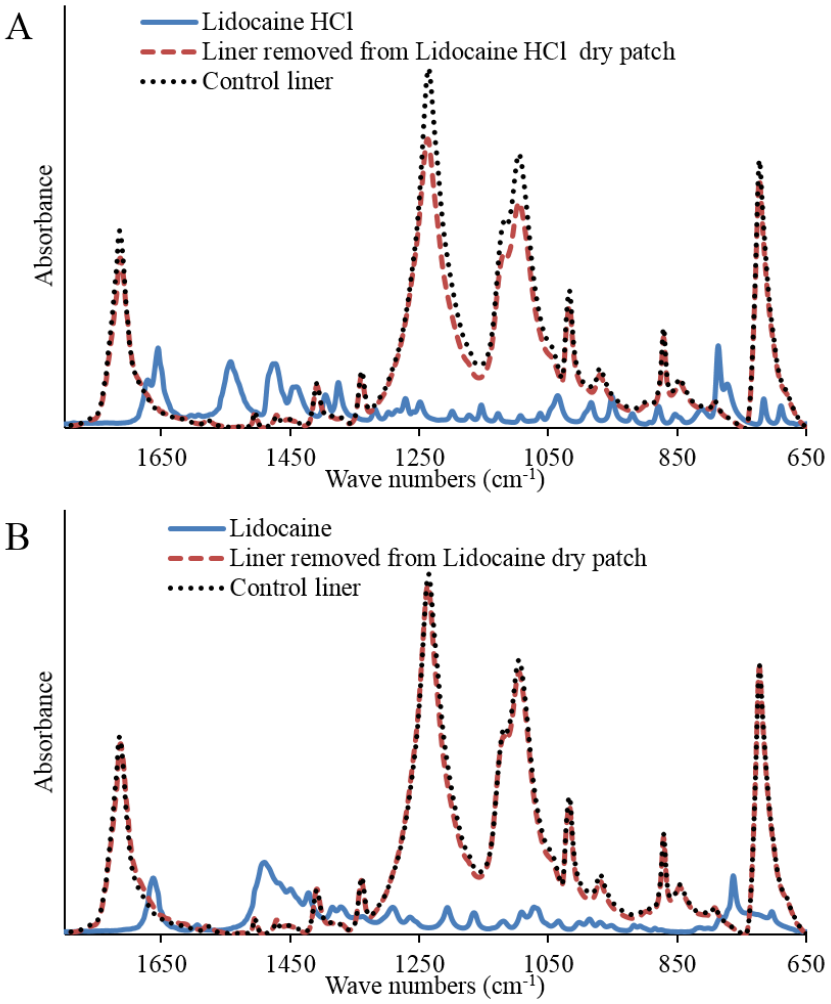

Figure 6.3 ATR-FTIR to examine the existence of drug on liner after removed from Lidocaine HCl dry patch (A) and Lidocaine dry patch (B).

6.3.2. *In vitro* release study

Drug release from lidocaine and lidocaine HCl dry patches was compared with that from the commercial patch, Lidoderm using Franz diffusion cells. A cellulose nitrate membrane was placed between the donor compartment and the receptor compartment. A patch with 1 cm^2 was pressed on the membrane. The receptor compartment contained 4.8 ml of PBS solution. The cells were placed inside a chamber with temperature controlled at 32 °C, and there was a magnetic stirrer in the receptor cell with a stirring speed of 100 rpm. The receptor solutions were withdrawn at pre-set time intervals and replaced with fresh ones.

Three replicates were conducted for each group. Lidocaine concentration in receptor solutions were analyzed by HPLC.

Compared to the commercial patch which has a controlled release over time, the dry patches had an initial burst of release and almost no more drug was collected after 1 hour (**Figure 6.4**). Although the absolute cumulative release amount from the commercial patch is higher than dry patches, less than 15% of drug was release from the commercial patch at the end of 6 hours, while the corresponding percentage release for lidocaine HCl dry patch and lidocaine dry patch were 86.5% and 56.4%, respectively.

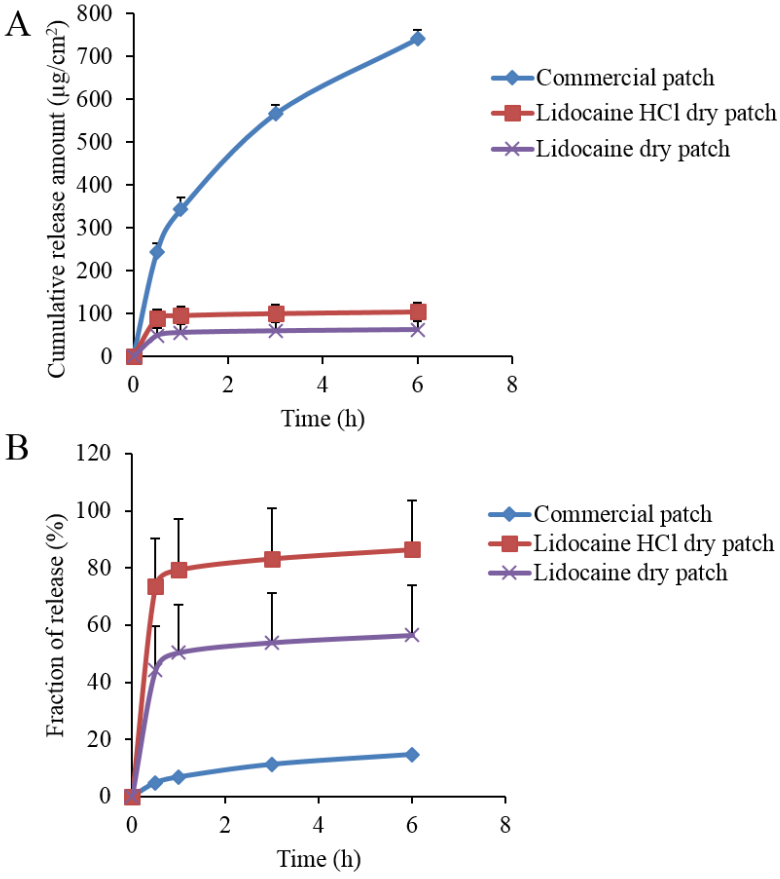

Figure 6.4 Drug release from different patches. (A) Cumulative release amount. (B) Fraction of release

6.3.3. *In vitro* skin permeation study

Figure 6.5 showed the lidocaine permeation profile of the base form and salt form through human skin either with or without microneedle pretreatment. No matter in solution or formulated in patch, lidocaine HCl had a low permeability through intact skin, while lidocaine, the base form was much more effectively delivered through skin than the salt form when applied on intact skin. When the skin was pretreated with microneedles, there was a significant increase in the delivery of lidocaine HCl across skin by 83.3 times. However, microneedle pretreatment showed no enhancement effect on the skin permeation of lidocaine solution from the permeation profile graphs. Although the cumulative amount of lidocaine delivery for lidocaine HCl solution across microneedle treated skin was not significant higher than that for lidocaine solution on intact skin, the former group showed a first order release profile ($r^2 = 0.9981$) and had a much steady flux over time. When the drugs were formulated into patches, including the commercial patch and dry patch, microneedles were found to have similar effect with that when drugs were in solution. When the skin was pretreated with microneedles, there was a significant increase in the drug permeation from lidocaine HCl dry patch across skin by around 9 times. But microneedles showed much less enhancement on the drug permeation from the lidocaine patches. More specifically, the drug permeation curves from the commercial patch were almost overlapped regardless the skin was microneedle pretreated or not. On the other hand, microneedle pretreatment increased the drug permeation from lidocaine dry patch slightly.

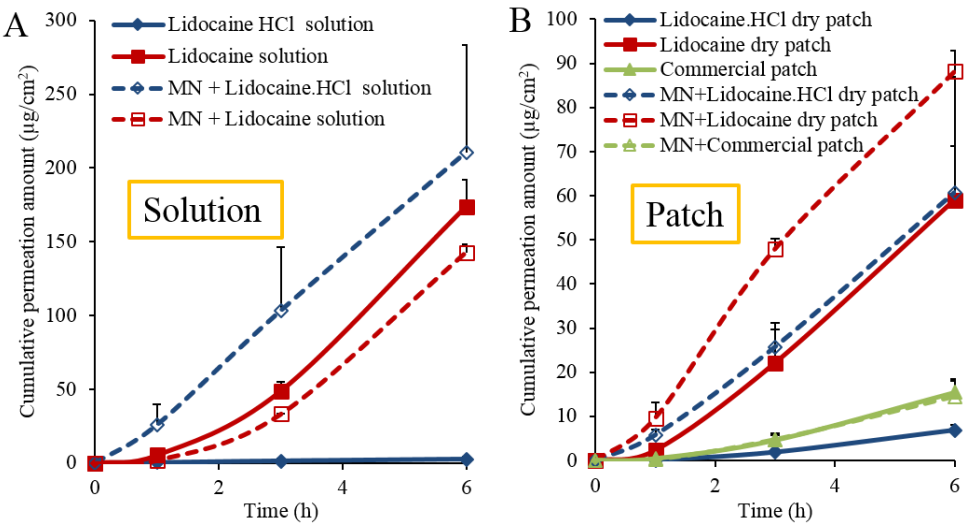

Figure 6.5 *In vitro* skin permeation test to study the effect of microneedle (MN) pretreatment on lidocaine skin transport with base form and hydrochloride form used. (A) When the drugs were in solution. (B) When the drugs were formulated into patches.

6.3.4. *In vivo* study on pigs

Figure 6.6 showed the skin lidocaine concentration after 6 hours' application of different patches with or without microneedles treatment on pigs. It was found that lidocaine dry patch generally resulted in a higher lidocaine concentration than lidocaine HCl dry patch, but lower than the commercial patch when the patches were applied on intact pig skin. Considering the commercial patch, Lidoderm may have one-hour delay in anaesthesia effect, the resulted skin lidocaine concentration at 1 h was set as therapeutic level (243, 244). When the pig skin was treated with microneedles, lidocaine HCl dry patch resulted in a lidocaine concentration higher than the therapeutic level as early as 10 min and the skin lidocaine concentration was steadier over time than that with the commercial patch. Microneedles also promoted Lidocaine dry patch performance by enhancing the skin lidocaine concentration. However, the commercial patch with microneedle pretreatment did not perform better than the commercial patch itself.

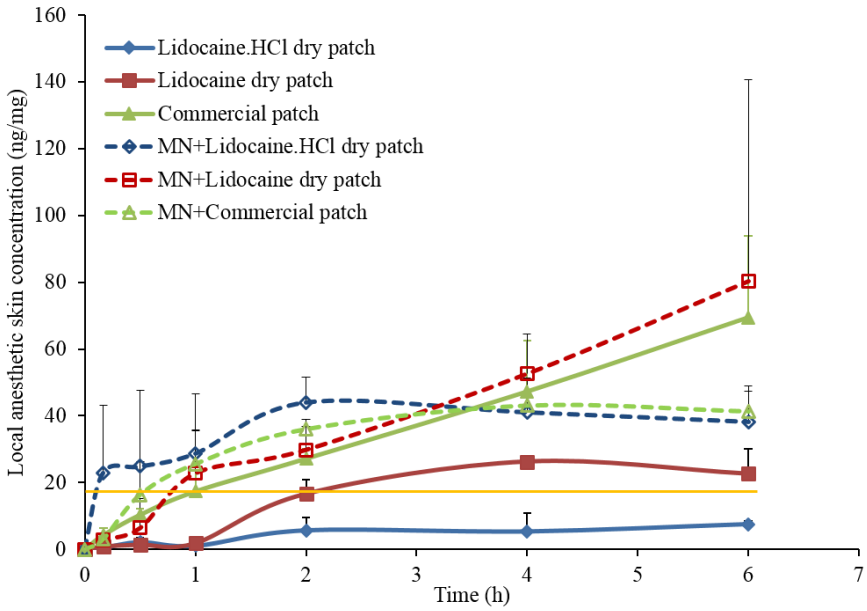

Figure 6.6 *In vivo* study on pigs to measure the skin lidocaine concentration when different patches were used with or without microneedles (MN).

6.4. Discussion

From *in vitro* skin permeation study when drug solutions were tested, it was observed that lidocaine was much more effectively delivered through skin than its hydrochloride salt when applied on intact skin. This is because the intact skin is much more permeable to lipophilic drug (lidocaine, log P = 2.63) than hydrophilic drug (lidocaine HCl, log P ≤ 0), as suggested by previous paper that the lipid bilayers in the *stratum corneum* is the main pathway for percutaneous absorption (245). After human skin was pretreated with microneedles, the amount of lidocaine HCl permeated though skin increased more than 80 times. Under passive diffusion in intact skin, the hydrophilic drug molecule, lidocaine HCl, had difficulty in permeating the lipid-based *stratum corneum*. However, when lipid barrier was overcome by microneedles with microchannels created, significant increase in the drug permeation was observed, which supports the fact that alternate route of permeation exists with the pretreatment of microneedle. This is consistent with previous report that microneedle pretreatment created aqueous passages in the skin, which facilitated the

delivery of hydrophilic molecules through the skin (83). A decreased lag time further ascertained the presence of an alternative permeation pathway. But microneedles had limited effect on lidocaine base delivery. It indicated that the permeation pathway of lidocaine remained the same even when micro-channels were created in the stratum corneum. Lidocaine did not utilize the aqueous pathway created by microneedles in the skin, probably because of its low aqueous solubility.

Lidocaine and Lidocaine HCl were further formulated into dry patch by spray coating to be screened for a microneedle assisted system. Because of the high resistance in skin absorption process, a very high amount of drug is usually used in a thick conventional drug-in-adhesive patch to ensure the effectiveness of patch although only a small portion is absorbed by skin. On the contrary, the dry patch described here is much thinner and more than 40 times less drug was loaded yet the effectiveness can be maintained. A thin patch or film can also be potentially applied buccal or sublingual besides transdermal (246). Furthermore, we don't have to consider the drug adhesive compatibility and thus a variety of drug molecules can be adopted in the dry patch system. The spray coating itself is also a very easy and cost-effective process. The resulted "dry patch" is solvent and adhesive free, thus a better long-term stability during storage is expected (242). In pharmaceutical industry, spray coating has been widely used in the coating process of granular solids and tablets with coatings of the millimeter thicknesses (247). It was also proposed to coat the surface of microneedle arrays and other medical devices (248, 249). However, application of spray coating in transdermal patches/films has not been reported to our knowledge.

Initially we had the concern that the dry state of drug in the spray coated dry patches may have difficulty in skin permeation, since drug have to be dissolved to a thermodynamic state and then utilize a certain pathway in the stratum corneum. Furthermore, the release study indicated that almost no more drug was released from dry patches after 1 hour and

the lower amount of drug was released from dry patches than that from commercial patch (**Figure 6.4**). Surprisingly in *in vitro* skin permeation study, lidocaine dry patch showed an even higher permeability than the commercial patch although 40 times less drug was loaded in the dry patch. After 6 hours, around 50% of drug in lidocaine dry patch permeated through skin. It indicated that water in the skin itself was enough for hydrating the patch and dissolving drug after occlusion of dry patch on skin. On the other hand, the drug had to be released from the adhesive matrix of commercial patch before reaching the skin surface, while the thin layer of drug on dry patch seemed more easily accessible to skin surface without the hindrance of vehicle matrix under limited skin hydration condition. On the other hand, even when drugs were formulated into patches, microneedles showed its preference in increasing the skin permeation of hydrophilic drug, lidocaine HCl.

Dermal pharmacokinetics of lidocaine was measured by biopsy analysis as reported (27). As expected, although lidocaine HCl dry patch resulted in a low skin concentration on intact skin *in vivo*, lidocaine HCl dry patch with microneedle assistance led to a skin concentration higher than therapeutic level in 10 min. Besides, a steady effective skin concentration with time up to 6 hours was obtained with the microneedle plus lidocaine HCl dry patch application. This is different from previous reports where only a short term effect was obtained with lidocaine coated microneedles or microneedle pretreatment plus lidocaine injection application (27, 28). The result demonstrated that the lidocaine HCl dry patch can resulted in an effective skin lidocaine concentration over 6 hours yet with a much faster onset of effect with the assistance of microneedles, although drug loading in lidocaine HCl dry patch was 40 times less than the commercial patch.

Our study demonstrated that lidocaine HCl was preferred in a microneedle assisted system, which is different from the drug selection standard for a conventional percutaneous drug delivery. Besides, a non-adhesive patch with low drug loading can achieve a satisfactory

effect *in vivo* with microneedle assistance. It overcame the limitations of conventional drug-in-adhesive patch, such as complicated patch design, waste of drug, and delayed drug effect. This preliminary study demonstrated the possibility of spray coated dry patch as a delivery vehicle used together with microneedle pretreatment. In future study, long term stability of the dry patches system needs to be further investigated. In order to be applied on skin conveniently, the patch was proposed to have a peripheral layer of adhesive. Current in *vivo* study only demonstrated 6 hours' effectiveness, and there is one concern that the current dry patch may not support an effectiveness for a longer time because of the low drug loading. Nevertheless, the spray coating process is quite flexible, the drug loading may be increased by using a higher concentration of spraying solution or multiple layers of coating. Furthermore, the dry patch plus microneedle pretreatment system is a two-step method. A simplified way is possible by incorporating the thin patch with a microneedle applicator device with a patch housing compartment, then the patch can be dispensed for application to a target site automatically after microneedle application (250).

6.5. Conclusion

In this study, it was demonstrated that the hydrophilic lidocaine HCl molecule is preferred in a microneedle system other than the lipophilic lidocaine molecule. Furthermore, we applied spray coating in the patch fabrication. The spray coating process is cost-effective and a variety of drug molecules are expected to be adapted in the adhesive-free patch system. The resulted lidocaine HCl dry patch plus microneedle pretreatment system can achieve similar effectiveness as the commercial lidocaine patch yet with a faster onset of 10 min, although 40 times less drug was loaded in the spray coated patch.

Chapter 7 Conclusions and future work

7.1. Conclusions

This thesis addresses the issues that influence the effective and safe use of microneedles as skin pretreatment for drug delivery. These findings are very important for a reasonable design of a microneedle system and the correct use of microneedles for effective skin permeation enhancement. Meanwhile, antimicrobial microneedles were proposed to reduce the risk of infection associated with microneedle usage. Some of the findings are patented. Brief conclusions from the studies were summarized below.

When studying the delivery efficacy of microneedle assisted transdermal drug delivery, it was observed that microneedle application force can influence the performance of skin permeation of copper peptide by affecting the depth and percentage of microneedle penetration through skin. The skin permeation of copper peptide can be enhanced by microneedle pretreatment at a high thumb force with minimal skin disturbance. Regarding the safety of the delivery, it was found that copper peptide has a low potential of inducing skin irritation response when compared to copper chloride and copper acetate. Besides, human epidermis and rat skin may not be suitable models for *in vitro* skin permeation study when microneedles are used. It further confirmed that enhanced delivery of copper peptide by microneedles is safe to skin. Besides, IL-1α, IL-8, FOSL1, and HSPA1A are potential *in vitro* biomarkers that can be used in adjunct to MTT assay in identifying irritants and assessing the skin irritation potential of copper compounds.

On the other hand, a series of novel QAS copolymers with improved biocompatibility was synthesized and they can form effective and durable coatings via a thermal-curing process. The new QAS copolymers have a great potential to be used as a safer substitute for the current monomeric QAS coating agents. Furthermore, in order to reduce the risk of

infection associated with microneedle use, microneedles with durable and effective antimicrobial properties were developed by coating with a QAS copolymer after plasma treatment and good biocompatibility of the antimicrobial microneedles were demonstrated.

Lastly, an adhesive and solvent free lidocaine HCl patch plus microneedle pretreatment system was fabricated and it can achieve similar effectiveness as the commercial lidocaine patch yet with a faster onset of 10 min, although 40 times less drug was loaded in the patch.

7.2. Future work

Following future work was proposed to further address the issues associated with the use of microneedle as permeation enhancer for percutaneous drug delivery.

Another important factor critical to microneedle-assisted drug delivery is the lifetime of the micro-sized channels created in the skin. On one hand, rapid closure of the microchannels when the patch is applied on the skin, may result in sub-therapeutic levels in the body. On the other hand, if the microchannels remain open even after removal of the patch, it may result in problems such as irritation, infection and contamination of the site (251). Therefore, it is important to understand formation and closure of microchannels following microporation. Several groups reported their study on pore closure and provided important insights regarding the study of microchannel lifetime (31, 84, 252) . However, there are still limited studies available on the mechanisms of restoring skin barrier function following microneedle treatment. More future studies should be carried out.

Further optimization has to be done for lidocaine HCl dry patch system. Besides, we can include a peripheral layer of adhesive for skin adhesion, and integrate the patch with a microneedle applicator device for an easier application.

Other coating methods other than flood coating can be developed for antimicrobial coating.

The QAS copolymer can also be used to coat other microneedle product, such as Dermaroller®, to confer the antimicrobial activity.

Chapter 8 Appendix

8.1. Appendix to Chapter 4

8.1.1. FE-SEM analysis

FE-SEM was applied to analyze the antimicrobial mechanism of QAS copolymer by investigating bacteria morphology change. *S. aureus* was adjusted to a concentration of 10^9 cells/ml before incubating with or without PMT-10% (to a final concentration of 2×MIC) for 0.5 h, and the obtained solutions were centrifuged at 4000 rpm for 5 min. The precipitated bacteria were rinsed twice with PBS, immobilized with 2.5% glutaraldehyde for 60 min, and again rinsed with water twice. Cell dehydration was performed using a series of ethanol/water solutions (35, 50, 70, 90, 95, and 100%), and the final dehydrated sample was transferred onto carbon tape and dried at room temperature for 2 days. Platinum sputtering was applied to coat the dry samples before FE-SEM (JSM-6700F, JEOL, Japan).

As mentioned earlier, the QAS copolymers are able to disrupt the cytoplasmic membrane of bacteria via the interaction between the cationic quaternary ammonium group of the polymers and the anionic bacterial cell surfaces. This membranelytic mechanism was further investigated by using SEM to characterize the morphology change of *S. aureus* cells after incubation with the QAS copolymer. Since there were not much solid residues that could be found after mixing polymer with bacteria at the same concentration (10^5 cells/ml) with the MIC test, a higher bacteria concentration (10^9 cells/ml) was used for SEM testing. As another evidence to show the efficiency of QAS copolymers, the cloudy bacterial solution became semi-transparent after the incorporation of PMT-10%, and a significant reduction in the amounts of bacterial residue pellets were observed after the centrifugation. The SEM images of *S. aureus* with and without treatment were shown in **Appendix 1**Error!

Reference source not found.**A** and **B** respectively. It can be found that survival *S. aureus* treated with an above MIC concentration of PMT-10% had obvious membrane blebbing and was covered by the mixture of QAS copolymer and sticky intracellular constituents.

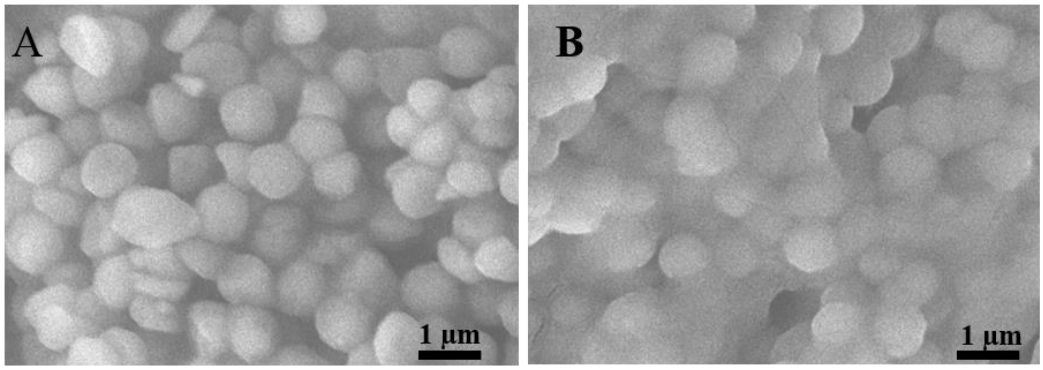

Appendix 1 SEM images of *S. aureus* before (A) and after (B) 30 min treatment with PMT -10% at 2 ×MIC.

8.2. Appendix to Chapter 6

8.2.1. Surface characterization by atomic force microscopy (AFM)

In order to evaluate the coating evenness after coating, the topography of the backing films with or without lidocaine HCl coating was examined by easyScan 2 FlexAFM (NanoSurf, Switzerland) in noncontact mode. The AFM imaging showed that the backing layer are very smooth both before and after the drug coating, which indicated the drug is evenly distributed on the backing layer (**Appendix 2**Error! Reference source not found.).

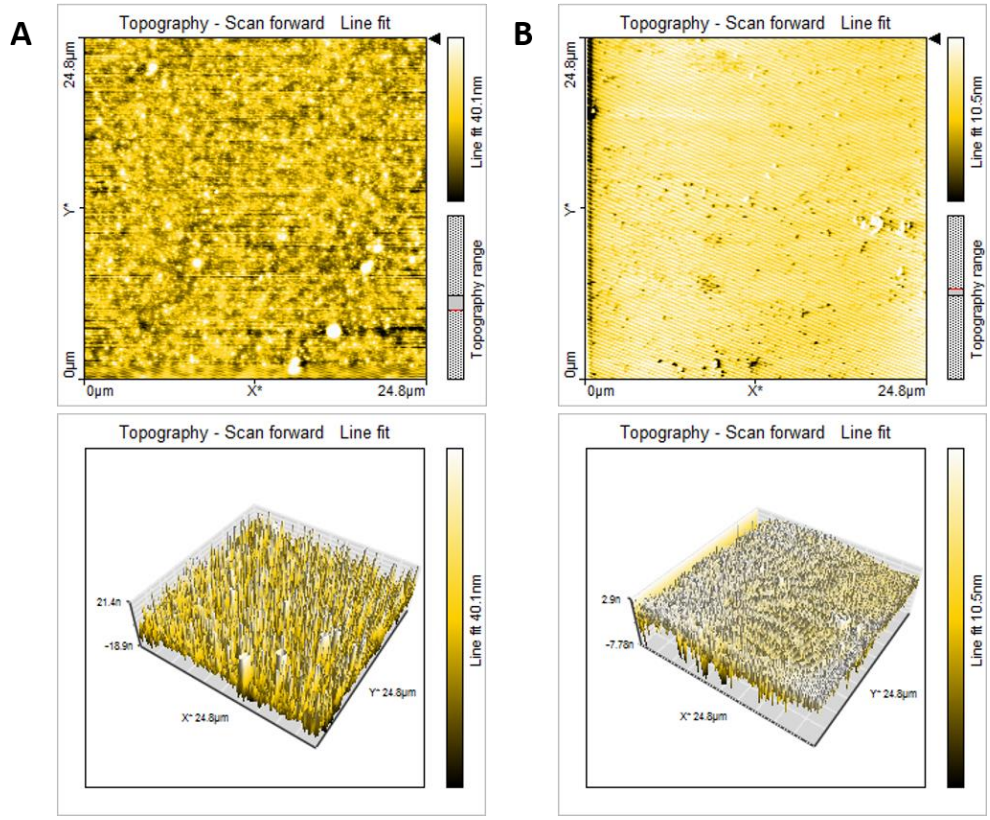

Appendix 2 AFM imaging. (A) Backing film with surface roughness of 5.3 nm. (B) Lidocaine HCl dry patch with surface roughness of 1.3 nm.

8.2.2. Thermal analysis by differential scanning calorimetry (DSC)

DSC analysis of drugs and the respective dry patch were performed using a differential scanning calorimeter DSC Q200 V24.4 Build 116 Model (TA Instruments, Water LLC). Around 5 mg of drug powder or dry patch (liner removed) was sealed in aluminum pans and heated from 20 to 250 °C with a heating rate of 20 °C/min under a nitrogen gas flow rate of 30 ml/min. The results were analyzed using TA Universal Analysis 2000 V4.5A Build 4.5.05 software.

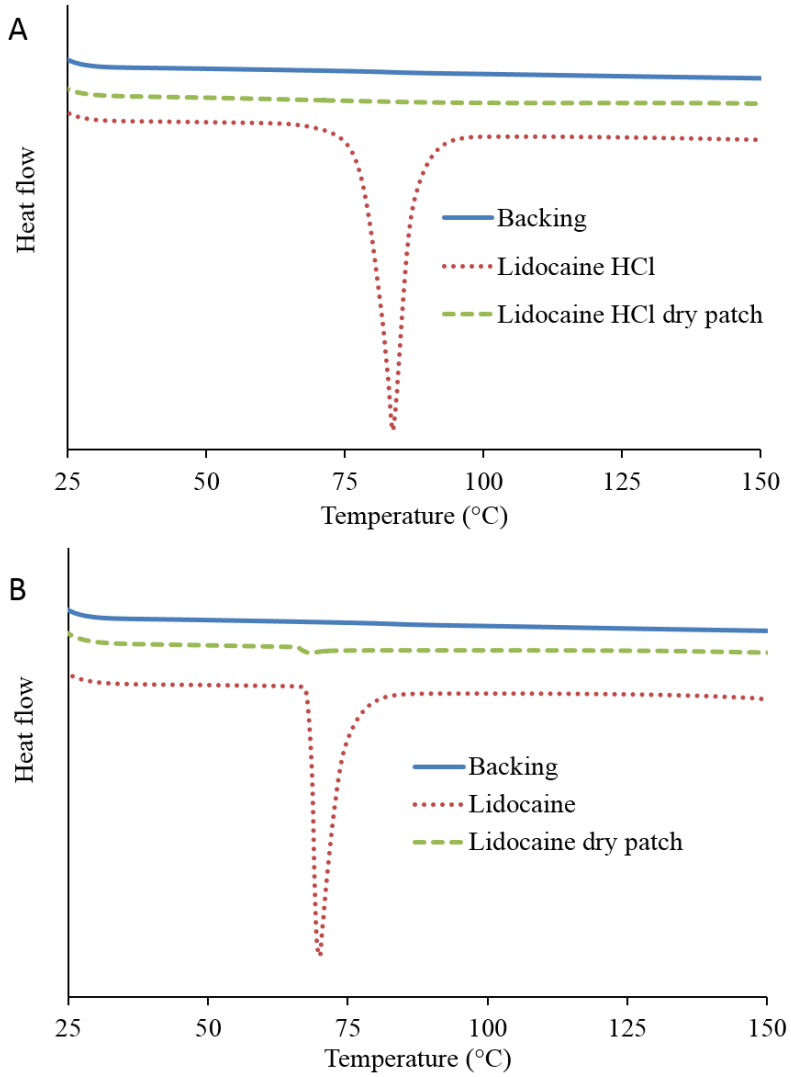

Appendix 3 Thermal analysis by DSC. (A) Lidocaine HCl and dry patch (liner removed). (B) Lidocaine and dry patch (liner removed).

The DSC thermograms of lidocaine and lidocaine HCl monohydrate powder showed that there was a sharp endothermic peak at around 69.9 and 83.7 °C due to the crystalline form of lidocaine and lidocaine hydrochloride. For lidocaine HCl dry patch, no melting endothermic peak was observed, which suggests that lidocaine HCl may exist as amorphous state on the dry patch. However, for lidocaine dry patch, the small endothermic peak may indicate the crystalline form of lidocaine on dry patch (**Appendix 3**).

Furthermore, no crystalline structure was observed on lidocaine HCl dry patch by AFM as well (**Appendix 2**).

8.3. The formulation effect of oligodeoxynucleotides (ODNs) on microneedle-assisted drug delivery

Direct cell-cell communication through connexin 43 (Cx43) gap junction channels played an important role in the wound healing process. Downregulation of Cx43 expression at skin wound sites can dramatically improve the rate and quality of healing, which was associated with a reduced inflammatory response, enhanced keratinocyte proliferation and wound fibroblast migration (253). The treatment with Cx43 antisense oligodeoxynucleotides (ODNs) was shown to downregulate the Cx43 protein levels in the early stage of skin healing process and result in a dramatic increase in the wound closure rate (254). Although the Cx43 antisense gel is effective for the healing of many open wound, it is not effective for pressure ulcers, where the skin is intact, because the ODNs with a molecular weight of 9308 Da have difficulty in conquering the *stratum corneum* barrier. Here we proposed the use of microneedles to facilitate the delivery of the antisense ODN drug into the skin. The effect of formulation type and drug concentration was evaluated. Since the microneedles were used as pretreatment, the micro-sized pores may close with time, which can influence the possibility of sustained drug delivery. In this study, a preliminary *in vivo* test was conducted to study the pore closure time as well. The work is still ongoing.

8.3.1. Concentration and formulation effect on drug delivery

Human dermatomed cadaver skin was defrosted and hydrated in tap water for around 30 min. The skin was then spread over a PDMS substrate mounted on a Styrofoam board with epidermis side up. After the skin surface tapped dry by Kimwipes, the microneedles (3M^{TM}

MSS) were applied on the skin with a hand force of around 20 N for 10 s. 10 µl of different concentrations (1 µM, 5 µM, 10 µM) of Fluorescence labelled Cx43 antisense ODNs either in water or in 30% Pluronic F127 gel was applied on the microneedle treated area immediately. After 2 hours, the excess DNA sample on skin surface was wiped off with wetted Kimwipes for 3 times. Then the skin was fixed in 10% Neutral Buffered Formalin (Sigma-Aldrich, US) in the fridge for 2 days. After that, the skin was imaged by using a fluorescent Stereoscopic Nikon SMZ1500 microscope (Melville, NY) to have a top view of all the microneedle spots.

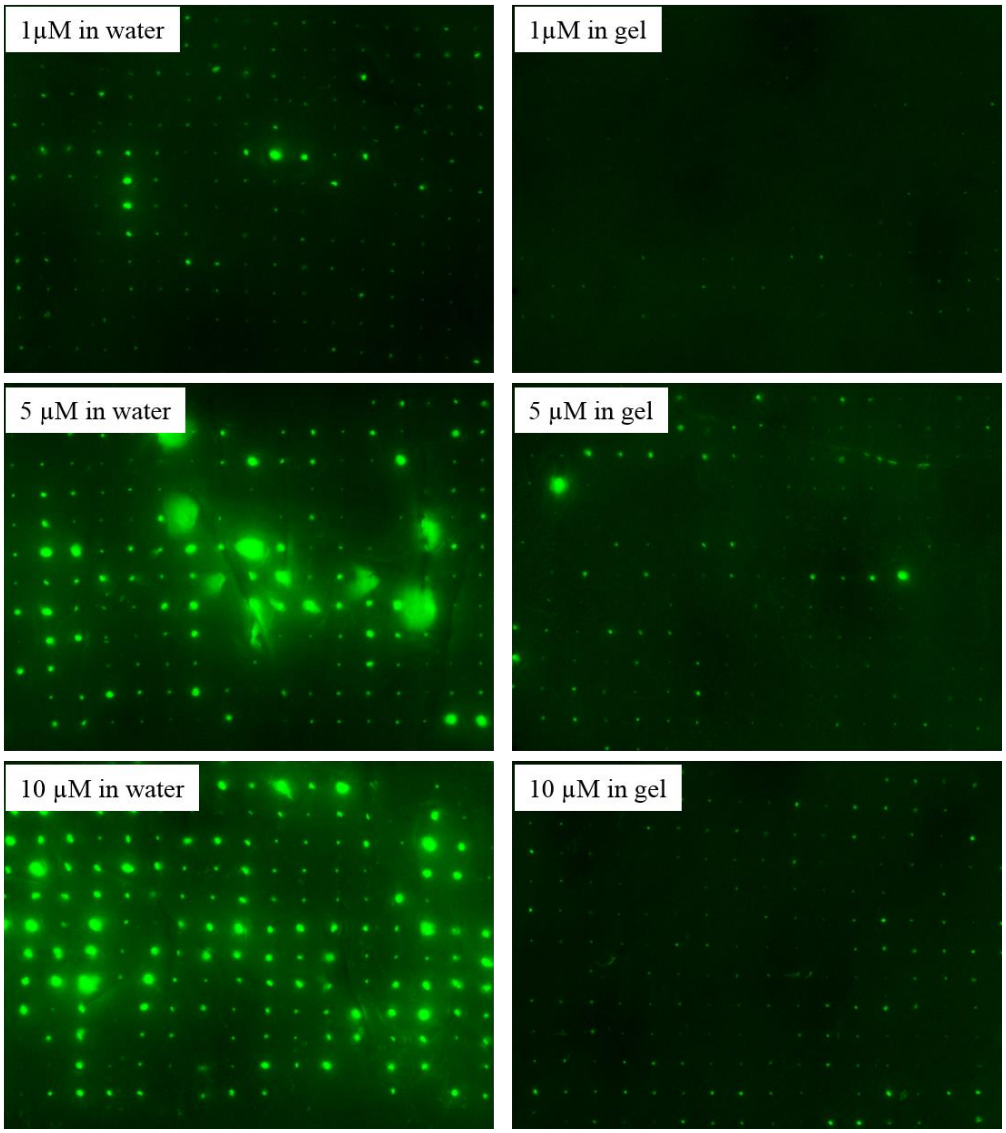

Appendix 4 The surface images of human cadaver skin with different formulations of fluorescence-labeled antisense ODNs after MN treatment.

In **Appendix 4**, clear patterned fluorescence dots retained on skin surface indicated that ODN drug penetrated the human skin through passages created by microneedles. For both solution and gel formulations, the higher the drug concentration, the more and brighter fluorescence dots were observed. The intensity of the fluorescence on ODN solution treated human skin are stronger than that on gel treated human skin at the same drug concentration. . It indicated that the gel may form another barrier for the percutaneous drug delivery, since

the drug has to transport from the gel sample to the skin surface first before it can be absorbed by the skin through the micro-sized passages.

8.3.2. Observation of drug penetration into skin after microneedle treatment

After human dermatomed skin was treated by 3M MSS with a hand force of around 20 N for 10 s, 20 µl of Fluorescence labelled Cx43 antisense ODNs either in water or in 30% Pluronic F127 was applied on the microneedle treated area immediately. After 2 hours, the excess DNA sample on skin surface was wiped off with wetted Kimwipes for 3 times. Then the skin was fixed in 10% Neutral Buffered Formalin (Sigma-Aldrich, US) in the fridge for 2 days, followed by sucrose equilibration overnight in fridge to protect skin samples from ice forming in the embedding step. Then the skin samples were embedding in OCT medium and cut in 14 µm thick sections from the *stratum corneum* side to the dermis side. The thin section was transferred to a glass slide and rehydrated in PBS for 10 min. After the skin section was tapped dry by tissue paper, a drop of DAPI solution was put on the skin section for 10 min. Then the DAPI solution was washed off and a drop of glycerol was put on the skin section followed by covered with a coverslip. The coverslip was then sealed with nail polishing liquid. The processed skin sectioning samples were then imaged by using a Leica confocal microscope.

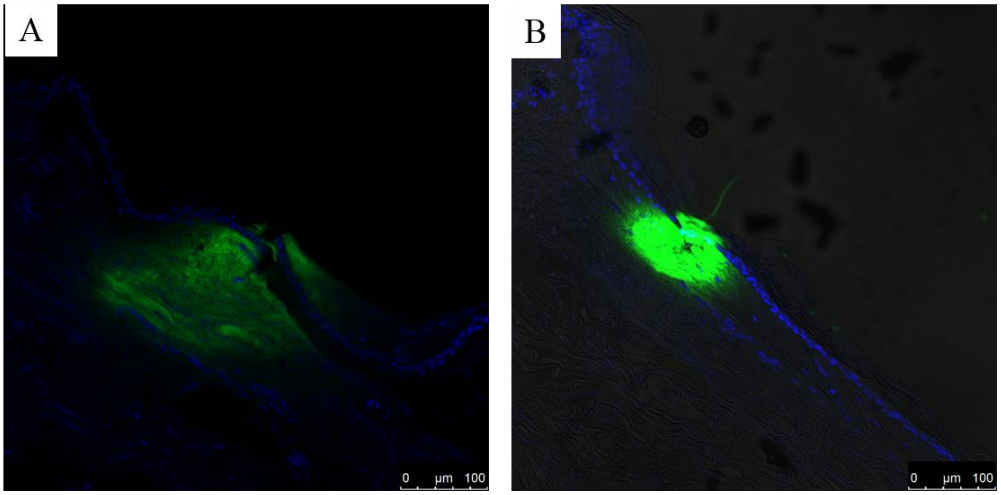

Appendix 5 Skin penetration of fluorescence-labeled antisense ODNs. (A) and (B) are the histological section of human skin stained with DAPI by applying with fluorescence-labeled antisense ODN solution sample and gel sample, respectively.

From **Appendix 5**, it was observed that the fluorescent antisense ODNs passed through the sites of *stratum corneum* perforation and go deep into the dermis layer of the skin. The solution sample can diffuse deeper into the skin than the gel sample. It indicated that we should control the gel viscosity to optimize the drug delivery into skin.

8.3.3. *In vivo* percutaneous delivery of antisense ODNs on the mouse skin.

Mice were anaesthetized with isoflurane gas. Then hair on the back was shaved to minimum 4 cm (H) × 3 cm (W) followed by hair removal cream (Nair™) application and removal after 1 min. The skin was further sterilized by 70% ethanol wipe for 3 times. Then the 3M MSS was pressed on skin for 10 s and 1 µM antisense ODNs in 15% Pluronic F127 gel was spread on the microneedle treated area. After 10 min to allow antisense ODNs to be absorbed into skin, Tegaderm™ film was carefully covered around the gel. Then the mouse was put back into cage with water and food feeding. After 4 hours, the mouse was sacrificed and the treated skin was cut and put into embedding solution. The skin samples was then imaged by using a fluorescent microscope to have a top view of the microneedle spots. After that, the skin samples were subjected to histological sectioning and staining.

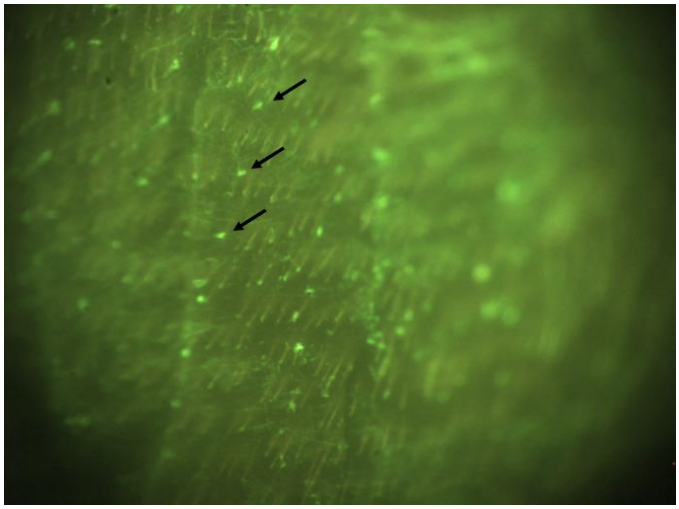

Appendix 6 The image of mouse skin at 4 h after MN pretreatment plus antisense ODN gel treatment.

From **Appendix 6**, it was observed that the passages created by microneedles were still visible at 4 h after microneedle pretreatment. However, no green fluorescence was found deep into skin during the histological section observation. It may because the concentration of antisense ODNs used in the gel is too low, or because of the fast degradation of antisense ODNs in skin. Further study should be carried out.

References

1. Prausnitz MR, Langer R. Transdermal drug delivery. Nat Biotechnol. 2008;26:1261-1268.

2. FDA. Approved drug products with therapeutic equivalence evaluations. 2015 11 Nov. Available from: www.FDA.gov.

3. Pegoraro C, MacNeil S, Battaglia G. Transdermal drug delivery: from micro to nano. Nanoscale. 2012;4:1881-1894.

4. Kreilgaard M. Dermal pharmacokinetics of microemulsion formulations determined by in vivo microdialysis. Pharm Res. 2001;18(3):367-373.

5. Cevc G. Drug delivery across the skin. Expert Opin Investig Drugs. 1997;6(12):1887-1937.

6. Kwan YH, Tung YK, Kochhar JS, Poh AL, Kang L. Handbook of Cosmeceutical Excipients. Cambridge, UK: Woodhead Publishing; 2014.

7. Michniak-Kohn BB, Wertz PW, Al-Khalili M, Meidan VM. Skin: Physiology and penetration pathways. In: Meyer RR, editor. Delivery System Handbook for Personal Care and Cosmetic Products. Norwich, NY: William Andrew Publishing; 2005. p. 77-100.

8. Mitragotri S. Breaking the skin barrier. Adv Drug Deliv Rev. 2004;56(5):555-556.

9. Yamashita F, Hashida M. Mechanistic and empirical modeling of skin permeation of drugs. Adv Drug Deliv Rev. 2003;55(9):1185-1199.

10. Nemanic MK, Elias PM. In situ precipitation: a novel cytochemical technique for visualization of permeability pathways in mammalian stratum corneum. J Histochem Cytochem. 1980;28(6):573-578.

11. Williams AC, Barry BW. Terpenes and the lipid-protein-partitioning theory of skin penetration enhancement. Pharm Res. 1991;8(1):17-24.

12. Paudel KS, Milewski M, Swadley CL, Brogden NK, Ghosh P, Stinchcomb AL. Challenges and opportunities in dermal/transdermal delivery. Ther Deliv. 2010;1(1):109-131.

13. Kanikkannan N. Iontophoresis-based transdermal delivery systems. BioDrugs. 2002;16:339-347.

14. Kajimoto K, Yamamoto M, Watanabe M, Kigasawa K, Kanamura K, Harashima H, Kogure K. Noninvasive and persistent transfollicular drug delivery system using a combination of liposomes and iontophoresis. Int J Pharm. 2011;403(1-2):57-65.

15. Garland MJ, Caffarel-Salvador E, Migalska K, Woolfson AD, Donnelly RF. Dissolving polymeric microneedle arrays for electrically assisted transdermal drug delivery. J Control Release. 2012;159:52-59.

16. Escobar-Chávez JJ, Bonilla-Martínez D, Villegas-González MA, Revilla-Vázquez AL. Electroporation as an efficient physical enhancer for skin drug delivery. J Clin Pharmacol. 2009;49:1262-1283.

17. Mitragotri S, Kost J. Low-frequency sonophoresis: a review. Adv Drug Deliv Rev. 2004;56:589-601.

18. Polat BE, Blankschtein D, Langer R. Low-frequency sonophoresis: application to the transdermal delivery of macromolecules and hydrophilic drugs. Expert Opin Drug Deliv. 2010;7:1415-1432.

19. Lee JW, Gadiraju P, Park JH, Allen MG, Prausnitz MR. Microsecond thermal ablation of skin for transdermal drug delivery. J Control Release. 2011;154:58-68.

20. Bramson J, Dayball K, Evelegh C, Wan YH, Page D, Smith A. Enabling topical immunization via microporation: a novel method for pain-free and needle-free delivery of adenovirus-based vaccines. Gene Ther. 2003;10(3):251-260.

21. Bachhav YG, Summer S, Heinrich A, Bragagna T, Böhler C, Kalia YN. Effect of controlled laser microporation on drug transport kinetics into and across the skin. Journal of controlled release. 2010;146:31-36.

22. Levin G, Gershonowitz A, Sacks H, Stern M, Sherman A, Rudaev S, Zivin I, Phillip M. Transdermal delivery of human growth hormone through RF-microchannels. Pharm Res. 2005;22:550-555.

23. Badkar AV, Smith AM, Eppstein JA, Banga AK. Transdermal delivery of interferon alpha-2B using microporation and iontophoresis in hairless rats. Pharm Res. 2007;24:1389-1395.

24. Gerstel MS, Place VA Drug delivery device. US 3964482 A, 1976.

25. Henry S, McAllister DV, Allen MG, Prausnitz MR. Microfabricated microneedles: a novel approach to transdermal drug delivery. J Pharm Sci. 1998;87(8):922-925.

26. Donnelly RF, Singh TRR, Morrow DIJ, Woolfson AD. Microneedles: Design, microfabrication and optimization. In. Microneedle-Mediated Transdermal and Intradermal Drug Delivery: John Wiley & Sons, Ltd; 2012. p. 20-56.

27. Zhang Y, Brown K, Siebenaler K, Determan A, Dohmeier D, Hansen K. Development of lidocaine-coated microneedle product for rapid, safe, and prolonged local analgesic action. Pharm Res. 2012;29:170-177.

28. Duan D, Moeckly C, Gysbers J, Novak C, Prochnow G, Siebenaler K, Albers L, Hansen K. Enhanced delivery of topically-applied formulations following skin pre-treatment with a hand-applied, plastic microneedle array. Current drug delivery. 2011;8:557-565.

29. Burton Sa, Ng C-Y, Simmers R, Moeckly C, Brandwein D, Gilbert T, Johnson N, Brown K, Alston T, Prochnow G, Siebenaler K, Hansen K. Rapid intradermal delivery of liquid formulations using a hollow microstructured array. Pharm Res. 2011;28:31-40.

30. Prausnitz MR, Mikszta JA, Cormier M, Andrianov AK. Microneedle-based vaccines. Curr Top Microbiol Immunol. 2009;333:369-393.

31. Gupta J, Gill HS, Andrews SN, Prausnitz MR. Kinetics of skin resealing after insertion of microneedles in human subjects. J Control Release. 2011;154(2):148-155.

32. Haq MI, Smith E, John DN, Kalavala M, Edwards C, Anstey A, Morrissey A, Birchall JC. Clinical administration of microneedles: skin puncture, pain and sensation. Biomed Microdevices. 2009;11(1):35-47.

33. Lee JW, Park JH, Prausnitz MR. Dissolving microneedles for transdermal drug delivery. Biomaterials. 2008;29:2113-2124.

34. Donnelly RF, Raj Singh TR, Woolfson AD. Microneedle-based drug delivery systems: microfabrication, drug delivery and safety. Drug delivery. 2010;17:187-207.

35. Li H, Yu Y, Faraji Dana S, Li B, Lee CY, Kang L. Novel engineered systems for oral, mucosal and transdermal drug delivery. J Drug Target. 2013;21(7):611-629.

36. Park JH, Allen MG, Prausnitz MR. Biodegradable polymer microneedles: fabrication, mechanics and transdermal drug delivery. J Control Release. 2005;104(1):51-66.

37. Lee JW, Han MR, Park JH. Polymer microneedles for transdermal drug delivery. J Drug Target. 2012.

38. Hirschberg HJ, van de Wijdeven GG, Kraan H, Amorij JP, Kersten GF. Bioneedles as alternative delivery system for hepatitis B vaccine. J Control Release. 2010;147(2):211-217.

39. Hirschberg HJ, van de Wijdeven GG, Kelder AB, van den Dobbelsteen GP, Kersten GF. Bioneedles as vaccine carriers. Vaccine. 2008;26(19):2389-2397.

40. Ito Y, Murakami A, Maeda T, Sugioka N, Takada K. Evaluation of self-dissolving needles containing low molecular weight heparin (LMWH) in rats. Int J Pharm. 2008;349(1-2):124-129.

41. Lee K, Lee CY, Jung H. Dissolving microneedles for transdermal drug administration prepared by stepwise controlled drawing of maltose. Biomaterials. 2011;32(11):3134-3140.

42. Li G, Badkar A, Nema S, Kolli CS, Banga AK. In vitro transdermal delivery of therapeutic antibodies using maltose microneedles. Int J Pharm. 2009;368(1-2):109-115.

43. Donnelly RF, Morrow DI, Singh TR, Migalska K, McCarron PA, O'Mahony C, Woolfson AD. Processing difficulties and instability of carbohydrate microneedle arrays. Drug Dev Ind Pharm. 2009;35(10):1242-1254.

44. Bariya SH, Gohel MC, Mehta TA, Sharma OP. Microneedles: an emerging transdermal drug delivery system. J Pharm Pharmacol. 2012;64(1):11-29.

45. Donnelly RF, Majithiya R, Singh TR, Morrow DI, Garland MJ, Demir YK, Migalska K, Ryan E, Gillen D, Scott CJ, Woolfson AD. Design, optimization and characterisation of polymeric microneedle arrays prepared by a novel laser-based micromoulding technique. Pharm Res. 2011;28(1):41-57.

46. You SK, Noh YW, Park HH, Han M, Lee SS, Shin SC, Cho CW. Effect of applying modes of the polymer microneedle-roller on the permeation of L-ascorbic acid in rats. J Drug Target. 2010;18(1):15-20.

47. Kochhar JS, Goh WJ, Chan SY, Kang L. A simple method of microneedle array fabrication for transdermal drug delivery. Drug Dev Ind Pharm. 2012;39(2):299-309.

48. Park JH, Allen MG, Prausnitz MR. Polymer microneedles for controlled-release drug delivery. Pharm Res. 2006;23(5):1008-1019.

49. Sullivan SP, Koutsonanos DG, Del Pilar Martin M, Lee JW, Zarnitsyn V, Choi SO, Murthy N, Compans RW, Skountzou I, Prausnitz MR. Dissolving polymer microneedle patches for influenza vaccination. Nat Med. 2010;16:915-920.

50. Migalska K, Morrow DIJ, Garland MJ, Thakur R, Woolfson AD, Donnelly RF. Laser-engineered dissolving microneedle arrays for transdermal macromolecular drug delivery. Pharm Res. 2011;28:1919-1930.

51. Kochhar JS, Zou S, Chan SY, Kang L. Protein encapsulation in polymeric microneedles by photolithography. Int J Nanomedicine. 2012;7:3143-3154.

52. Pegoraro C, MacNeil S, Battaglia G. Transdermal drug delivery: from micro to nano. Nanoscale. 2012;4(6):1881-1894.

53. Kim YC, Park JH, Prausnitz MR. Microneedles for drug and vaccine delivery. Adv Drug Deliv Rev. 2012;64(14):1547-1568.

54. Prausnitz MR. Microneedles for transdermal drug delivery. Adv Drug Deliv Rev. 2004;56(5):581-587.

55. van der Maaden K, Jiskoot W, Bouwstra J. Microneedle technologies for (trans)dermal drug and vaccine delivery. J Control Release. 2012;161(2):645-655.

56. Gill HS, Prausnitz MR. Coated microneedles for transdermal delivery. J Control Release. 2007;117:227-237.

57. Choi HJ, Bondy BJ, Yoo DG, Compans RW, Kang SM, Prausnitz MR. Stability of whole inactivated influenza virus vaccine during coating onto metal microneedles. J Control Release. 2013;166(2):159-171.

58. Kommareddy S, Baudner BC, Bonificio A, Gallorini S, Palladino G, Determan AS, Dohmeier DM, Kroells KD, Sternjohn JR, Singh M, Dormitzer PR, Hansen KJ, O'Hagan DT. Influenza subunit vaccine coated microneedle patches elicit comparable immune responses to intramuscular injection in guinea pigs. Vaccine. 2013;31(34):3435-3441.

59. Gill HS, Prausnitz MR. Coating formulations for microneedles. Pharm Res. 2007;24(7):1369-1380.

60. Ito Y, Kashiwara S, Fukushima K, Takada K. Two-layered dissolving microneedles for percutaneous delivery of sumatriptan in rats. Drug Dev Ind Pharm. 2011;37(12):1387-1393.

61. Chu LY, Choi SO, Prausnitz MR. Fabrication of dissolving polymer microneedles for controlled drug encapsulation and delivery: Bubble and pedestal microneedle designs. J Pharm Sci. 2010;99(10):4228-4238.

62. Park JH, Choi SO, Kamath R, Yoon YK, Allen MG, Prausnitz MR. Polymer particle-based micromolding to fabricate novel microstructures. Biomed Microdevices. 2007;9(2):223-234.

63. Kochhar JS, Goh WJ, Chan SY, Kang L. A simple method of microneedle array fabrication for transdermal drug delivery. Drug Dev Ind Pharm. 2013;39(2):299-309.

64. Chen B, Wei J, Tay FH, Wong Y, Iliescu C. Silicon microneedle array with biodegradable tips for transdermal drug delivery. Microsystem Technologies. 2008;14(7):1015-1019.

65. Lee K, Kim JD, Lee CY, Her S, Jung H. A high-capacity, hybrid electro-microneedle for in-situ cutaneous gene transfer. Biomaterials. 2011;32(30):7705-7710.

66. Banga AK. Microporation applications for enhancing drug delivery. Expert Opin Drug Deliv. 2009;6(4):343-354.

67. Davis SP, Martanto W, Allen MG, Prausnitz MR. Hollow metal microneedles for insulin delivery to diabetic rats. IEEE Trans Biomed Eng. 2005;52:909-915.

68. Hafeli UO, Mokhtari A, Liepmann D, Stoeber B. In vivo evaluation of a microneedle-based miniature syringe for intradermal drug delivery. Biomed Microdevices. 2009;11(5):943-950.

69. Martanto W, Moore JS, Kashlan O, Kamath R, Wang PM, O'Neal JM, Prausnitz MR. Microinfusion using hollow microneedles. Pharm Res. 2006;23(1):104-113.

70. Gupta J, Felner EI, Prausnitz MR. Minimally invasive insulin delivery in subjects with type 1 diabetes using hollow microneedles. Diabetes Technol Ther. 2009;11(6):329-337.

71. Amirouche F, Zhou Y, Johnson T. Current micropump technologies and their biomedical applications. Microsystem Technologies. 2009;15(5):647-666.

72. Ashraf MW, Tayyaba S, Nisar A, Afzulpurkar N, Bodhale DW, Lomas T, Poyai A, Tuantranont A. Design, fabrication and analysis of silicon hollow microneedles for transdermal drug delivery system for treatment of hemodynamic dysfunctions. Cardiovascular engineering. 2010;10(3):91-108.

73. Cui Q, Liu C, Zha X. Study on a piezoelectric micropump for the controlled drug delivery system. Microfluidics and Nanofluidics. 2007;3(4):377-390.

74. Martanto W, Baisch SM, Costner EA, Prausnitz MR, Smith MK. Fluid dynamics in conically tapered microneedles. AIChE Journal. 2005;51(6):1599-1607.

75. Yung KL, Yan X, Chunlei K, Liu H, Tam KF, Ko SM, Kwan FY, Thomas MHL. Sharp tipped plastic hollow microneedle array by microinjection moulding. Journal of Micromechanics and Microengineering. 2012;22(1):015016.

76. Singh TR, Dunne NJ, Cunningham E, Donnelly RF. Review of patents on microneedle applicators. Recent Pat Drug Deliv Formul. 2011;5(1):11-23.

77. Oh JH, Park HH, Do KY, Han M, Hyun DH, Kim CG, Kim CH, Lee SS, Hwang SJ, Shin SC, Cho CW. Influence of the delivery systems using a microneedle array on the permeation of a hydrophilic molecule, calcein. European journal of pharmaceutics and biopharmaceutics. 2008;69(3):1040-1045.

78. Verbaan FJ, Bal SM, van den Berg DJ, Dijksman JA, van Hecke M, Verpoorten H, van den Berg A, Luttge R, Bouwstra JA. Improved piercing of microneedle arrays in dermatomed human skin by an impact insertion method. J Control Release. 2008;128(1):80-88.

79. Wu XM, Todo H, Sugibayashi K. Effects of pretreatment of needle puncture and sandpaper abrasion on the in vitro skin permeation of fluorescein isothiocyanate (FITC)-dextran. Int J Pharm. 2006;316(1-2):102-108.

80. Yan G, Warner KS, Zhang J, Sharma S, Gale BK. Evaluation needle length and density of microneedle arrays in the pretreatment of skin for transdermal drug delivery. Int J Pharm. 2010;391(1-2):7-12.

81. Kochhar JS, Quek TC, Soon WJ, Choi J, Zou S, Kang L. Effect of microneedle geometry and supporting substrate on microneedle array penetration into skin. J Pharm Sci. 2013;102(11):4100-4108.

82. Verbaan FJ, Bal SM, van den Berg DJ, Groenink WH, Verpoorten H, Luttge R, Bouwstra JA. Assembled microneedle arrays enhance the transport of compounds varying over a large range of molecular weight across human dermatomed skin. J Control Release. 2007;117(2):238-245.

83. Banks SL, Pinninti RR, Gill HS, Crooks PA, Prausnitz MR, Stinchcomb AL. Flux across [corrected] microneedle-treated skin is increased by increasing charge of naltrexone and naltrexol in vitro. Pharm Res. 2008;25(7):1677-1685.

84. Milewski M, Brogden NK, Stinchcomb AL. Current aspects of formulation efforts and pore lifetime related to microneedle treatment of skin. Expert Opin Drug Deliv. 2010;7(5):617-629.

85. Bal SM, Caussin J, Pavel S, Bouwstra JA. In vivo assessment of safety of microneedle arrays in human skin. Eur J Pharm Sci. 2008;35(3):193-202.

86. Noh YW, Kim TH, Baek JS, Park HH, Lee SS, Han M, Shin SC, Cho CW. In vitro characterization of the invasiveness of polymer microneedle against skin. Int J Pharm. 2010;397(1-2):201-205.

87. Donnelly RF, Singh TR, Tunney MM, Morrow DI, McCarron PA, O'Mahony C, Woolfson AD. Microneedle arrays allow lower microbial penetration than hypodermic needles in vitro. Pharm Res. 2009;26(11):2513-2522.

88. Kumar A, Li X, Sandoval MA, Rodriguez BL, Sloat BR, Cui Z. Permeation of antigen protein-conjugated nanoparticles and live bacteria through microneedle-treated mouse skin. Int J Nanomedicine. 2011;6:1253-1264.

89. Prausnitz M, Mikszta J, Cormier M, Andrianov A. Microneedle-based vaccines. In: Compans RW, Orenstein WA, editors. Vaccines for Pandemic Influenza: Springer Berlin Heidelberg; 2009. p. 369-393.

90. Pickart L, Thaler MM. Tripeptide in human serum which prolongs survival of normal liver cells and stimulates growth in neoplastic liver. Nat New Biol. 1973;243(124):85-87.

91. Maquart FX, Pickart L, Laurent M, Gillery P, Monboisse JC, Borel JP. Stimulation of collagen synthesis in fibroblast cultures by the tripeptide-copper complex glycyl-L-histidyl-L-lysine-Cu2+. FEBS Lett. 1988;238(2):343-346.

92. Buffoni F, Pino R, Dal Pozzo A. Effect of tripeptide-copper complexes on the process of skin wound healing and on cultured fibroblasts. Arch Int Pharmacodyn Ther. 1995;330(3):345-360.

93. Wegrowski Y, Maquart FX, Borel JP. Stimulation of sulfated glycosaminoglycan synthesis by the tripeptide-copper complex glycyl-L-histidyl-L-lysine-Cu2+. Life Sci. 1992;51(13):1049-1056.

94. Siméon A, Emonard H, Hornebeck W, Maquart F-X. The tripeptide-copper complex glycyl-L-histidyl-L- lysine-Cu2+ stimulates matrix metalloproteinase-2 expression by fibroblast cultures. Life Sciences. 2000;67(18):2257-2265.

95. Siméon A, Wegrowski Y, Bontemps Y, Maquart FX. Expression of glycosaminoglycans and small proteoglycans in wounds: modulation by the tripeptide-copper complex glycyl-L-histidyl-L-lysine-Cu(2+). J Invest Dermatol. 2000;115(6):962-968.

96. McCormack MC, Nowak KC, Koch RJ. The effect of copper tripeptide and tretinoin on growth factor production in a serum-free fibroblast model. Arch Facial Plast Surg. 2001;3(1):28-32.

97. Kang YA, Choi HR, Na JI, Huh CH, Kim MJ, Youn SW, Kim KH, Park KC. Copper-GHK increases integrin expression and p63 positivity by keratinocytes. Arch Dermatol Res. 2009;301(4):301-306.

98. Choi HR, Kang YA, Ryoo SJ, Shin JW, Na JI, Huh CH, Park KC. Stem cell recovering effect of copper-free GHK in skin. J Pept Sci. 2012;18(11):685-690.

99. Pickart L. The human tri-peptide GHK and tissue remodeling. J Biomater Sci Polym Ed. 2008;19(8):969-988.

100. Hostynek JJ, Dreher F, Maibach HI. Human skin retention and penetration of a copper tripeptide in vitro as function of skin layer towards anti-inflammatory therapy. Inflamm Res. 2010;59(11):983-988.

101. Philips N, Hwang H, Chauhan S, Leonardi D, Gonzalez S. Stimulation of cell proliferation and expression of matrixmetalloproteinase-1 and interluekin-8 genes in dermal fibroblasts by copper. Connect Tissue Res. 2010;51(3):224-229.

102. Maquart FX, Bellon G, Chaqour B, Wegrowski J, Patt LM, Trachy RE, Monboisse JC, Chastang F, Birembaut P, Gillery P, et al. In vivo stimulation of connective tissue accumulation by the tripeptide-copper complex glycyl-L-histidyl-L-lysine-Cu2+ in rat experimental wounds. J Clin Invest. 1993;92(5):2368-2376.

103. Gorouhi F, Maibach HI. Role of topical peptides in preventing or treating aged skin. Int J Cosmet Sci. 2009;31(5):327-345.

104. Lamb J. The Connectivity Map: a new tool for biomedical research. Nat Rev Cancer. 2007;7(1):54-60.

105. Iorio F, Bosotti R, Scacheri E, Belcastro V, Mithbaokar P, Ferriero R, Murino L, Tagliaferri R, Brunetti-Pierri N, Isacchi A, di Bernardo D. Discovery of drug mode of action and drug repositioning from transcriptional responses. Proc Natl Acad Sci U S A. 2010;107(33):14621-14626.

106. Campbell JD, McDonough JE, Zeskind JE, Hackett TL, Pechkovsky DV, Brandsma CA, Suzuki M, Gosselink JV, Liu G, Alekseyev YO, Xiao J, Zhang X, Hayashi S, Cooper JD, Timens W, Postma DS, Knight DA, Marc LE, James HC, Avrum S. A gene expression signature of emphysema-related lung destruction and its reversal by the tripeptide GHK. Genome Med. 2012;4(8):67.

107. Huang PJ, Huang YC, Su MF, Yang TY, Huang JR, Jiang CP. In vitro observations on the influence of copper peptide aids for the LED photoirradiation of fibroblast collagen synthesis. Photomed Laser Surg. 2007;25(3):183-190.

108. Pollard JD, Quan S, Kang T, Koch RJ. Effects of copper tripeptide on the growth and expression of growth factors by normal and irradiated fibroblasts. Arch Facial Plast Surg. 2005;7(1):27-31.

109. Harvey L. Mineral bioavailability. Nutrition & Food Science. 2001;31(4):179-182.

110. Driscoll MS, Kwon EK, Skupsky H, Kwon SY, Grant-Kels JM. Nutrition and the deleterious side effects of nutritional supplements. Clin Dermatol. 2010;28(4):371-379.

111. Chan S, Gerson B, Subramaniam S. The role of copper, molybdenum, selenium, and zinc in nutrition and health. Clin Lab Med. 1998;18(4):673-685.

112. Araya M, Pena C, Pizarro F, Olivares M. Gastric response to acute copper exposure. Sci Total Environ. 2003;303(3):253-257.

113. Reynolds JEF, Prasad AB (eds.) Martindale, the extra pharmacopoeia. Lodon: The Pharmaceutical Press; 1982.

114. Pickart L, Freedman JH, Loker WJ, Peisach J, Perkins CM, Stenkamp RE, Weinstein B. Growth-modulating plasma tripeptide may function by facilitating copper uptake into cells. Nature. 1980;288(5792):715-717.

115. Pickart L. The need for improved skin regenerative copper peptides. 2014 17 Apr. Available from: http://skinbiology.com/copper-peptides-need-for-improved.html.

116. Mulder GD, Patt LM, Sanders L, Rosenstock J, Altman MI, Hanley ME, Duncan GW. Enhanced healing of ulcers in patients with diabetes by topical treatment with glycyl-l-histidyl-l-lysine copper. Wound Repair Regen. 1994;2(4):259-269.

117. Bishop JB, Phillips LG, Mustoe TA, VanderZee AJ, Wiersema L, Roach DE, Heggers JP, Hill DP, Jr., Taylor EL, Robson MC. A prospective randomized evaluator-blinded trial of two potential wound healing agents for the treatment of venous stasis ulcers. J Vasc Surg. 1992;16(2):251-257.

118. Wu Y, Qiu Y, Zhang S, Qin G, Gao Y. Microneedle-based drug delivery: studies on delivery parameters and biocompatibility. Biomed Microdevices. 2008;10(5):601-610.

119. Mohammed YH, Yamada M, Lin LL, Grice JE, Roberts MS, Raphael AP, Benson HA, Prow TW. Microneedle enhanced delivery of cosmeceutically relevant peptides in human skin. PLoS One. 2014;9(7):e101956.

120. Godin B, Touitou E. Transdermal skin delivery: predictions for humans from in vivo, ex vivo and animal models. Adv Drug Deliv Rev. 2007;59(11):1152-1161.

121. Mah CS, Kochhar JS, Ong PS, Kang L. A miniaturized flow-through cell to evaluate skin permeation of endoxifen. Int J Pharm. 2013;441(1-2):433-440.

122. Hostynek JJ, Dreher F, Maibach HI. Human skin penetration of a copper tripeptide in vitro as a function of skin layer. Inflamm Res. 2011;60(1):79-86.

123. Tinggi U, Maher W. Determination of trace elements in biological tissues by aluminum block digestion and spike-height flame atomic absorption spectrometry. Microchemical Journal. 1986;33(3):304-308.

124. Davis SP, Landis BJ, Adams ZH, Allen MG, Prausnitz MR. Insertion of microneedles into skin: measurement and prediction of insertion force and needle fracture force. J Biomech. 2004;37(8):1155-1163.

125. Park JH, Yoon YK, Choi SO, Prausnitz MR, Allen MG. Tapered conical polymer microneedles fabricated using an integrated lens technique for transdermal drug delivery. IEEE Trans Biomed Eng. 2007;54(5):903-913.

126. Tran S-L, Puhar A, Ngo-Camus M, Ramarao N. Trypan blue dye enters viable cells incubated with the pore-forming toxin HlyII of Bacillus cereus. PLoS ONE. 2011;6(9):e22876.

127. Marieb EN, Hoehn K. Human Anatomy & Physiology. Boston: Pearson; 2007.

128. Andrews SN, Jeong E, Prausnitz MR. Transdermal delivery of molecules is limited by full epidermis, not just stratum corneum. Pharm Res. 2013;30(4):1099-1109.

129. Robert LB, Jeffrey JY, Margaret EKK. Determination of percutaneous absorption by in vitro techniques. In. Percutaneous Absorption: CRC Press; 2005. p. 265-269.

130. Hostynek JJ. Factors determining percutaneous metal absorption. Food Chem Toxicol. 2003;41(3):327-345.

131. Endo T, Miyagi M, Ujiie A. Simultaneous determination of glycyl-L-histidyl-L-lysine and its metabolite, L-histidyl-L-lysine, in rat plasma by high-performance liquid chromatography with post-column derivatization. J Chromatogr B Biomed Sci Appl. 1997;692(1):37-42.

132. Gibbs S. In vitro Irritation Models and Immune Reactions. Skin Pharmacology and Physiology. 2009;22(2):103-113.

133. Simon GA, Maibach HI. The pig as an experimental animal model of percutaneous permeation in man: qualitative and quantitative observations--an overview. Skin Pharmacol Appl Skin Physiol. 2000;13(5):229-234.

134. Institute of Medicine FaNB. Dietary Reference Intakes for Vitamin A, Vitamin K, Arsenic, Boron, Chromium, Copper, Iodine, Iron, Manganese, Molybdenum, Nickel, Silicon, Vanadium, and Zinc. The National Academies Press. 2015 19 Jan. Available from: http://www.nal.usda.gov/fnic/DRI/DRI_Vitamin_A/vitamin_a_full_report.pdf.

135. WHO/FAO/IAEA. Trace elements in human nutrition and health. World Health Organization. 2015 19 Jan. Available from: http://whqlibdoc.who.int/publications/1996/9241561734_eng_fulltext.pdf.

136. Stanford JB, Mikolajczyk RT. Mechanisms of action of intrauterine devices: update and estimation of postfertilization effects. Am J Obstet Gynecol. 2002;187(6):1699-1708.

137. Hostynek JJ, Maibach HI. Skin irritation potential of copper compounds. Toxicol Mech Methods. 2004;14(4):205-213.

138. Hostynek JJ. Corrosion chemistry of copper: Formation of potentially skin-diffusible compounds. In: Hostynek JJ, Maibach HI, editors. Copper and the Skin. Boca Raton, Florida: CRC Press; 2006. p. 7-19.

139. Li H, Low Y, Chong H, Zin M, Lee C-Y, Li B, Leolukman M, Kang L. Microneedle-mediated delivery of copper peptide through skin. Pharmaceutical Research. 2015;32(8):2678-2689.

140. Walker WR, Beveridge SJ, Whitehouse MW. Dermal copper drugs: the copper bracelet and cu(II) salicylate complexes. Agents Actions Suppl. 1981;8:359-367.

141. Ma Z, Moulton B. Supramolecular medicinal chemistry: mixed-ligand coordination complexes. Molecular pharmaceutics. 2007;4(3):373-385.

142. El Brahmi N, El Kazzouli S, Mignani SM, Essassi EM, Aubert G, Laurent R, Caminade A-M, Bousmina MM, Cresteil T, Majoral J-P. Original multivalent copper(II)-conjugated phosphorus dendrimers and corresponding mononuclear copper(II) complexes with antitumoral activities. Molecular Pharmaceutics. 2013;10(4):1459-1464.

143. Kheirolomoom A, Mahakian LM, Lai C-Y, Lindfors HA, Seo JW, Paoli EE, Watson KD, Haynam EM, Ingham ES, Xing L, Cheng RH, Borowsky AD, Cardiff RD, Ferrara KW. Copper−doxorubicin as a nanoparticle cargo retains efficacy with minimal toxicity. Molecular Pharmaceutics. 2010;7(6):1948-1958.

144. Ramadan S, Guo L, Li Y, Yan B, Lu W. Hollow copper sulfide nanoparticle-mediated transdermal drug delivery. Small. 2012;8(20):3143-3150.

145. Miller TR, Wagner JD, Baack BR, Eisbach KJ. Effects of topical copper tripeptide complex on CO2 laser-resurfaced skin. Arch Facial Plast Surg. 2006;8(4):252-259.

146. Fishel FM. Pesticide toxicity profile: Copper-based pesticides 2015 21st July. Available from: http://www.edis.ifas.ufl.edu/pdffiles/PI/PI10300.pdf.

147. Fage SW, Faurschou A, Thyssen JP. Copper hypersensitivity. Contact Dermatitis. 2014;71(4):191-201.

148. EC. Opinion on the Murine Local Lymph Node Assay (LLNA) adopted by the SCCNFP during the 12th plenary meeting of 3 May 2000. 2015 21st July. Available from: http://ec.europa.eu/health/scientific_committees/consumer_safety/opinions/sccnfp_opinions_97_04/sccp_out114_en.htm.

149. Anderson SE, Siegel PD, Meade BJ. The LLNA: A brief review of recent advances and limitations. J Allergy (Cairo). 2011;2011:424203.

150. Miles A, Berthet A, Hopf NB, Gilliet M, Raffoul W, Vernez D, Spring P. A new alternative method for testing skin irritation using a human skin model: A pilot study. Toxicology in Vitro. 2014;28(2):240-247.

151. EC. Ban on animal testing - European Commission. 2015 21st July. Available from: http://ec.europa.eu/growth/sectors/cosmetics/animal-testing/index_en.htm.

152. Basketter D, Darlenski R, Fluhr JW. Skin irritation and sensitization: mechanisms and new approaches for risk assessment. Skin Pharmacol Physiol. 2008;21(4):191-202.

153. Niwa M, Nagai K, Oike H, Kobori M. Evaluation of the skin irritation using a DNA microarray on a reconstructed human epidermal model. Biol Pharm Bull. 2009;32(2):203-208.

154. Zhang Q, Dai T, Zhang L, Zhang M, Xiao X, Hu H, Zou P, Liu X, Xiang Q, Su Z, Huang Y, He QY. Identification of potential biomarkers for predicting acute dermal irritation by proteomic analysis. J Appl Toxicol. 2011;31(8):762-772.

155. D'Addario C, Dell'Osso B, Palazzo MC, Benatti B, Lietti L, Cattaneo E, Galimberti D, Fenoglio C, Cortini F, Scarpini E, Arosio B, Di Francesco A, Di Benedetto M, Romualdi P, Candeletti S, Mari D, Bergamaschini L, Bresolin N, Maccarrone M, Altamura AC. Selective DNA methylation of BDNF promoter in bipolar disorder: differences among patients with BDI and BDII. Neuropsychopharmacology. 2012;37(7):1647-1655.

156. Chen H, Li S, Meng T, Zhang L, Dai T, Xiang Q, Su Z, Zhang Q, Huang Y. HSP27 as a biomarker for predicting skin irritation in human skin and reconstructed organotypic skin model. Toxicol Lett. 2014;226(2):124-131.

157. van de Sandt J, Roguet R, Cohen C, Esdaile D, Ponec M, Corsini E, Barker C, Fusenig N, Liebsch M, Benford D, de Fraissinette Ade B, Fartasch M. The use of human keratinocytes and human skin models for predicting skin irritation. Altern Lab Anim. 1999;27(5):723-743.

158. Brosin A, Wolf V, Mattheus A, Heise H. Use of XTT-assay to assess the cytotoxicity of different surfactants and metal salts in human keratinocytes (HaCaT). A feasible method for in vitro testing of skin irritants. Acta Derm Venereol. 1997;77(1):26-28.

159. Dhingra N, Gulati N, Guttman-Yassky E. Mechanisms of contact sensitization offer insights into the role of barrier defects vs. intrinsic immune abnormalities as drivers of atopic dermatitis. J Invest Dermatol. 2013;133(10):2311-2314.

160. Borlon C, Godard P, Eskes C, Hartung T, Zuang V, Toussaint O. The usefulness of toxicogenomics for predicting acute skin irritation on in vitro reconstructed human epidermis. Toxicology. 2007;241(3):157-166.

161. Welss T, Basketter DA, Schroder KR. In vitro skin irritation: facts and future. State of the art review of mechanisms and models. Toxicol In Vitro. 2004;18(3):231-243.

162. Wilhelm KP, Bottjer B, Siegers CP. Quantitative assessment of primary skin irritants in vitro in a cytotoxicity model: comparison with in vivo human irritation tests. Br J Dermatol. 2001;145(5):709-715.

163. Wilheilm KP, Samblebe M, Siegers CP. Quantitative in vitro assessment of N-alkyl sulphate-induced cytotoxicity in human keratinocytes (HaCaT). Comparison with in vivo human irritation tests. Br J Dermatol. 1994;130(1):18-23.

164. Sanchez L, Mitjans M, Infante MR, Vinardell MP. Potential irritation of lysine derivative surfactants by hemolysis and HaCaT cell viability. Toxicology Letters. 2006;161(1):53-60.

165. Seth R, Yang S, Choi S, Sabean M, Roberts EA. In vitro assessment of copper-induced toxicity in the human hepatoma line, Hep G2. Toxicol In Vitro. 2004;18(4):501-509.

166. Sanchez L, Mitjans M, Infante MR, Vinardell MP. Determination of interleukin-1alpha in human NCTC 2544 keratinocyte cells as a predictor of skin irritation from lysine-based surfactants. Toxicol Lett. 2006;167(1):40-46.

167. Gröne A. Keratinocytes and cytokines. Veterinary Immunology and Immunopathology. 2002;88(1–2):1-12.

168. Wright HL, Moots RJ, Bucknall RC, Edwards SW. Neutrophil function in inflammation and inflammatory diseases. Rheumatology (Oxford). 2010;49(9):1618-1631.

169. Mohamadzadeh M, Miiller M, Hultsch T, Enk A, Saloga J, Knop J. Enhanced expression of IL-8 in normal human keratinocytes and human keratinocyte cell line HaCaT in vitro after stimulation with contact sensitizers., tolerogens and irritants. Experimental Dermatology. 1994;3(6):298-303.

170. Coquette A, Berna N, Vandenbosch A, Rosdy M, Poumay Y. Differential expression and release of cytokines by an in vitro reconstructed human epidermis following exposure to skin irritant and sensitizing chemicals. Toxicology in Vitro. 1999;13(6):867-877.

171. Coquette A, Berna N, Vandenbosch A, Rosdy M, De Wever B, Poumay Y. Analysis of interleukin-1α (IL-1α) and interleukin-8 (IL-8) expression and release in in vitro reconstructed human epidermis for the prediction of in vivo skin irritation and/or sensitization. Toxicology in Vitro. 2003;17(3):311-321.

172. Verde P, Casalino L, Talotta F, Yaniv M, Weitzman JB. Deciphering AP-1 function in tumorigenesis: fra-ternizing on target promoters. Cell Cycle. 2007;6(21):2633-2639.

173. Evellin S, Galvagni F, Zippo A, Neri F, Orlandini M, Incarnato D, Dettori D, Neubauer S, Kessler H, Wagner EF, Oliviero S. FOSL1 controls the assembly of endothelial cells into capillary tubes by direct repression of alphav and beta3 integrin transcription. Mol Cell Biol. 2013;33(6):1198-1209.

174. Scieglinska D, Piglowski W, Chekan M, Mazurek A, Krawczyk Z. Differential expression of HSPA1 and HSPA2 proteins in human tissues; tissue microarray-based immunohistochemical study. Histochem Cell Biol. 2011;135(4):337-350.

175. Freedman JH, Ciriolo MR, Peisach J. The role of glutathione in copper metabolism and toxicity. J Biol Chem. 1989;264(10):5598-5605.

176. Mazurowska L, Mojski M. Biological activities of selected peptides: skin penetration ability of copper complexes with peptides. J Cosmet Sci. 2008;59(1):59-69.

177. Lintner K, Peschard O. Biologically active peptides: from a laboratory bench curiosity to a functional skin care product. Int J Cosmet Sci. 2000;22(3):207-218.

178. ECVAM. Statement on the validity of in-vitro tests for skin irritation. 2015 27th August. Available from: https://eurl-ecvam.jrc.ec.europa.eu/validation-regulatory-acceptance/docs-skin-irritation-1/DOC5-ESAC2007.pdf.

179. Kenawy el R, Worley SD, Broughton R. The chemistry and applications of antimicrobial polymers: a state-of-the-art review. Biomacromolecules. 2007;8(5):1359-1384.

180. Blaszykowski C, Sheikh S, Thompson M. A survey of state-of-the-art surface chemistries to minimize fouling from human and animal biofluids. Biomater Sci. 2015;3(10):1335-1370.

181. Trampuz A, Widmer AF. Infections associated with orthopedic implants. Current Opinion in Infectious Diseases. 2006;19(4):349-356.

182. Tenke P, Riedl CR, Jones GL, Williams GJ, Stickler D, Nagy E. Bacterial biofilm formation on urologic devices and heparin coating as preventive strategy. International Journal of Antimicrobial Agents. 2004;23 Suppl 1:S67-74.

183. Song J, Kong H, Jang J. Bacterial adhesion inhibition of the quaternary ammonium functionalized silica nanoparticles. Colloids and Surfaces B: Biointerfaces. 2011;82(2):651-656.

184. Siedenbiedel F, Tiller JC. Antimicrobial polymers in solution and on surfaces: overview and functional principles. Polymers. 2012;4(1):46-71.

185. Advincula R. Polymer brushes by anionic and cationic surface-initiated polymerization (SIP). In: Jordan R, editor. Surface-initiated polymerization I: Springer Berlin Heidelberg; 2006. p. 107-136.

186. Hammond PT. Engineering materials layer-by-layer: Challenges and opportunities in multilayer assembly. AIChE Journal. 2011;57(11):2928-2940.

187. Friedrich J. Mechanisms of plasma polymerization – reviewed from a chemical point of view. Plasma Processes and Polymers. 2011;8(9):783-802.

188. Roosjen A, Norde W, Mei H, Busscher H. The use of positively charged or low surface free energy coatings versus polymer brushes in controlling biofilm formation. In: Grundke K, Stamm M, Adler H-J, editors. Characterization of Polymer Surfaces and Thin Films. Berlin Heidelberg: Springer 2006. p. 138-144.

189. Cheng G, Xue H, Zhang Z, Chen S, Jiang S. A switchable biocompatible polymer surface with self-sterilizing and nonfouling capabilities. Angew Chem Int Ed Engl. 2008;47(46):8831-8834.

190. Pearson HA, Andrie JM, Urban MW. Covalent attachment of multilayers (CAM): a platform for pH switchable antimicrobial and anticoagulant polymeric surfaces. Biomaterials Science. 2014;2(4):512-521.

191. Ramstedt M, Cheng N, Azzaroni O, Mossialos D, Mathieu HJ, Huck WT. Synthesis and characterization of poly(3-sulfopropylmethacrylate) brushes for potential antibacterial applications. Langmuir. 2007;23(6):3314-3321.

192. Alves D, Olivia Pereira M. Mini-review: Antimicrobial peptides and enzymes as promising candidates to functionalize biomaterial surfaces. Biofouling. 2014;30(4):483-499.

193. Kazemzadeh-Narbat M, Lai BF, Ding C, Kizhakkedathu JN, Hancock RE, Wang R. Multilayered coating on titanium for controlled release of antimicrobial peptides for the prevention of implant-associated infections. Biomaterials. 2013;34(24):5969-5977.

194. Gao G, Lange D, Hilpert K, Kindrachuk J, Zou Y, Cheng JT, Kazemzadeh-Narbat M, Yu K, Wang R, Straus SK, Brooks DE, Chew BH, Hancock RE, Kizhakkedathu JN. The biocompatibility and biofilm resistance of implant coatings based on hydrophilic polymer brushes conjugated with antimicrobial peptides. Biomaterials. 2011;32(16):3899-3909.

195. Wach J-Y, Bonazzi S, Gademann K. Antimicrobial surfaces through natural product hybrids. Angew Chem Int Ed Engl. 2008;47(37):7123-7126.

196. Zhang F, Shi ZL, Chua PH, Kang ET, Neoh KG. Functionalization of titanium surfaces via controlled living radical polymerization: from antibacterial surface to surface for osteoblast adhesion. Industrial & Engineering Chemistry Research. 2007;46(26):9077-9086.

197. Aumsuwan N, Heinhorst S, Urban MW. Antibacterial surfaces on expanded polytetrafluoroethylene; penicillin attachment. Biomacromolecules. 2007;8(2):713-718.

198. Aumsuwan N, McConnell MS, Urban MW. Tunable antimicrobial polypropylene surfaces: simultaneous attachment of penicillin (Gram +) and gentamicin (Gram -). Biomacromolecules. 2009;10(3):623-629.

199. Tang F, Zhang L, Zhang Z, Cheng Z, Zhu X. Cellulose filter paper with antibacterial activity from surface-initiated ATRP. Journal of Macromolecular Science®, Part A: Pure and Applied Chemistry. 2009;46(10):989-996.

200. Costa F, Carvalho IF, Montelaro RC, Gomes P, Martins MC. Covalent immobilization of antimicrobial peptides (AMPs) onto biomaterial surfaces. Acta biomaterialia. 2011;7(4):1431-1440.

201. Qin GT, Lopez A, Santos C, McDermott AM, Cai CZ. Antimicrobial peptide LL-37 on surfaces presenting carboxylate anions. Biomaterials Science. 2015;3(5):771-778.

202. Cho WM, Joshi BP, Cho H, Lee KH. Design and synthesis of novel antibacterial peptide-resin conjugates. Bioorg Med Chem Lett. 2007;17(21):5772-5776.

203. Bagheri M, Beyermann M, Dathe M. Immobilization reduces the activity of surface-bound cationic antimicrobial peptides with no influence upon the activity spectrum. Antimicrob Agents Chemother. 2009;53(3):1132-1141.

204. Hilpert K, Elliott M, Jenssen H, Kindrachuk J, Fjell CD, Korner J, Winkler DF, Weaver LL, Henklein P, Ulrich AS, Chiang SH, Farmer SW, Pante N, Volkmer R, Hancock RE. Screening and characterization of surface-tethered cationic peptides for antimicrobial activity. Chem Biol. 2009;16(1):58-69.

205. Onaizi SA, Leong SS. Tethering antimicrobial peptides: current status and potential challenges. Biotechnol Adv. 2011;29(1):67-74.

206. Tiller JC, Lee SB, Lewis K, Klibanov AM. Polymer surfaces derivatized with poly(vinyl-N-hexylpyridinium) kill airborne and waterborne bacteria. Biotechnol Bioeng. 2002;79(4):465-471.

207. Lee SB, Koepsel RR, Morley SW, Matyjaszewski K, Sun Y, Russell AJ. Permanent, nonleaching antibacterial surfaces. 1. Synthesis by atom transfer radical polymerization. Biomacromolecules. 2004;5(3):877-882.

208. Isquith AJ, Abbott EA, Walters PA. Surface-bonded antimicrobial activity of an organosilicon quaternary ammonium chloride. Appl Microbiol. 1972;24(6):859-863.

209. Windler L, Height M, Nowack B. Comparative evaluation of antimicrobials for textile applications. Environ Int. 2013;53:62-73.

210. USEPA. Reregistration eligibility decision for trimethoxysilyl quaternary ammonium chloride compounds. In: Agency USEP, editor. Washington, DC: United States Environmental Protection Agency, Prevention, Pesticides and Toxic Substances; 2007.

211. Ruiz Oropeza A, Fischer Friis U, Duus Johansen J. Occupational contact urticaria caused by didecyl dimethyl ammonium chloride. Contact Dermatitis. 2011;64(5):297-298.

212. Iwata M, Tanizaki H, Fujii H, Endo Y, Fujisawa A, Tanioka M, Miyachi Y, Kabashima K. Contact Urticaria Due to a Face Mask Coated with Disinfectant Liquid Spray. Acta Derm Venereol. 2015;95(5):628-629.

213. Erdem M, Yuksel E, Tay T, Cimen Y, Turk H. Synthesis of novel methacrylate based adsorbents and their sorptive properties towards p-nitrophenol from aqueous solutions. J Colloid Interface Sci. 2009;333(1):40-48.

214. Imazato S, Kinomoto Y, Tarumi H, Ebisu S, Tay FR. Antibacterial activity and bonding characteristics of an adhesive resin containing antibacterial monomer MDPB. Dent Mater. 2003;19(4):313-319.

215. Egger S, Lehmann RP, Height MJ, Loessner MJ, Schuppler M. Antimicrobial properties of a novel silver-silica nanocomposite material. Appl Environ Microbiol. 2009;75(9):2973-2976.

216. Chen S, Chen S, Jiang S, Mo Y, Luo J, Tang J, Ge Z. Study of zwitterionic sulfopropylbetaine containing reactive siloxanes for application in antibacterial materials. Colloids and Surfaces B: Biointerfaces. 2011;85(2):323-329.

217. French GL. Bactericidal agents in the treatment of MRSA infections--the potential role of daptomycin. Journal of Antimicrobial Chemotherapy. 2006;58(6):1107-1117.

218. Carmona-Ribeiro AM, de Melo Carrasco LD. Cationic antimicrobial polymers and their assemblies. International Journal of Molecular Sciences. 2013;14(5):9906-9946.

219. Buffet-Bataillon S, Tattevin P, Bonnaure-Mallet M, Jolivet-Gougeon A. Emergence of resistance to antibacterial agents: the role of quaternary ammonium compounds--a critical review. Int J Antimicrob Agents. 2012;39(5):381-389.

220. Gong SQ, Niu LN, Kemp LK, Yiu CK, Ryou H, Qi YP, Blizzard JD, Nikonov S, Brackett MG, Messer RL, Wu CD, Mao J, Bryan Brister L, Rueggeberg FA, Arola DD, Pashley DH, Tay FR. Quaternary ammonium silane-functionalized, methacrylate resin composition with antimicrobial activities and self-repair potential. Acta biomaterialia. 2012;8(9):3270-3282.

221. Song J, Kong H, Jang J. Bacterial adhesion inhibition of the quaternary ammonium functionalized silica nanoparticles. Colloids Surf B Biointerfaces. 2011;82(2):651-656.

222. Isquith AJ, Abbott EA, Walters PA. Surface-bonded antimicrobial activity of an organosilicon quaternary ammonium chloride. Applied Microbiology. 1972;24(6):859-863.

223. Donnelly RF, Singh TR, Alkilani AZ, McCrudden MT, O'Neill S, O'Mahony C, Armstrong K, McLoone N, Kole P, Woolfson AD. Hydrogel-forming microneedle arrays exhibit antimicrobial properties: potential for enhanced patient safety. Int J Pharm. 2013;451(1-2):76-91.

224. Boehm RD, Miller PR, Singh R, Shah A, Stafslien S, Daniels J, Narayan RJ. Indirect rapid prototyping of antibacterial acid anhydride copolymer microneedles. Biofabrication. 2012;4(1):011002.

225. Gittard SD, Narayan RJ, Jin C, Ovsianikov A, Chichkov BN, Monteiro-Riviere NA, Stafslien S, Chisholm B. Pulsed Laser Deposition of Antimicrobial Silver Coating on Ormocer® Microneedles. Biofabrication. 2009;1(4):41001-41001.

226. Bragg PD, Rainnie DJ. The effect of silver ions on the respiratory chain of Escherichia coli. Can J Microbiol. 1974;20(6):883-889.

227. Feng QL, Wu J, Chen GQ, Cui FZ, Kim TN, Kim JO. A mechanistic study of the antibacterial effect of silver ions on Escherichia coli and Staphylococcus aureus. J Biomed Mater Res. 2000;52(4):662-668.

228. Yamanaka M, Hara K, Kudo J. Bactericidal actions of a silver ion solution on Escherichia coli, studied by energy-filtering transmission electron microscopy and proteomic analysis. Appl Environ Microbiol. 2005;71(11):7589-7593.

229. Gupta A, Silver S. Molecular Genetics: Silver as a biocide: Will resistance become a problem? Nat Biotech. 1998;16(10):888-888.

230. Gittard SD, Miller PR, Jin C, Martin TN, Boehm RD, Chisholm BJ, Stafslien SJ, Daniels JW, Cilz N, Monteiro-Riviere NA. Deposition of antimicrobial coatings on microstereolithography-fabricated microneedles. JOM. 2011;63(6):59-68.

231. Boehm RD, Miller PR, Schell WA, Perfect JR, Narayan RJ. Inkjet printing of amphotericin B onto biodegradable microneedles using piezoelectric inkjet printing. JOM. 2013;65(4):525-533.

232. Boehm RD, Daniels J, Stafslien S, Nasir A, Lefebvre J, Narayan RJ. Polyglycolic acid microneedles modified with inkjet-deposited antifungal coatings. Biointerphases. 2015;10(1):011004.

233. Park SY, Lee HU, Lee YC, Kim GH, Park EC, Han SH, Lee JG, Choi S, Heo NS, Kim DL, Huh YS, Lee J. Wound healing potential of antibacterial microneedles loaded with green tea extracts. Mater Sci Eng C Mater Biol Appl. 2014;42:757-762.

234. Li H, Bao H, Bok KX, Lee CY, Li B, Zin MT, Kang L. High durability and low toxicity antimicrobial coatings fabricated by quaternary ammonium silane copolymers. Biomater Sci. 2015.

235. Duan DC, Rendon S Liquid crystalline polymer microneedles. WO/2012/074576 2011.

236. Wang B, Eberhardt W, Kück H. Plasma pre-treatment of liquid crystal polymer and subsequent metallization by PVD. Vacuum. 2006;81(3):325-328.

237. Kazuo N, Yasutaka T, Kazuto K, Norihiro I, Yoshihiro I, Mohammed Rafiqul I. Surface Modification of Polymer Films by Pulsed Oxygen Plasma. Japanese Journal of Applied Physics. 2007;46(7R):4246.

238. Grice EA, Segre JA. The skin microbiome. Nature reviews Microbiology. 2011;9(4):244-253.

239. Nair K, Whiteside B, Grant C, Patel R, Tuinea-Bobe C, Norris K, Paradkar A. Investigation of plasma treatment on micro-injection moulded microneedle for drug delivery. Pharmaceutics. 2015;7(4):471.

240. Shingade G. Review on: Recent trend on transdermal drug delivery system. Journal of Drug Delivery and Therapeutics. 2012;2(1):66-75.

241. Wokovich AM, Prodduturi S, Doub WH, Hussain AS, Buhse LF. Transdermal drug delivery system (TDDS) adhesion as a critical safety, efficacy and quality attribute. European Journal of Pharmaceutics and Biopharmaceutics. 2006;64(1):1-8.

242. Subedi RK, Oh SY, Chun MK, Choi HK. Recent advances in transdermal drug delivery. Arch Pharm Res. 2010;33(3):339-351.

243. DailyMed - LIDODERM - lidocaine patch. NDC Code(s): 63481-687. 2015 13 sep. Available from: http://dailymed.nlm.nih.gov/dailymed/drugInfo.cfm?setid=5ffefcdc-ebfa-4dc8-b484-719658da9d6d.

244. Hellgren U, Kihamia CM, Premji Z, Danielson K. Local anaesthetic cream for the alleviation of pain during venepuncture in Tanzanian schoolchildren. Br J Clin Pharmacol. 1989;28(2):205-206.

245. Mitragotri S. Modeling skin permeability to hydrophilic and hydrophobic solutes based on four permeation pathways. J Control Release. 2003;86(1):69-92.

246. Kellner T, Ehmann HM, Schrank S, Kunert B, Zimmer A, Roblegg E, Werzer O. Crystallographic textures and morphologies of solution cast Ibuprofen composite films at solid surfaces. Molecular pharmaceutics. 2014;11(11):4084-4091.

247. Turton R, Cheng XX. The scale-up of spray coating processes for granular solids and tablets. Powder Technology. 2005;150(2):78-85.

248. McGrath MG, Vrdoljak A, O'Mahony C, Oliveira JC, Moore AC, Crean AM. Determination of parameters for successful spray coating of silicon microneedle arrays. International Journal of Pharmaceutics. 2011;415(1–2):140-149.

249. Weber J, Kocur GJ Method for spray-coating a medical device having a tubular wall such as a stent. US6861088 B2, 2005.

250. Frederickson FL, Johnson MD Microneedle array applicator device and method of array application. US8784363 B2, 2014.

251. Kalluri H, Banga AK. Formation and closure of microchannels in skin following microporation. Pharm Res. 2011;28(1):82-94.

252. Bal S, Kruithof AC, Liebl H, Tomerius M, Bouwstra J, Lademann J, Meinke M. In vivo visualization of microneedle conduits in human skin using laser scanning microscopy. Laser Phys Lett. 2010;7:242-246.

253. Mori R, Power KT, Wang CM, Martin P, Becker DL. Acute downregulation of connexin43 at wound sites leads to a reduced inflammatory response, enhanced keratinocyte proliferation and wound fibroblast migration. J Cell Sci. 2006;119(Pt 24):5193-5203.

254. Qiu C, Coutinho P, Frank S, Franke S, Law LY, Martin P, Green CR, Becker DL. Targeting connexin43 expression accelerates the rate of wound repair. Curr Biol. 2003;13(19):1697-1703.